Chemical and Biological Oceanographic Conditions in the Gulf of St. Lawrence During 2024

Marjolaine Blais, Stephanie A. Clay, Peter S. Galbraith, and Michel Starr

Regional Sciences Branch
Québec Region
Pelagic and Ecosystemic Sciences Division
Fisheries and Oceans Canada
Maurice Lamontagne Institute
850, Route de la Mer
Mont-Joli, QC
G5H 3Z4

2025

Canadian Technical Report of
Hydrography and Ocean Sciences 405

Fisheries and Oceans Canada | Pêches et Océans Canada

Canada

Canadian Technical Report of Hydrography and Ocean Sciences

Technical reports contain scientific and technical information of a type that represents a contribution to existing knowledge but which is not normally found in the primary literature. The subject matter is generally related to programs and interests of the Oceans and Science sectors of Fisheries and Oceans Canada.

Technical reports may be cited as full publications. The correct citation appears above the abstract of each report. Each report is abstracted in the data base *Aquatic Sciences and Fisheries Abstracts.*

Technical reports are produced regionally but are numbered nationally. Requests for individual reports will be filled by the issuing establishment listed on the front cover and title page.

Regional and headquarters establishments of Ocean Science and Surveys ceased publication of their various report series as of December 1981. A complete listing of these publications and the last number issued under each title are published in the *Canadian Journal of Fisheries and Aquatic Sciences*, Volume 38: Index to Publications 1981. The current series began with Report Number 1 in January 1982.

Rapport technique canadien sur l'hydrographie et les sciences océaniques

Les rapports techniques contiennent des renseignements scientifiques et techniques qui constituent une contribution aux connaissances actuelles mais que l'on ne trouve pas normalement dans les revues scientifiques. Le sujet est généralement rattaché aux programmes et intérêts des secteurs des Océans et des Sciences de Pêches et Océans Canada.

Les rapports techniques peuvent être cités comme des publications à part entière. Le titre exact figure au-dessus du résumé de chaque rapport. Les rapports techniques sont résumés dans la base de données *Résumés des sciences aquatiques et halieutiques*.

Les rapports techniques sont produits à l'échelon régional, mais numérotés à l'échelon national. Les demandes de rapports seront satisfaites par l'établissement auteur dont le nom figure sur la couverture et la page de titre.

Les établissements de l’ancien secteur des Sciences et Levés océaniques dans les régions et à l'administration centrale ont cessé de publier leurs diverses séries de rapports en décembre 1981. Vous trouverez dans l'index des publications du volume 38 du *Journal canadien des sciences halieutiques et aquatiques*, la liste de ces publications ainsi que le dernier numéro paru dans chaque catégorie. La nouvelle série a commencé avec la publication du rapport numéro 1 en janvier 1982.

Canadian Technical Report
of Hydrography and Ocean Sciences 405

2025

Chemical and Biological Oceanographic Conditions in the Gulf of St. Lawrence During 2024

[1]Marjolaine Blais, [2]Stephanie A. Clay, [1]Peter S. Galbraith, and [1]Michel Starr

[1]Regional Sciences Branch
Quebec region
Pelagic and Ecosystemic Sciences Division
Fisheries and Oceans Canada
Maurice Lamontagne Institute
850, Route de la Mer
Mont-Joli, QC
G5H 3Z4

[2] Fisheries and Oceans Canada
Maritimes Region
Bedford Institute of Oceanography
P.O. Box 1006
Dartmouth, Nova Scotia
B2Y 4A2

Cat. No. Fs 97-18/405E-PDF ISBN 978-0-660-78830-2 ISSN 1488-5417
https://doi.org/10.60825/gmbq-jf70

Correct citation for this publication:

Blais, M., Clay, S.A., Galbraith, P.S., and Starr, M. 2025. Chemical and Biological Oceanographic Conditions in the Gulf of St. Lawrence During 2024. Can. Tech. Rep. Hydrogr. Ocean. Sci. 405: vi + 87 p. https://doi.org/10.60825/gmbq-jf70

TABLE OF CONTENTS

ABSTRACT

Blais, M., Clay, S.A., Galbraith, P.S., and Starr, M. 2025. Chemical and Biological Oceanographic Conditions in the Gulf of St. Lawrence During 2024. Can. Tech. Rep. Hydrogr. Ocean. Sci. 405: vi + 87 p. https://doi.org/10.60825/gmbq-jf70

This report presents an overview of chemical and biological oceanographic conditions in the Estuary and Gulf of St. Lawrence in 2024 relative to long-term means, based on data from the Atlantic Zone Monitoring Program (AZMP) and regional programs. Oxygen saturation reached record lows at 200 m in the Estuary and northwest Gulf, and at 250 m in the latter. Nutrient inventories were generally below normal in surface waters and above normal in deep layers. Vertically integrated chlorophyll *a* inventories were near or slightly below normal, except in the Estuary and northwest Gulf, where they were above normal. Remote sensing observations showed slightly below-normal surface chlorophyll *a* on the Magdalen Shallows, and near or above normal elsewhere. Spring blooms were early or near normal, while fall blooms were delayed. Zooplankton biomass was generally low in the Gulf, despite above-normal abundances of *Calanus finmarchicus*, mainly due to very low *Calanus hyperboreus* levels at several sites. Small calanoids, non-copepods, and warm-water copepods abundances were mostly below or near normal. *Calanus finmarchicus* showed an early phenology.

RÉSUMÉ

Blais, M., Clay, S.A., Galbraith, P.S., and Starr, M. 2025. Chemical and Biological Oceanographic Conditions in the Estuary and Gulf of St. Lawrence During 2024. Can. Tech. Rep. Hydrogr. Ocean. Sci. 405: vi + 87 p. https://doi.org/10.60825/gmbq-jf70

Ce rapport présente un aperçu des conditions océanographiques chimiques et biologiques dans l'estuaire et le golfe du Saint-Laurent en 2024 en comparaison aux moyennes à long terme, basé sur les données du Programme de monitorage de la zone atlantique (PMZA) et de programmes régionaux. La saturation en oxygène a atteint des creux records à 200 m dans l'estuaire et le nord-ouest du golfe, ainsi qu'à 250 m dans ce dernier. Les inventaires d'éléments nutritifs étaient généralement sous la normale dans la couche de surface, et au-dessus de la normale dans la couche profonde. Les inventaires de chlorophylle *a* intégrés verticalement étaient près de la normale ou légèrement inférieurs, sauf dans l'estuaire et le nord-ouest du Golfe où ils étaient supérieurs. La télédétection a révélé que les concentrations de chlorophylle *a* à la surface étaient légèrement inférieures à la normale sur le plateau madelinien, et près ou supérieure à la normale ailleurs. Les floraisons printanières étaient hâtives ou proches de la normale, tandis que celles d'automne étaient retardées. La biomasse de zooplancton était généralement faible dans le golfe, malgré des abondances supérieures à la normale de *Calanus finmarchicus*, en raison de très faibles abondances de *Calanus hyperboreus* à plusieurs sites. Les petits calanoïdes, non-copépodes et copépodes d'eaux chaudes étaient généralement sous ou près de la normale. *Calanus finmarchicus* a montré une phénologie hâtive.

1. INTRODUCTION

The Atlantic Zone Monitoring Program (AZMP) was implemented in 1998 (Therriault et al. 1998), with the aim of 1) increasing Fisheries and Oceans Canada's (DFO) capacity to understand, describe, and forecast the state of the marine ecosystem, and 2) quantifying the changes in the ocean's physical, chemical, and biological properties, and the predator–prey relationships of marine resources. AZMP provides data to support the sound development of ocean activities. A critical element of the AZMP observational program is the annual assessment of the distribution and variability of physical, chemical and biological properties of the water column. This report focuses on oxygen, nutrients, and plankton communities.

A description of the spatiotemporal distribution of nutrients (nitrate, silicate, and phosphate), and chlorophyll *a* (chl *a*) concentrations provides important information on biogeochemical cycling, water-mass movements and on the location, timing, and magnitude of biological production cycles. A description of the phytoplankton and zooplankton communities, distributions and phenologies provides important information on the organisms forming the base of marine food webs. Biogeochemical and plankton production cycles play a pivotal role in supporting healthy marine ecosystems, and their understanding is crucial for an ecosystem approach to fisheries management.

The AZMP derives its information on the state of the marine ecosystem from a combination of satellite remote sensing and *in situ* data collected at a network of sampling locations (high-frequency monitoring stations, cross-shelf sections) in each DFO region (Québec, Gulf, Maritimes, Newfoundland and Labrador; see Figure 1 for section locations in the St. Lawrence Gulf and Estuary) visited at a frequency of weekly to once annually (Galbraith et al. 2025b). The sampling design of the zonal AZMP provides valuable information on the natural variability in physical, chemical, and biological properties of the Northwest Atlantic continental shelf. Cross-shelf sections and ecosystem trawl surveys provide a broad-scale overview of the conditions but are limited in their seasonal coverage. Strategically located high-frequency monitoring stations complement the sampling by providing more detailed information on seasonal-scale changes in ecosystem properties. In recent years, automated oceanographic buoys have also complemented core observations, with high temporal resolution data.

In this document, we review the chemical and biological (lower trophic levels) oceanographic conditions in the Estuary and Gulf of St. Lawrence in 2024. For conciseness, the term Gulf is used to refer to the entire St. Lawrence Estuary and Gulf bioregion thereafter in the document. Changes in the physical pelagic environment influence both plankton community composition and annual biological production cycles, with implications for the energy transfer to higher trophic levels. Readers should refer to Galbraith et al. (2025a) for a complete description of the physical conditions that prevailed in the Gulf in 2024.

2. METHODS

2.1 SAMPLING

All sample collection and processing steps meet the standards of AZMP protocols (Mitchell et al. 2002). Field measurements included in this report were collected during dedicated AZMP surveys carried out in winter, early summer, and fall (generally in March, June, and October) of each year, and at two high-frequency monitoring stations (Figure 1). Oceanographic

measurements made during multidisciplinary surveys (August and September; hereafter referred to as late summer surveys), and during the mackerel egg survey (June) were included for all years (2006–2024) for which data are available. In this document, stations were grouped into four main regions for which biochemical indices are presented (Figure 1):

(1) Estuary/northwest Gulf: this region is generally deep (> 200 m) and cold at the surface in summer. It is strongly influenced by freshwater runoff from the St. Lawrence River, by upwelling/mixing of cold intermediate (CIL) waters, and by dense waters inflowing along the Laurentian Channel in deeper waters;

(2) Northeast Gulf: this region, with deep channels and a relatively wide shelf (shallower than 100 m), is characterized by high surface salinity;

(3) Central Gulf/Cabot Strait: this region is generally deep (> 200 m), and is directly influenced by deep waters that mix at the continental slope (warm North Atlantic Central Water that has a Gulf Stream signature and cold Labrador Current water) and enter the Gulf through Cabot Strait;

(4) Magdalen Shallows: this region is shallow (<100 m) and warm at the surface in summer. It is largely influenced by the Gaspé Current.

These regions are consistent with those used for the DFO Ecosystem Approach to Fisheries Management. Due to sparse data, biogeochemical indices are not reported for Mécatina Trough and Northumberland Strait (Figure 1).

Table 1 lists the 2024 sampling surveys and Figure 2 and Figure 3 summarize the sampling effort during the seasonal surveys and at the high-frequency monitoring stations, respectively. Rimouski station (depth 320 m) has been sampled since 1991—about weekly throughout the summer, once or twice a month in early spring and late fall, and rarely in winter (except during the March survey) due to the presence of sea ice. It is representative of conditions in the Estuary/northwestern Gulf. In 2024, Rimouski station was visited on 24 occasions. Shediac Valley station (depth 84 m) is representative of conditions on the Magdalen Shallows and of the Estuary outflow. Shediac Valley station is at best sampled once monthly between May and November, with nearly absent coverage from December through April, except during the March survey. Shediac Valley station was visited six times in 2024; however, no visit occurred in July or August. In addition to the occupations at the high-frequency monitoring stations, automated oceanographic buoys equipped with temperature, salinity, and fluorescence surface sensors (data collected every 30 minutes) have been deployed at the high-frequency stations since 2002 and 2004 at Rimouski and Shediac Valley stations, respectively. Buoys are typically deployed in late April/early May, and recovered in late October/early November.

Sampling along the oceanographic sections and at the high-frequency monitoring stations includes a Conductivity-Temperature-Depth profile (CTD; temperature, salinity, fluorescence, dissolved oxygen) as well as discrete water sampling using Niskin bottles at multiple depths (~ 2 m, 10 m, 15 m, 25 m, 50 m, 100 m, 200 m, 300 m, 400 m, bottom). Water from the Niskin bottles is collected for the analysis of dissolved oxygen (Winkler method), nutrients (Seal Analytical AutoAnalyzer 3 or Alpkem AutoAnalyzer), chl *a* concentration (fluorometer), and phytoplankton enumeration (inverted microscopy) (Mitchell et al. 2002). Finally, mesozooplankton (<1 cm, hereafter referred to as zooplankton) is collected with bottom-to-surface vertical ring net tows (75 cm diameter, 200 µm mesh) for most surveys. Taxonomists

are responsible for the identification, enumeration, and bulk biomass (dry weight) measurements of zooplankton samples collected during regular AZMP surveys (early summer and fall surveys) and the September southern Gulf multidisciplinary survey. Zooplankton samples collected during the August multidisciplinary survey and mackerel egg survey are processed semi-automatically using the ZooImage 5.5.2 software package (Grosjean et al. 2018), following the methodology described in Plourde et al. (2019) and Blais et al. (2023). Since methods are different, and considering the larger mesh size of nets deployed during the mackerel egg survey (333 µm mesh), which prevents the capture of early copepodite stages (CI–CIII, and up to CIV for small species; Nichols and Thompson 1991), ZooImage derived indices are excluded from annual abundance estimates. September survey results, limited to the Magdalen Shallows and based on a different set of stations each year, are also reported separately and excluded from the annual indices.

2.2 IN SITU METRICS

2.2.1 Oxygen

Oxygen concentration profiles are used to monitor hypoxic conditions in the Gulf. Oxygen concentrations were measured using a Sea-Bird SBE43 probe mounted on the CTD and calibrated against seawater samples, collected from most casts, and analyzed by Winkler titration (for the calibration procedure, see Sea-Bird application notes 64-1, -2, -3). Annual mean values were calculated from gridded 2 km^2 fields using inverse-distance-weighted interpolation, spatially averaged by region and season.

2.2.2 Nutrients and phytoplankton

Nutrient and chl *a* concentrations (a proxy for phytoplankton biomass) collected along the AZMP sections and at the high-frequency monitoring stations were depth-integrated (i.e., 0–100 m for chl *a*; 0–50 m, 50–150 m, and 150 m–bottom for nutrients) using the trapezoidal method. In 2016 and 2017, winter vertical profiles of nutrients all over the Gulf revealed that nutrient concentrations were relatively homogeneous in the upper 50 m of the water column. Therefore, for typical years when vertical nutrient profiles are not available, including 2024, winter nutrient inventories 0–50m were estimated using surface concentrations, assuming the nutrient concentrations were uniform in the mixed layer. Spring nutrient drawdown was estimated as the difference between the March and June nitrate inventories (0–50 m), and is used as a proxy for phytoplankton spring production since the early summer sampling occurs after the spring bloom. Phytoplankton taxonomic identification is performed for the high-frequency monitoring stations, and has been since the beginning of the program, and since 2014 across the Gulf of St Lawrence. For the Shediac Valley time series, counts performed by two different taxonomists were used in this report, whereas previous versions relied on only one. Overlapping counts enabled the estimation of correction factors to align the counts between taxonomists. Annual mean counts are based on the first taxonomist from 1999 to 2015, both from 2016 to 2023, and the second taxonomist in 2024.

2.2.3 Zooplankton

Since zooplankton samples are generally collected over the entire water column (or 0–50 m during the mackerel egg survey), zooplankton indices represent depth-integrated metrics. Only taxonomist-analyzed samples collected during early summer and fall AZMP surveys were included in the calculation of regional zooplankton annual anomalies. Appendix 1 lists species

included in each copepod index. Since 2018, *Calanus finmarchicus* and *C. glacialis* have been distinguished using prosome length and a genetic criterion (Parent et al. 2011).

We use the time series at Rimouski station to describe *C. finmarchicus* phenology and its evolution as adequate sampling and stage identification started 30 years ago. Zooplankton sampling at Rimouski station prior to 2005 and the use of AZMP standard nets (*i.e.*, 75 cm diameter, 200 µm mesh bottom-to-surface ring net tows; Mitchell et al. 2002) is described in Blais et al. (2024). The phenology of *C. finmarchicus* was characterized using the following steps: (1) stage-relative abundances were normalized (proportion of a copepodite stage/maximum proportion for the stage) within each year for CI–III, CIV, CV, and CVI (male and female) and (2) stage proportions were smoothed using a LOESS function (locally estimated scatterplot smoothing).

2.3 SATELLITE REMOTE SENSING OF OCEAN COLOR AND BLOOM METRICS

Satellite ocean colour data provide large-scale images of surface phytoplankton biomass (as indexed by chl *a* concentration). Daily satellite composite images within four ocean colour polygons (northwest Gulf, northeast Gulf, Magdalen Shallows, and Cabot Strait; Figure 4) supplement our ship-based observations, especially regarding the spring bloom phenology, and provide seasonal coverage and a large-scale context for interpreting survey data. However, since ocean colour imagery only provides surface coverage (i.e., a few metres at best), it should be used as complementary information to the in situ survey data.

In this report, characteristics of phytoplankton blooms were derived from daily composites of satellite images of remote sensing reflectance (4 km spatial resolution) obtained from the Ocean Colour Climate Change Initiative (OC-CCI, 1998–2024) dataset, provided by the Plymouth Marine Laboratory as part of the European Space Agency (ESA) climate change initiative. These composites were converted to chl *a* concentration using the POLY4 algorithm, with coefficients tuned to the Gulf of Saint Lawrence (Clay et al. 2019, Clay 2025). This dataset integrates observations from multiple satellite sensors (e.g., SeaWiFS, MODIS, VIIRS), thereby extending the time series back to 1998 and improving spatial and temporal coverage compared to previous reports, which previously relied solely on data from NASA's Moderate Resolution Imaging Spectroradiometer (MODIS) "Aqua" sensor, launched in July 2002. By enhancing regional coverage, the use of the OC-CCI product also improves the accuracy of bloom estimates (Sathyendranath et al. 2019). However, it also introduces differences in seasonal metrics and anomalies, which may not align with those reported in previous assessments based on the MODIS-only dataset.

The timing of the spring phytoplankton bloom was derived by applying a LOESS function to the daily averages of log-10 transformed chl *a* concentration (weighted by percent coverage within the polygon, down to a minimum of 20%), and then by fitting a shifted Gaussian to the smoothed curve (Zhai et al. 2011). The start of the spring bloom corresponds to the day when chl *a* concentration reaches 20% of the maximum spring bloom amplitude, and the peak timing is the day at which fitted chl *a* concentration reaches its maximum. Initiation of the fall bloom was calculated by applying the threshold method described in Layton et al. (2022) on the LOESS-smoothed daily averages of the log-10 transformed chl *a* concentration. Fall bloom start corresponds to the day when chl *a* concentration rises above the threshold of 5% over the

annual median, and remains above it for at least 14 consecutive days. Parameters used to fit the Gaussian curves are described in Appendix 2.

To characterize spring and fall bloom intensities but also phytoplankton production occurring in other seasons, seasonal chl *a* averages are reported. The season boundaries, which are considered unique to each polygon, are defined by the timing (start and end) of the spring and fall bloom over the climatology. Winter starts on January 1st until the spring bloom starts, and summer starts at the end of the spring bloom and ends at the start of the fall bloom. Fall ends on December 31st.

All ocean-colour polygons are located outside of the St. Lawrence River plume because satellite-based chl *a* concentration estimates in such areas are unreliable due to contamination by river inputs loaded with coloured matter of terrestrial origin. For the same reason, polygons exclude areas within 1 km of the coast, and over 5 km away where freshwater influence is stronger. This also explains why spring bloom metrics in the Estuary cannot be derived from ocean colour data. However, high-temporal-resolution information on the phytoplankton dynamics at the surface of the Estuary is available from the surface fluorescence sensor on the oceanographic buoy located at Rimouski station and presented in this document. To increase the accuracy of daily chl *a* concentration estimates, data from the buoy sensor were examined to remove data collected during daytime to remove potential bias due to the influence of high light intensity on phytoplankton pigments and daily outliers (± 3 SD). The cleaned dataset was then calibrated against weekly in situ chl *a* concentrations measured at Rimouski station using a linear regression (R^2 = 0.25, p <0.001, n = 1486).

2.4 ANNUAL ANOMALY SCORECARDS

Normalized anomalies for the chemical and biological indices presented in scorecards were computed for the high-frequency monitoring station and oceanographic regions. These anomalies are calculated as the difference between the variable's average for the season or for the complete year and the variable's climatological mean (usually 1999–2020); this number is then divided by the standard deviation over the climatological period.

Anomalies are presented as scorecards, with positive anomalies depicted as shades of red, negatives as blues, and anomalies within ± 0.5 SD as white (considered as normal conditions, *i.e.*, similar to the climatology). A standard set of indices representing anomalies of nitrate inventories in the mid-layer (50–150 m), phytoplankton biomass and bloom dynamics, mesozooplankton biomass, and the abundance of dominant mesozooplankton species, and groups (*C. finmarchicus, Pseudocalanus* spp., total copepods, and total non-copepods) are produced for each AZMP region (Casault et al. 2025; Bélanger et al. 2024). To visualize Northwest Atlantic shelf-scale patterns of environmental variation, a zonal scorecard including observations from all AZMP regions is presented in Galbraith (2025b).

Annual nutrient, phytoplankton, and zooplankton index anomalies are based on the mean annual inventory (mmol m^{-2} for nutrients, mg chl *a* m^{-2} for phytoplankton biomass), density (cells L^{-1} for phytoplankton abundance, individuals m^{-2} for zooplankton abundance), or biomass (g m^{-2} for zooplankton biomass), estimated at both high-frequency monitoring stations and in all Gulf regions of Figure 1. These annual estimates are derived from general linear models (GLM) of the form:

$Log_{10}(y) = \alpha + \beta_{YEAR} + \delta_{MONTH} + \varepsilon$ for the high-frequency monitoring stations, and
$Log_{10}(y) = \alpha + \beta_{YEAR} + \delta_{STATION} + \gamma_{SEASON} + \varepsilon$ for the regions,

Where *y* is the response variable, either expressed as inventory or density, α is the intercept, and ε is the error (following a gaussian distribution). The GLM is applied to each region separately. For the high-frequency monitoring stations, β and δ are the categorical effects for year and month, respectively. For the regions, β, δ, and γ are the categorical effects of year, station, and season, respectively. We log-10 transformed inventories and density values before computing anomalies to compensate for the skewed distribution of observations. We added one unit to *Density* terms for the abundance indices (phytoplankton and zooplankton counts) to account for observations with values of zero. An estimate of the least-square means based on type III sums of squares is used as an estimate of the annual average. Results of the GLM (significance of each factor and adjusted coefficients of the regression) are presented in Appendices 3 to 7. Four seasons (winter, early summer, late summer, and fall) are included in the GLM to estimate the annual average of surface nutrient inventories; three seasons are used to estimate the annual average of deeper nutrient inventories and phytoplankton indices (no data collection during winter); and two seasons (early summer and fall) are used to calculate annual estimates of zooplankton indices. Zooplankton data collected during mackerel egg survey or late summer surveys are presented separately, and their time series are based on seasonal arithmetic means.

3. OBSERVATIONS

3.1 PHYSICAL ENVIRONMENT

Stratification is one of the key physical parameters influencing primary production. For this reason, we present the upper water column stratification, calculated as the density difference between the surface and 50 m depth. In 2024, the timing of the spring freshet was near normal, but the runoff of the St. Lawrence River at Québec City was near normal to lower than normal during spring and fall, and above normal during summer (Figure 6 in Galbraith et al. 2025a). This led to a slightly delayed onset of stratification in spring and weaker-than-normal stratification during monitoring at the Rimouski station, where stratification was only higher than normal in the fall, consistent with the pattern observed in the previous year (Figure 5). However, at the Shediac Valley station, stratification was either normal or higher than normal throughout seasonal monitoring during 2024 (Figure 5). Similarly, in the northern Gulf, stratification generally ranged from near normal to lower than normal during most months, whereas in the central and southern Gulf, it was predominantly near normal to higher than normal (Figure 6Figure 6). Overall, stratification was generally lower in 2024 compared to the previous monthly measurements in 2023.

3.2 DEEP OXYGEN

Hypoxic waters (i.e. <30% saturation levels) were observed near 150 m deep in late April/early May 2024 at the Rimouski station, with most waters deeper than 200 m classified as severely hypoxic (i.e., <20% saturation levels; Figure 7). Compared to the climatology, where hypoxic waters are typically restricted below 200 m, and severely hypoxic waters below 250 m, 2024 observations indicate a reduced upper limit of hypoxia (Figure 7). The bottom layer (270–320 m) at Rimouski station reached its lowest monthly average oxygen saturation levels in October, dropping to 11%, which is nearly half the climatological value for that time of the year (Figure 8). This represents the third-lowest monthly average in the time series, following the record lows (10.5%) recorded in September and October 2022. Oxygen saturation was below 10% at the bottom in October and November (Figure 7).

In the Gulf, minimum oxygen saturation levels (below 15% saturation at 300 m in recent years) were observed in the deep waters of the Estuary (Figure 9). Hypoxic waters extended along the channel from the Estuary to the centre of Anticosti Island (Figure 9). Hypoxic waters were also present at the heads of the Anticosti and Esquiman channels in 2024, regions where hypoxia was absent in the climatology. Detailed vertical profiles along the deep channels also shows that severely hypoxic waters (<20% saturation) extended from the Estuary to the northwest Gulf in waters deeper than 225 m (Figure 10). In the Anticosti and Esquiman Channels, hypoxic waters were found slightly below 200 m, extending down to about 275 m, and spanned nearly 150 and 125 km, respectively, from the heads of these channels (Figure 11 and 12).

As a consequence, there has been a major increase in both the area at 300 m and the volume covered by hypoxic waters in the Gulf since 2015, with record-high values observed in 2023 (Figure 13). The area and volume estimated in 2024 therefore represent a decrease from these record highs, but in different proportions. The decrease in hypoxic water area at 300 m (approximately 30%) is much larger than the decrease in volume (approximately 12%). The annual average time series suggest that saturation levels at 300 m in 2024 remained similar or above those measured in 2023 (Figure 14). At depths of 250 m and 300 m in Cabot Strait, oxygen levels increased to values comparable to those observed in 2015 (Figure 14). However, at 200 and 250 m in the Estuary and northwest Gulf, 2024 saturation levels were generally lower than in 2023, setting new record lows at 200 m in both regions, and at 250 metres in the northwest Gulf. In 2024, the annual average dissolved oxygen saturation levels in the Estuary were 12% (38 µM) at 300 m, and 24% (77 µM) in bottom waters (> 100 m) in 2024 (Figure 14).

3.3 NUTRIENTS

Distributions of dissolved inorganic nutrients (nitrate, silicate, phosphate) strongly co-vary in space and time (Brickman and Petrie 2003). For this reason, and because nitrogen availability controls phytoplankton growth in coastal waters of the Gulf, emphasis in this document is given to the variability in nitrate concentrations and inventories, even though the distributions of other nutrients are also briefly discussed. In this document, we use the term “nitrate” to refer to the sum of nitrate and nitrite (NO_3^-+NO_2^-).

3.3.1 High-frequency monitoring stations

The two high-frequency monitoring stations typically exhibit a seasonal cycle of surface nitrate inventories: a spring/summer drawdown linked to biological uptake, a summer minimum, and a subsequent increase during fall/winter once water column mixing intensifies due to cooling processes and wind forcing (Figure 15). Seasonal stratification and mixing processes inversely influence the mid-layer nitrate inventories since this layer supplies the surface one (Figure 15). Surface and mid-layer nitrate inventories at Rimouski station are typically two to three times higher and about three to four times higher, respectively, than those at Shediac Valley station (Figure 15).

In 2024, surface nitrate inventories at the Rimouski station ranged from normal to below normal, with the exception of one above-normal inventory observed in July (Figure 15). Vertical nitrate profiles confirm the surface layer was indeed replenished with nitrate in mid July (Figure 16). The mid-layer nitrate inventory was below normal during spring/early summer, and again in the fall, but near or above normal between these periods (Figure 15). The deep layer showed negative anomalies throughout the year, particularly in November, when nitrate inventories were strongly below normal from 100 m depth to the bottom (Figure 16).

At the Shediac Valley, surface and bottom nitrate inventories were mostly close to normal, except in April when the surface inventory was higher than normal, suggesting a delayed spring bloom, as nitrate is typically depleted by this time, and again in September in the subsurface layer (Figure 15, 16).

3.3.2 Gulf regions

The spatial distribution of nitrate in the surface layer during winter 2024 was similar to the climatology, with maximum inventories in the Estuary and around the Gaspé Peninsula. However, nitrate inventories were below normal across the Gulf, especially in the northeast Gulf (Figure 17). These winter inventories are calculated from the sample collected at ~2 m depth, assuming that concentrations are uniform over the 0–50 m layer. The estimated nitrate drawdown during spring was generally lower than normal, which could suggest a low-intensity phytoplankton spring bloom, except for the lower Estuary (Figure 17). Surface layer nitrate inventories remained below normal during early summer in most of the Gulf, except in the northwest Gulf and at two stations in Baie des Chaleurs, south of the Gaspé Peninsula (Figure 18). During late summer, a plume of nutrient-rich surface waters extending south of the Gaspé Peninsula towards the eastern side of Northumberland Strait led to positive nitrate anomalies in these areas (Figure 19). Above-normal nitrate levels were also observed in the surface layer north of Anticosti Island during the same season. Surface layer nitrate inventories were again below normal during fall across the Gulf (Figure 20). Mid-layer nitrate inventory anomalies varied widely both spatially and seasonally, but generally indicated below-normal inventories along the Laurentian Channel (Figure 18–20). Deep nitrate inventories shifted from being mostly above normal in early summer to predominantly below normal in fall, with late summer showing negative anomalies in the western Gulf and positive anomalies in the eastern Gulf (Figure 18–20).

3.3.3 Scorecards

Annual averages of all nutrients were mostly negative in the surface layer across the Gulf, a pattern mainly observed since 2010 (Figure 21). A linear regression of surface layer nitrate annual averages indicates a significant decrease (p <0.001) of slightly over 20% in the Gulf when comparing the 1999–2009 and 2010–2024 periods. In the mid-layer, annual average nutrient inventories were mostly near normal, with a few positive anomalies, contrasting with the dominant negative anomalies observed over the past two years (Figure 22). In the deep layer, nutrient inventories showed strong coherence in their patterns across the Gulf (Figure 23): nitrate inventories were mostly below normal, while silicate and phosphate inventories were above normal. In the central Gulf/Cabot Strait regions, this year marks the end of a four-year period of strong positive anomalies in deep nitrate (Figure 23).

The Redfield-Brzezinski C:Si:N:P ratio, which assumes equilibrium between phytoplankton composition and the deep-ocean nutrient inventory, is 106:15:16:1 (Redfield 1958; Brzezinski 1985). In the deep waters of the Gulf, the N:P ratio is lower than the target of 16, with climatological averages ranging from 11.0 to 12.7, while the Si:N ratios tend to be higher than the target of 0.94, ranging between 1.3 and 2.1 (Figure 23). The climatological N:P (Si:N) ratio is highest (lowest) at the entrance of the Laurentian Chanel and decreases (increases) as water progresses up the deep channel from Cabot Strait to the Estuary. In 2024, deep-layer N:P (Si:N) ratios reached record lows (highs) in almost all regions. These patterns of lower-than-normal N:P and higher-than-normal Si:N have persisted over the past eight years across much of the

Gulf and have intensified in recent years, particularly at Rimouski and in the Estuary/northwest Gulf region, where new nutrient ratio records have been set annually since 2022 (Figure 23).

3.4 PHYTOPLANKTON

3.4.1 High-frequency monitoring stations

Seasonal patterns of water-column integrated chl *a* concentrations differ between the two high-frequency monitoring stations. At Rimouski station, maximum chl *a* is typically reached during early summer, and stays at relatively high levels until late summer/early fall. In contrast, at Shediac Valley station, the maximum is reached in early spring (no chl *a* data in March but high surface nutrient levels indicate that the bloom has not yet begun) before diminishing rapidly, and staying low for the remainder of the production cycle (Figure 24). From June onward, chl *a* inventories are typically two to three times higher at Rimouski station than at Shediac Valley station (Figure 24).

In 2024, chl *a* inventories at Rimouski station were generally normal or above normal, reaching their highest value in late July (Figure 24). The highest chl *a* concentration was measured at the surface during the station's first visit in May, suggesting that the phytoplankton spring bloom had already begun (Figure 25). Phytoplankton biomass is typically confined within the upper 25 m of the water column, but in 2024, noticeable biomass was also observed between 25 and 75 m in late May, as well as during July and August (Figure 25).

At the Shediac Valley, chl *a* inventories were below normal in April, and considerably above normal in May (Figure 24), corroborating nutrient observations that suggested a delayed spring phytoplankton bloom. While high phytoplankton biomass at this station often extends to the bottom of the water column during the spring bloom, in 2024, it was mostly restricted to the upper 30 m (Figure 25).

Apart from one observation in May, phytoplankton abundances were below normal until late July at the Rimouski station (Figure 26). From that point onward, they were either near or above normal. Diatoms largely dominated the phytoplankton community in May and August, while flagellates were clearly dominant in March, June and during fall. The proportion of diatoms was particularly lower than normal in June. Conversely, the proportion of dinoflagellates was higher than normal in March and during the fall (Figure 26).

At Shediac Valley, phytoplankton abundances were generally close to or slightly above normal, except in early May when they were considerably above normal, and numerically dominated by diatoms (Figure 27). Diatoms accounted for a substantial proportion of the phytoplankton community between March and May, but their proportion declined to nearly negligible levels afterward, and remained much lower than the climatological average (Figure 27).

3.4.2 Gulf regions

Chlorophyll *a* inventories are typically highest in the Estuary and around the Gaspé Peninsula during early and late summer. This region becomes less of a phytoplankton hotspot in the fall, as chl *a* maxima typically expand into the central Gulf and northern Magdalen Shallows (Figure 28). In early and late summer 2024, chl *a* inventories (0–100 m) were mostly below normal across the Gulf (Figure 28), with some exceptions in the Estuary/northwest Gulf in June and in Jacques-Cartier Strait, north of Anticosti Island, in August. During the fall, chl *a* inventories were generally near or above normal, except in parts of the eastern Gulf. Positive anomalies were

particularly strong along the northern shore of the Gulf, similar to conditions in 2023 (Blais et al., 2024), and in Chaleur Bay (Figure 28).

In 2024, phytoplankton cell abundances during winter across the Gulf were generally lower than during early summer, which typically corresponds to a post-bloom period characterized by low cell abundance. Winter communities were largely dominated by flagellates, although diatoms accounted for over 50% of cells at two locations, Shediac Valley and east of Northumberland Sound, a composition more typical of bloom conditions (Figure 29). The high phytoplankton biomass observed in the Estuary/northwest Gulf during early summer, and in the Estuary during fall, was associated with a relatively high proportion of diatoms. Flagellates remained the dominant taxa at other locations (Figure 29).

3.4.3 Scorecards

Overall, annual averages of chl *a* inventories were slightly below normal on the Magdalen Shallows, above normal at the Rimouski station and in the Estuary/northwest Gulf region, and near normal elsewhere (Figure 30). For the seventh consecutive year, a larger-than-usual fall bloom was observed in the Estuary/northwest Gulf (Figure 30). Over the past decade, positive fall chl *a* anomalies have been common throughout the Gulf (Figure 30), with fall biomass increasing by ~40% between the 1999–2013 and 2014–2024 periods.

Since 2018, total phytoplankton abundances have regularly shown positive anomalies, driven by higher-than-normal abundances of flagellates and dinoflagellates in most regions. During the same period, the Estuary/northwest Gulf region (including the Rimouski station) has been the only area to almost consistently indicate positive anomalies in diatom abundance (Figure 31). A similar pattern was observed in 2024, although only the Rimouski station exhibited a positive anomaly in diatom abundance. Dinoflagellate abundances have been strongly above normal on the Magdalen Shallows over the past four years, including in 2024 (Figure 31).

3.4.4 Satellite remote sensing and oceanographic buoy data

Observations from the oceanographic buoy at the Rimouski station are included in this section, as they align well with satellite remote sensing data in terms of both temporal and vertical (thin surface layer) resolution, providing comparable indices of phytoplankton biomass. Surface chl *a* concentrations estimated from the buoy in 2024 suggest a phenology similar to that observed from water samples collected at the Rimouski station (Figure 24), with concentration peaks in mid-May, July, and late September (Figure 32). Chlorophyll *a* concentrations from the buoy were above normal during these periods, as well as in the fall, and were close to or slightly above normal otherwise (Figure 32).

In most remote sensing ocean colour polygons, winter phytoplankton biomass was above normal (Figure 32). Phytoplankton biomass maxima reached during the spring bloom were also generally higher than the climatological average (Figure 32). However, the strongest spring bloom positive anomalies appeared to have occurred in the central Gulf, although there is no defined polygon for that area (Figure 33). In the northwest Gulf, phytoplankton biomass peaks were notably observed during the summer and late summer months, consistent with both *in situ* chl *a* samples and buoy fluorescence observations. A similar, albeit less intense, summer bloom also occurred in the Cabot Strait polygon. Fall blooms began in the northern Gulf in September, and extended southward in October (Figure 34). Phytoplankton biomass was above normal during these fall blooms (Figure 32).

Spring bloom timing in 2024 was slightly earlier than normal in the northeast Gulf, earlier in Cabot Strait, and near normal in other regions (Figure 35). Since 2016, spring bloom timing has

been generally normal or earlier than normal across the Gulf. In contrast, the fall bloom occurred later than normal in all regions, a pattern consistently observed since 2011. Bloom curve fits for 2024 are available in Appendix 2.

Overall, annual averages suggest that surface phytoplankton biomass in 2024 was above normal at the Rimouski station and in the northeast Gulf, below normal on the Magdalen Shallows, and near normal in other regions (Figure 35). Seasonal anomalies of surface chl *a* have shifted around 2014 from predominantly negative to positive, with the trend especially pronounced in winter and fall (Figure 35). On an annual basis, surface phytoplankton biomass has increased significantly over the time series ($p < 0.001$).

3.5 ZOOPLANKTON

3.5.1 High-frequency-monitoring stations

In 2024, zooplankton biomass at the Rimouski station was consistently below the climatological average throughout the year, except in November. At Shediac Valley, biomass was mostly near normal (Figure 36). Copepods abundance was also generally below normal at the Rimouski station (Figure 37). The copepod community composition was relatively similar to the climatology, although the relative contribution of *C. hyperboreus* was considerably reduced in 2024 (Figure 37). In contrast, both *C. finmarchicus* and *C. glacialis* accounted for a larger-than-normal proportions.

Non-copepods abundance at the Rimouski station was highly variable, ranging from slightly below normal to well above normal (Figure 38). The *Euphausiacea* group dominated the non-copepod community until fall, and the *Ostracoda* group became dominant in October and November (Figure 38).

At Shediac Valley, copepods abundance was near to below normal (Figure 39). Similar to Rimouski, a lower-than-normal proportion of *C. hyperboreus,* and a higher-than-normal proportion of *C. finmarchicus* were observed at Shediac. *Triconia longicornis*, which typically accounts for 10–20% of copepod abundance, was nearly absent from samples in 2024 (Figure 39). Non-copepods abundance was generally within normal ranges (Figure 40). *Cirripedia* showed above-normal proportions in spring, while *Echinoderma* and *Bryozoa* did so in the fall (Figure 40).

At the Rimouski station, the abundances of *C. finmarchicus* was generally near normal until September, after which it increased to above-normal levels for the remainder of the year (Figure 41). The proportion of early copepodite stages (CI–CIII) seemingly peaked in May, when sampling began, and remained relatively high (approximately 20%) until November (Figure 41). At Shediac Valley, *C. finmarchicus* abundances were also generally close to normal. The peak in early copepodite stages occurred in May, compared to April in the climatology, and CI–CIII stages again dominated the *C. finmarchicus* population in September (Figure 41).

In 2024, *C. hyperboreus* abundances were below normal at both high-frequency monitoring stations (Figure 42). For all 2024 samples, the *C. hyperboreus* population consisted of stages CIV, CV and CVI, with the proportion of the CVI stage being nearly three times higher than normal, while the CIV stage was about half the normal level (Figure 42). In contrast, at Shediac Valley, the population was dominated by early copepodite stages in spring, and the overall composition in 2024 was comparable to the climatology (Figure 42).

At the Rimouski station, the abundance of *Pseudocalanus* spp. abundances was below normal during most of the year (Figure 43). Early copepodite stages peaked in May and October but were nearly absent otherwise. At Shediac Valley, *Pseudocalanus* spp. abundances were near normal in spring and early summer, but fell below normal during the fall (Figure 43).

Long-term trends in the phenology of *C. finmarchicus* at Rimouski station (1994–2024) show a clear shift toward earlier development (Figure 44). Two indices, one being the first day of year when the normalized CIV proportion exceeds 35%, and the second one being the day of year when peak CIV proportion is reached, have indicated negative anomalies consistently since 2012, especially during 2021–2023. In 2024, the phenology remained earlier than normal although not as extreme as during 2021–2023. A second pulse of early life stages, observed in late summer during 2010–2014, and again in 2021–2023, was present in 2024, albeit with reduced intensity compared to the preceding three years (Figure 44).

3.5.2 Gulf regions

Zooplankton biomass is typically concentrated in the deep channels of the Gulf, where the large copepod *C. hyperboreus* is more abundant. As a result, biomass tends to be lower in the coastal stations of each section, and on the Magdalen Shallows. This spatial pattern persisted in 2024, although biomass during early summer in the western Magdalen Shallows approached observations in the deep channels (Figure 45). During early summer, biomass levels were generally near or below normal across the Gulf. By fall, conditions varied, ranging from below normal in the central Gulf/Cabot Strait region to above normal in the Estuary/northwest Gulf region (Figure 45).

The highest abundances of *C. finmarchicus* were observed in the northwest Gulf, and on the western side of the Magdalen Shallows during early summer 2024 (Figure 46Figure 47). In the fall, *C. finmarchicus* abundances were relatively high and homogenous across the Estuary/northwest Gulf region, resulting in a seasonal record high for that region (Figure 46Figure 47). Seasonal abundances of *C. finmarchicus* were near to above normal for most regions, except for the lower-than-normal values in the central Gulf/Cabot Strait during early summer.

In early summer, *C. hyperboreus* was most abundant in the southernmost transects but remained below normal, except over the Magdalen Shallows (Figure 47). In the fall, the abundance distribution of *C. hyperboreus* was concentrated in the deep channels, mirroring the biomass distribution. A record-low abundance was observed in the Estuary/northwest Gulf region during fall, marking a new record low that followed the previous year's record low. Elsewhere, fall abundances ranged from below normal in the central Gulf/Cabot Strait region to above normal on the Magdalen Shallows (Figure 47).

Pseudocalanus spp. generally exhibited lower-than-normal abundances in 2024 (Figure 48). However, areas of high abundances were observed near the Magdalen Islands in early summer, and on the northern side of the northeast Gulf section during the fall (Figure 48).

The 2024 seasonal averages for zooplankton indices from the mackerel egg survey on the Magdalen Shallows and from the northern Gulf late-summer survey (ZooImage) generally align with the AZMP time series (Figure 49). *C. finmarchicus* was much more abundant than normal during early summer on the Magdalen Shallows (particularly the western side). In contrast, the abundances of *C. hyperboreus* and small calanoids were slightly below normal. In the northern Gulf during late summer, only *C. finmarchicus* showed above-normal abundances; the other indices were consistently below normal (*C. hyperboreus*) (Figure 49). Consistent with previous observations, September zooplankton biomass on the Magdalen Shallows was slightly below normal, with *C. hyperboreus* abundances being the second lowest in the time series, after last year (Figure 50). *Pseudocalanus* spp. abundances also remained below normal (Figure 50).

3.5.3 Scorecards

The time series of annual zooplankton biomass anomalies highlights recent major changes in the community, with mostly near-normal to negative anomalies across the Gulf since 2009

(Figure 51). A linear regression of annual zooplankton biomass averages reveals a significant decline in the Gulf over the time series (p <0.001), with an estimated reduction of approximately 25% when comparing the periods 2001–2008 and 2009–2024. The Magdalen Shallows is the only region showing consistently normal to above-normal biomass levels in recent years. In 2024, annual zooplankton biomass anomalies were mostly below normal to near normal (Figure 51).

The abundance of large *Calanus* spp is a dominant contributor to the zooplankton biomass. Annual *C. finmarchicus* abundances were above normal in most regions in 2024, similar to last year's anomaly patterns. Their abundance was at record high in the northeast Gulf and the second highest levels in the Estuary/northwest Gulf (Figure 52). *C. hyperboreus*, however, showed strong negative anomalies, including record-low abundances at the Rimouski station and in the Estuary/northwest Gulf (Figure 53). This represents the fourth consecutive year of strong and widespread negative anomalies for *C. hyperboreus*. An exception was the Magdalen Shallows, where *C. hyperboreus* anomalies were positive in 2024. In the northern Gulf, the high abundance of *C. finmarchicus* compensated for the low abundance of *C. hyperboreus,* leading to a positive anomaly for large calanoid abundance, while other regions exhibited near- to below-normal values (Figure 52).

The general decrease in zooplankton biomass over time has coincided with increases in the abundance of *Pseudocalanus* spp., total copepods, non-copepods, small calanoids, and cyclopoids, for which positive anomalies have been regularly observed since around 2014 (Figure 52, 53: see Appendix 1 for a detailed list of species included in each of these indices). However, in 2024, these groups mostly exhibited neutral to negative anomalies, consistent with previous year observations. *Pseudocalanus* spp. reached record-low abundance at Rimouski and in the central Gulf/Cabot Strait region, as did the small calanoid index in the latter region (Figure 52, 53).

The abundance of warm-water copepods, which has also increased since 2011, showed neutral anomalies in 2024, with a record-low abundance observed at Shediac Valley (Figure 53). Cold-water copepods, which have exhibited frequent positive anomalies in most regions since 2016, continued this trend in 2024 (Figure 53), with regional variation driven by either *Calanus glacialis*, *Metridia longa*, or both species (not shown). In general, annual anomalies were consistent among the high-frequency monitoring stations and their associated Gulf regions (Figures 52, 53). This suggests a high degree of confidence in our annual estimates throughout the Gulf, even though data collection for the zooplankton indices is limited to early summer and fall surveys.

Following a decade of predominantly positive anomalies for most non-copepod taxa, the signals began to weaken in 2021, particularly in both the northeast Gulf and the central Gulf/Cabot Strait regions (Figure 54). This trend continued into 2024, with non-copepod levels generally ranging from near normal to below normal in these two regions. In contrast, anomalies for most taxa remained neutral to positive in the Estuary/northwest Gulf and on the Magdalen Shallows (Figure 54).

4. DISCUSSION

4.1 ENVIRONMENTAL CONDITIONS

The timing of the onset of water column stratification and its strength play a role in defining spring bloom phenology, phytoplankton production, species succession, and trophic interactions throughout the growth season (Levasseur et al. 1984). At the Rimouski station, stratification typically begins increasing in April, but in 2024, its onset was delayed until May, possibly due to

the low St. Lawrence river runoff during spring (Galbraith et al. 2025a). The higher-than-normal freshwater runoff during late summer, combined with a strong marine heatwave in the Estuary during fall (Galbraith et al. 2025a), likely contributed to the strong stratification observed at Rimouski station in the fall. In addition to the effect of water column stratification on phytoplankton dynamics, thermal properties of the surface, cold intermediate layer (CIL; correspond to the winter surface mixed layer that has been isolated from the atmosphere through seasonal warming and freshening of the surface layer), and deep-water masses play a role in defining zooplankton dynamics (Plourde et al. 2002). Galbraith et al. (2025a) reported on the physical conditions that prevailed in the Gulf during 2024, showing warmer-than-normal conditions for most indices, and water column layers, which likely had both direct and indirect effects on the chemical and biological conditions observed.

In the Gulf, dissolved oxygen concentrations below 100 µmol L^{-1} at 300 m (below 30% saturation) are considered hypoxic, and can negatively affect species such as Atlantic cod (Plante et al. 1998). Long-term AZMP data and historical records (Gilbert et al. 2005) confirm that the deep waters of the Estuary have consistently been hypoxic since 1984. Changes in dissolved oxygen of the deep waters entering the Gulf at the continental shelf are related to the varying proportions of Labrador Current water (LCW; colder/fresher, high dissolved oxygen levels) and North Atlantic Central Water (NACW; warmer/saltier, low dissolved oxygen levels), which together form the source of Gulf deep waters (McLellan 1957, Lauzier and Trites 1958, Gilbert et al. 2005). In recent years, the contribution of NACW to the deep Gulf waters has increased (Gilbert et al. 2005, Galbraith et al. 2025a), and was estimated to contribute nearly 100% in 2021 (Jutras et al. 2023). These deep waters take approximately three to four years to travel from Cabot Strait to the Estuary (Gilbert 2004). During this transit, oxygen levels further decline due to *in situ* respiration and oxidation of organic material by microbes. Thus, the record-low saturation levels measured in 2024 at 200 m in the Estuary and the northwest Gulf, and at 250 m in the latter, likely reflect this upstream propagation of oxygen-depleted water masses. However, the contribution of NACW to the deep Gulf waters has likely decreased in recent years, as suggested by the concurrent increase in oxygen levels and decrease in temperature in the deep waters of the Cabot Strait and central Gulf. As these more oxygen-rich waters travel up the Laurentian Chanel, an improvement in oxygen conditions is expected in the northwest Gulf and the Estuary, although conditions in the latter are likely to remain hypoxic.

Given the inherent properties of the Gulf source waters (NACW vs. LCW; Gilbert et al. 2005), changes in their mixing ratio at Cabot Strait imply that a decrease of 1.46 µmol L^{-1} of oxygen might be expected for each 0.1 °C temperature increase. However, deep oxygen concentrations at Cabot Strait in 2024 represent a decline of ca. 40 µmol L^{-1} compared to their levels in the early 1970s (ca. 190 µmol L^{-1} at 300 m; Gilbert et al. 2005), for a nearly 1.25 °C increase in temperature over the same period (Figure 50 in Galbraith et al. 2025a). In the Estuary, deep-water temperature at 300 m has increased by 1.72 °C over the past 50 years (Fig. 50 in Galbraith et al. 2025a), while oxygen concentration has decreased from ca. 105 µmol L^{-1} (Gilbert et al. 2005) to 37.8 µmol L^{-1}. This oxygen decline is more than twice what would be expected from the temperature changes according to the mixing ratio of source waters. Thus, warming of bottom water and reduced initial oxygen saturation levels through changes in the mixing ratio of source waters are not the only drivers of declining oxygen concentrations in the Gulf. Additional contributing factors that can cause variability in oxygen concentration of deep waters include changes in the vertical flux of organic matter, enhanced microbial respiration under warmer conditions, and a reduction of deep inflow transport and bottom water ventilation via increased stratification (Jutras et al. 2023).

Winter mixing is a critical process for bringing nutrient-rich deep water to the surface. In the Gulf, winter convection is driven by buoyancy loss of surface waters attributable to cooling and

reduced freshwater runoff, brine rejection associated with sea-ice formation, and wind-driven mixing prior to ice formation (Galbraith 2006). Warmer-than-normal surface waters during winter of 2024 limited sea-ice formation, and reduced the volume of winter mixed layer, thereby decreasing the availability of nutrients for spring primary production. Since 2010, various temperature and ice-cover indices have indicated important warming of the Gulf (Galbraith et al. 2025a). These anomalies are tied to a large decrease in the nitrate content of the surface layer over the time series, including 2024. Moreover, the particularly short sea-ice season in 2024 (Galbraith et al. 2025a) may also have prolonged phytoplankton production, as supported by the above-normal surface chl *a* concentrations in January and February across most ocean colour polygons.

The freshwater inflow from the St. Lawrence River also contributes to the nutrient surface layer inventory in areas under its influence, typically accounting for up to 35% of nutrient input to the Estuary (Lavoie et al. 2021). The intensity of freshwater inflow, and the resulting stratification, also influence the strength of upwelling at the head of the Laurentian Channel. Consequently, the weak freshwater runoff in early July 2024 was accompanied by a negative sea surface temperature (SST) anomaly in the Estuary, typical of upwelling events, and a replenishment of nutrients in the surface layer at Rimouski station. Similarly, weak stratification in August in the northeast Gulf resulted in upwelling (SST negative anomaly, Galbraith et al. 2025b) in that region, and likely enhanced phytoplankton production through nutrient replenishment.

Since 2012, positive anomalies in deep-water nitrate has regularly been observed in the central Gulf/Cabot Strait region in association with greater contribution of NACW to the water masses composition (Gilbert et al. 2005, Galbraith et al. 2025a, Jutras et al. 2023). As with the increase in oxygen, the return to normal of the deep nitrate anomaly in the central Gulf/Cabot Strait region in 2024 suggests a reduced contribution of the NACW water mass. In addition to water mass signatures, enhanced stratification over the past decade may have reduced exchanges between the upper layer and the CIL, favouring nutrient accumulation in the deep layers.

Notably, 2024 marked the eighth consecutive year of pronounced nutrient ratio anomalies in most deep waters of the Gulf, characterized by negative N:P and positive Si:N anomalies. The nutrient ratio anomalies even reached record levels in 2024 in most regions. Deep-water masses entering the Gulf through Cabot Strait possess distinct nutrient ratio signatures. However, as the water masses travel through the Laurentian Channel, their nutrient signatures are altered by microbial processes involved in nitrogen cycling, particularly denitrification, which typically occurs in hypoxic to anoxic conditions (see review by Hutchins and Capone 2022). The changes in nutrient ratios observed between Cabot Strait and the Estuary, along with concurrent decreases in nitrate concentrations and oxygen levels, point to denitrification as a key driver of nitrate loss in deep waters. A recent study by Pascal et al. (2024) further supports this interpretation, highlighting an intensification of fixed-nitrogen removal processes in the Estuary over the past decade, linked to the expansion of the hypoxic zone.

4.2 PHYTOPLANKTON

Except at Rimouski station, where sampling regularly covers the spring bloom period, phytoplankton production during the spring bloom must be inferred either from indirect indices, such as the difference between the nutrient inventory of the surface mixed layer from winter to early summer (drawdown), or from satellite observations. In 2024, the lower-than-normal nutrient drawdown during spring in the 0–50 m surface layer across most regions contrasts with the higher-than-normal phytoplankton biomass observed by remote sensing in the thin surface layer in April. This discrepancy may be explained by vertical phytoplankton distribution and early spring bloom phenology, as seen at Cabot Strait, where nutrient uptake likely began before the winter helicopter survey. Additionally, near-normal silicate concentrations in March (not shown)

may have supported the above-normal chl *a* levels, given that diatoms, which are key drivers of the spring bloom in the Gulf, require silicate. Although it is generally assumed that the intensity of the spring bloom is largely controlled by nutrient availability at the onset of stratification, overwintering copepod abundance and their grazing pressure are also key drivers of spring bloom dynamics (Sommer and Lengfellner 2008). Considering the low zooplankton biomass across the Gulf during the 2021–2024 period, and the below-normal abundances of *C. hyperboreus,* a major consumer of spring bloom production (Plourde et al. 2003), reduced grazing during spring may have played a key role in promoting a strong spring bloom in 2024 despite the low nitrate inventory in March.

A pattern of earlier spring bloom timing since 2016 has emerged from the new ocean colour indices. Under global warming scenarios, an earlier onset of stratification is expected to trigger an earlier spring bloom. Moreover, the increase in light availability resulting from the important reduction in sea-ice concentration is another factor that can contribute to an earlier phytoplankton bloom in the Gulf (Mei et al. 2024). However, the anticipated increase in precipitation and freshwater runoff could delay blooms by hindering the accumulation of phytoplankton biomass in the water column in regions influenced by freshwater (Levasseur et al. 1984, Zakardjian et al. 2000). In 2024, a year of lower-than-normal spring freshet, the timing of the bloom was either earlier than normal (Rimouski) or normal (northwest Gulf and Magdalen Shallows) in the regions under freshwater influence. Another foreseen outcome of the increased stratification under warmer conditions is the larger contribution of smaller-sized cells, known to perform better in nutrient-poor and highly stratified waters, to the phytoplankton assemblage (Legendre and Rassoulzadegan 1995). The taxonomic composition over the Gulf provided in this report supports this hypothesis, with mostly positive anomalies of flagellates since 2016. Warmer conditions, combined with increased freshwater input, may also promote harmful algal blooms (HABs) of toxin-producing dinoflagellates (Boivin-Rioux et al. 2021, Boivin-Rioux et al. 2022). The proportion of dinoflagellates was unusually high in 2024 on the Magdalen Shallows and at Shediac Valley station.

For most seasons, ocean colour data retrieved from remote sensing are complemented by *in situ* observations. These two data sources have often yielded differing seasonal anomaly patterns in phytoplankton biomass. Such divergences can be explained by several factors, including the vertical structure of phytoplankton in the water column; methodological differences in calculating seasonal anomalies (e.g., full seasonal coverage within ocean-colour polygons versus fewer discrete sampling days per Gulf region for in situ data, with AZMP survey timings shown in Figure 32); the alignment of in situ sampling with key phenological phases of phytoplankton; differences in the volume of water sampled by each method; and limitations such as cloud cover for remote sensing. Despite these divergences, both data sources suggest an increase in fall phytoplankton biomass since around 2016, which may have implications for higher trophic levels. The increased frequency of fall storms in recent years (Galbraith et al. 2025a), and the associated nutrient injections into the surface layer likely create favourable growth conditions for phytoplankton, especially when combined with reduced grazing pressure. The weak to near-normal stratification across the Gulf in October 2024 likely favoured high phytoplankton biomass during that period.

4.3 ZOOPLANKTON

Zooplankton biomass has generally been below normal in recent years, with several record-low levels in 2016–2017, and again in 2021–2023. Although no record lows were observed in 2024, biomass was still below normal in most Gulf regions. Lower biomass is typically associated with a decrease in the abundance of large zooplankton species. The mean weight of large calanoids (*e.g.*, *C. hyperboreus*: 3.5 mg per adult female) is between one and two orders of magnitude greater than that of small calanoids (*e.g.*, *Pseudocalanus* spp.: 0.02 mg per adult female)

(Conover and Huntley 1991, Plourde et al. 2003). Thus, low abundance of large calanoids has a greater impact on total zooplankton biomass than the high abundances of *Pseudocalanus* spp., which have been regularly observed over the 2014–2022 period. In these years, the increase in small calanoids often coincided with an increase in non-copepod abundance. Environmental factors such as temperature, food availability, phytoplankton size structure, interspecific competition, and predation pressure likely influence the dominance of distinct community types—those dominated by large calanoids versus those characterized by small calanoids and non-copepods (Hall et al. 1976; Daewel et al. 2014)—with potential implications for pelagic food web dynamics and pelago–benthic coupling. In 2024, however, the community composition resembled that of the 2000–2009 decade, despite low zooplankton biomass; *C. finmarchicus* was abundant, while the small calanoids and non-copepod community were near or below average.

Life cycle strategies vary among large copepod species, and so do the environmental drivers influencing their phenology. For instance, interannual variations in the abundance of *C. hyperboreus* and its phenology is mostly influenced by spring conditions, including timing of sea-ice retreat and water temperature (Plourde et al. 2003, Lehoux et al. 2021). In contrast, late summer and early fall environmental conditions influence the phenology of *C. finmarchicus,* as part of its population is still active during that period. Moreover, the timing of reproduction of each taxon relative to the freshet—considering its influence on water-mass circulation and transport (Runge et al. 1999), can considerably influence zooplankton spatial distribution. As a result, species may exhibit distinct spatial patterns depending on how their life cycles align with hydrological dynamics (Brennan et al. 2021).

In 2024, the negative anomalies of zooplankton biomass aligned with *C. hyperboreus* abundances across all regions, except the Magdalen Shallows, were likely driven by environmental conditions. The early sea-ice retreat could explain the early phenology of *C. hyperboreus*, as suggested by the absence of CI—CIII copepodite stages in May at the Rimouski station and the high CIV/CI-CIV ratio observed in June at Shediac Valley. The peak of *C. hyperboreus* early copepodite stages presumably occurred in April (no data available for that month) at Rimouski station, coinciding with the peak freshwater runoff (Galbraith et al. 2025a), which likely promoted their downstream export to the Magdalen Shallows. There, the high proportion of diapausing CIV and CV *C. hyperboreus* in early summer most likely favoured their retention in the region (Brennan et al. 2019). Additionally, the proportion of diapausing CIV individuals at Rimouski station was lower than normal, suggesting that *C. hyperboreus* recruitment was low in the Estuary in 2024, although not as low as in 2023 (Blais et al., 2024).

The peak timing of *C. finmarchicus* early copepodite stages in May 2024 at Rimouski station was coupled with the spring bloom in this area, probably enhancing their survival rates (Plourde et al. 2008). Their retention within the Estuary was further maximized by calmer hydrodynamic conditions following the spring freshet. However, the marked asymmetry in *C. finmarchicus* abundances between the western and eastern sides of the Magdalen Shallows section suggests that some level of transport still occurred between both regions. Under favourable conditions, *C. finmarchicus* can produce a second cohort that typically develops in late summer, a phenomenon observed with increasing frequency and strength since 2010. In 2024, rather than a distinct second cohort, the production of early *C. finmarchicus* copepodite stages was sustained throughout the summer until October, likely benefiting from the high phytoplankton biomass at the Rimouski station.

The northeast Gulf and the central Gulf/Cabot Strait regions are less influenced by freshwater inputs; zooplankton communities in these regions are likely shaped by factors such as CIL conditions, the volume and temperature of cold and saline Labrador Shelf water that flows into northeast Gulf through the Strait of Belle Isle, and the mixing ratio of source waters that enters the deep Laurentian Chanel via Cabot Strait (Shaw and Galbraith 2023). Variability in these

environmental drivers might explain why these two regions often show distinct zooplankton anomaly patterns compared to other parts of the Gulf. In 2024, the central Gulf/Cabot Strait region was the only area with negative anomalies for *C. finmarchicus* and large copepods. Such limited top-down control on phytoplankton growth may explain the strong spring bloom observed in the central Gulf in April, and could suggest increased export of organic matter to bottom waters.

4.4 PERSPECTIVES

The record-low oxygen saturation values in the St. Lawrence Estuary and the northwestern Gulf at depths of 200 and 250 m, along with the unprecedentedly low *C. hyperboreus* levels in these regions in 2024, highlight the urgent need for continued research on the ecological impacts of deoxygenation and shifting planktonic communities in the St. Lawrence system. The drivers behind the observed changes in nutrient inventories, phytoplankton biomass, and zooplankton community composition and size structure, how they interact and may evolve, are still not fully understood. While the roles of predation and changes in community structure remain to be clarified, some insight into the environmental influences on biological components can be gained from a simple correlation matrix (Figure 55). Among other things, this matrix shows that a cold CIL—typically associated with a stronger winter convection and delayed stratification—correlates with a later bloom start and high surface nitrate inventories. Zooplankton biomass is strongly positively correlated to a community dominated by large copepods, and inversely correlated with small calanoids and non-copepods as would be expected. Thermal properties of the water column and spring bloom dynamics—especially its timing—could be major drivers of zooplankton assemblage. Indeed, it seems that a cold water column favours high zooplankton biomass (negative correlation at all depths) while a cold deep layer reduces the abundance of non-copepods (positive correlation). Changes in phytoplankton community composition and species succession may also be important drivers for the zooplankton assemblage, though these variables were excluded from the correlation matrix due to limited time series outside of the high-frequency monitoring stations. It is possible that the highly stratified and nutrient-poor conditions have promoted the proliferation of flagellates in the Gulf, especially during years when reduced grazing pressure is expected (Cloern 2017, Cushing 1989, Ward et al. 2012). These environmental drivers may also trigger changes in the developmental timing of zooplankton taxa (not illustrated in Figure 55), such as the earlier development of large *Calanus*. Overall, these preliminary analyses highlight the importance of bottom-up controls in shaping zooplankton communities, although the relative importance of these processes, and potential interactions, is not yet well understood.

5. SUMMARY

This document summarizes the chemical and biological (plankton) conditions observed in the Gulf of St. Lawrence in 2024, within the broader context of warmer-than-normal conditions prevailing since 2010.

- At 250 m depth and below, dissolved oxygen concentrations remained low but relatively stable at Rimouski station and in the Estuary, slightly above the record lows of 2022. However, new record lows were observed at 200 m at both locations, as well as in the northwest Gulf where oxygen levels also reached a record low at 250 m. Average annual saturation levels were 12% (37 $\mu mol\, L^{-1}$) at 300 m and 24% (77 $\mu mol\, L^{-1}$) in the bottom waters of the Estuary in 2024.

- In general, nutrient inventories were below normal in the surface layer of the Gulf, near to above normal in the mid-layer, and mostly above normal in the deep layer, except for nitrate, which were below normal in most regions, and reached a record low at the Rimouski station.
- Since 2017, and strengthening through 2024, the positive anomalies in deep nutrient content have been associated with negative anomalies in the N:P ratio and positive anomalies in the Si:N ratio.
- Annual averages of *in situ* chl *a* inventory ranged from below normal on the Magdalen Shallows to above normal in the Estuary/northwest Gulf, where oceanographic surveys recorded higher-than-normal biomass.
- Flagellate abundances were generally higher than normal in 2024, a recurring pattern since 2016, while dinoflagellate abundances ranged from near to above normal. Diatom abundances were above normal only at Rimouski station.
- Ocean colour data revealed spatial heterogeneity in anomaly patterns. Anomalies were either neutral or positive in most polygons during winter, spring and summer. However, in fall, the two southernmost polygons exhibited lower-than-normal surface phytoplankton biomass, a first since 2009.
- The timing of spring blooms was early or normal, while fall blooms occurred later than normal in all polygons.
- Zooplankton biomass was generally below normal, continuing a pattern observed since 2009. Concomitantly, very low abundances of *C. hyperboreus* were observed almost everywhere in the Gulf, particularly at Rimouski station and in the Estuary/northwest Gulf, where record-low abundances were recorded for a third consecutive year.
- The abundances of *C. finmarchicus* were higher than normal in most regions, and reached a record high in the northeast Gulf.
- The phenology of large *Calanus* at Rimouski station was earlier than usual, although not as early as during the past three years.
- The shift in zooplankton community size structure toward a higher proportion of small copepods and non-copepods, observed over the past decade, was not evident in 2024. For a second consecutive year, the community composition resembled pre-2010 conditions, with several negative anomalies in small copepods, non-copepods and *Pseudocalanus* spp., and positive anomalies in *C. finmarchicus* across most regions.

ACKNOWLEDGEMENTS

The data used in this report would not be available without the amazing work of the AZMP team (Félix St-Pierre, David Leblanc, Caroline Lafleur, Anthony Ouellet, Nicolas Coulombe, Sylvain Dubé, Guillaume Mercier, Myranda Blouin, Michel Rousseau, Véronique Desborbes, Marie-Noëlle Bourassa and Hélèna Talbot) in organizing and carrying out AZMP surveys, analyzing samples, and ensuring quality control of the data. We thank Jean-Yves Couture, Marie-France Beaulieu, Caroline Lebel and Christian Turcotte for preparation and standardization of the phytoplankton and zooplankton data; Lindsay Beazley for providing data from Shediac Valley station; and Julien Laliberté for his assistance in processing the oceanographic buoy fluorescence data. We are grateful to Gary Maillet and Benoit Casault for their critical reviews.

REFERENCES

Bélanger, D., Maillet, G., Cyr, F., Doyle, G., Rastin, S., Ramsay, D., Dalton, B., and Pepin, P. 2024. Biogeochemical Oceanographic Conditions on the Newfoundland and Labrador Shelf during 2019 and 2020. DFO Can. Sci. Advis. Sec. Res. Doc. 2024/074. vi + 55 p.

Blais, M., Galbraith, P.S., Lizotte, M., Clay, S.A., and Starr, M. 2024. Chemical and Biological Oceanographic Conditions in the Estuary and Gulf of St. Lawrence during 2023. Can. Tech. Rep. Hydrogr. Ocean Sci. 385 : v + 84 p.

Blais, M., Galbraith, P.S., Plourde, S., Lehoux, C. and Devine, L. 2023. Chemical and Biological Oceanographic Conditions in the Estuary and Gulf of St. Lawrence during 2021. DFO Can. Sci. Advis. Sec. Res. Doc. 2023/045. iv + 74 p.

Boivin-Rioux, A., Starr, M., Chassé, J., Scarratt, M., Perrie, W., and Long, Z. 2021. Predicting the effects of climate change on the occurrence of the toxic dinoflagellate *Alexandrium catenella* along Canada's east coast. Front. Mar. Sci. 7:608021. doi:10.3389/fmars.2020.608021

Boivin-Rioux, A., Starr, M., Chassé, J., Scarratt, M., Perrie, W., Long, Z., and Lavoie, D. 2022. Harmful algae and climate change on the Canadian East Coast: Exploring occurrence predictions of *Dinophysis acuminata*, *D. norvegica*, and *Pseudo-nitzschia seriata*. Harmful Algae 112: 102183. doi: 10.1016/j.hal.2022.102183

Brennan, C.E., Maps, F., Gentleman, W.C., Plourde, S., Lavoie, D., Chassé, J., Lehoux, C., Krumhansl, K.A., and Johnson, C.L. 2019. How transport shapes copepod distributions in relation to whale feeding habitat : Demonstration of a new modelling framework. Prog. Oceanogr. 171: 1–21. doi:10.1016/j.pocean.2018.12.005.

Brennan, C.E., Maps, F., Gentleman, W.C., Lavoie, D., Chassé, J., Plourde, S., and Johnson, C.L. 2021. Ocean circulation changes drive shifts in Calanus abundance in North Atlantic right whale foraging habitat: A model comparison of cool and warm year scenarios. Prog. Oceanogr. 197:102629. https://doi.org/10.1016/j.pocean.2021.102629

Brickman, D., and Petrie, B. 2003. Nitrate, silicate and phosphate atlas for the Gulf of St. Lawrence. Can. Tech. Rep. Hydrogr. Ocean Sci. 231: xi + 152 pp.

Brzezinski, M. A. 1985. The Si:C:N ratio of marine diatoms: interspecific variability and the effect of some environmental variables. J. Phycol. 21: 347–357.

Casault, B., Johnson, C.L., Devred, E., and Beazley, L. 2025. Chemical and Biological Oceanographic Conditions on the Scotian Shelf and in the Eastern Gulf of Maine during 2023. Can. Tech. Rep. Fish. Aquat. Sci. 3658: vi + 57 p. https://doi.org/10.60825/4d69-8120

Clay, S. 2025. oceancolouR: Various Functions for Satellite and Data Analysis. R package version 0.0.0.9000, https://github.com/BIO-RSG/oceancolouR.

Clay, S., Layton, C., and Devred, E. 2021. BIO-RSG/PhytoFit: First release (Version v1.0.0). Zenodo. https://doi.org/10.5281/zenodo.4770754

Clay, S., Peña, A., DeTracey, B., and Devred, E. 2019. Evaluation of Satellite-Based Algorithms to Retrieve Chlorophyll-a Concentration in the Canadian Atlantic and Pacific Oceans. Remote Sensing, 11(22), 2609. https://doi.org/10.3390/rs11222609

Cloern, J.E. 2017. Why large cells dominate estuarine phytoplankton. Limnol. Oceanogr. doi: 10.1002/lno.10749

Conover, R. J., and Huntley, M. 1991. Copepods in ice-covered seas - Distribution, adaptations to seasonally limited food, metabolism, growth patterns and life cycle strategies in polar seas. J. Mar. Syst. 2: 1–41.

Cushing, D.H. 1989. A difference in structure between ecosystems in strongly stratified waters and in those that are only weakly stratified. J. Plankton Res. 11(1): 1–13.

Daewel, U., Hjøllo, S.S., Huret, M., Ji, R., Maar, M., Niiranen, S., Travers-Trolet, M., Peck, M.A., and van de Wolfshaar, K. E. 2014. Predation control of zooplankton dynamics: a review of observations and models. ICES J. Mar. Sci. 71(2): 254–271.

Galbraith, P.S. 2006. Winter water masses in the Gulf of St. Lawrence. J. Geophys. Res. 111, C06022, doi: 10.1029/2005JC003159.

Galbraith, P.S., Chassé, J., Shaw, J.-L., Lefaivre, D. and Bourassa, M.-N. 2025a. Physical Oceanographic Conditions in the Gulf of St. Lawrence during 2024. Can. Tech. Rep. Hydrogr. Ocean Sci. 397: v + 95 p. https://doi.org/10.60825/eznq-0815

Galbraith, P.S., Lizotte, M., Blais, M., Bélanger, D., Casault, B., Coyne, J., Layton, C., Azetsu-Scott, K., Beazley, L., Chassé, J., Clay, S., Cyr, F., Devred, E., Fudge, A., Gabriel, C.-E., Greenan, B., Hébert, A.-J., Johnson, C.L., Maillet, G., Penney, J., Rastin, S., Ringuette, M., Shaw, J.-L., Snook, S., Starr, M. 2025b. Oceanographic conditions in the Atlantic zone in 2024. Can. Tech. Rep. Hydrogr. Ocean. Sci. 400 : viii + 49 p. https://doi.org/10.60825/e92v-d229

Gilbert, D. 2004. Propagation of temperature signals from the northwest Atlantic continental shelf edge into the Laurentian Channel. ICES CM, 2004/N: 7, 12 pp.

Gilbert, D., Sundby, B., Gobeil, C., Mucci, A., and Tremblay, G.-H. 2005. A seventy-two-year record of diminishing deep-water oxygen in the St. Lawrence estuary: The Northwest Atlantic connection. Limnol. Oceanogr., 50(5): 1654–1666.

Grosjean, P., Denis K., and Wacquet G. 2018. ZooImage: Analysis of numerical plankton images. R package version 5.5.2. https://CRAN.R-project.org/package=zooimage

Hall, D.J., Threlkeld, S.T., Burns, C.W., and Crowley, P.H. 1976. The size-efficiency hypothesis and the size structure of zooplankton communities. Annu. Rev. Ecol. Evol. Syst. 7: 177–208.

Hutchins, D.A., and Capone, D.G. 2022. The marine nitrogen cycle: new developments and global change. Nat Rev Microbiol. 20: 401–414. https://doi.org/10.1038/s41579-022-00687-z

Jutras, M., Mucci, A., Chaillou, G., Nesbitt, W.A., and Wallace D.W.R. 2023. Temporal and spatial evolution of bottom-water hypoxia in the St. Lawrence estuarine system. Biogeosciences. 20: 839–849.

Lavoie, D., Lambert, N., Starr, M., Chassé, J., Riche, O., Le Clainche, Y., Azetsu-Scott, K., Béjaoui, B., Christian, J.R., and Gilbert, D. 2021 The Gulf of St. Lawrence biogeochemical model: A modelling tool for Fisheries and Ocean management. Front. Mar. Sci. 8:732269, doi: 10.3389/fmars.2021.732269.

Lauzier, L.M., and Trites, R.W. 1958. The deep waters of the Laurentian Channel. J. Fish. Res. Board Can. 15: 1247–1257.

Layton, C., Devred, E., DeTracey B. 2022. A comparison of phytoplankton spring bloom fitting methods using MODIS satellite-derived chlorophyll-a concentration for the Maritimes region. Can. Tech. Rep. Hydrogr. Ocean Sci. 340: vii +22 p.

Legendre L., and Rassoulzadegan, F. 1995. Plankton and nutrient dynamics in marine waters. Ophelia. 41(1): 153–172. doi: 10.1080/00785236.1995.10422042.

Lehoux, C., Plourde, S., Chamberland, J.-M., and Benoît, H. 2021. Linking interannual variations of capelin abundance indices in the Gulf of St. Lawrence to environmental proxies of bottom-up regulation of cohort strength. DFO Can. Sci. Advis. Sec. Res. Doc. 2021/068. iv + 51 p.

Levasseur, M., Therriault, J.-C., and Legendre, L. 1984. Hierarchical control of phytoplankton succession by physical factors. Mar. Ecol. Prog. Ser. 19: 211–222.

McLellan, H.J. 1957. On the distinctness and origin of the slope water off the Scotian Shelf and its easterly flow south of the Grand Banks. J. Fish. Res. Board Can. 14: 213–239.

Mei, Z.-P., Lavoie, D., Lambert, N., Starr, M., Chassé, J., Perrie, W. and Long, Z. (2024). Modelling the bottom-up effects of climate change on primary production in the Gulf of St. Lawrence and eastern Scotian Shelf. Front. Mar. Sci. 11:1416744. https://doi.org/10.3389/fmars.2024.1416744

Mitchell, M. R., Harrison, G., Pauley, K., Gagné, A., Maillet, G., and Strain, P. 2002. Atlantic Zonal Monitoring Program sampling protocol. Can. Tech. Rep. Hydrogr. Ocean Sci. 223: iv + 23 pp.

Nichols, J.H. and Thompson, A.B. 1991. Mesh selection of copepodite and nauplius stages of four calanoid copepod species. Journal of Plankton Research, 13(3): 661–671. https://doi.org/10.1093/plankt/13.3.661

Pascal, L., Cloutier-Artiwat, F., Zanon, A., Wallace D.W.R., and Chaillou, G. 2024. Fixed-nitrogen loss in a deoxygenating coastal ocean: Insights from the Estuary and Gulf of St. Lawrence. ESS Open Archive. doi: 10.22541/essoar.171560871.19656696/v1

Parent, G.J., Plourde, S. and Turgeon, J. 2011. Overlapping size ranges of *Calanus* spp. off the Canadian Arctic and Atlantic coasts: impact on species' abundances. J. Plankton Res. 33:1654–1665

Plante, S., Chabot, D., and Dutil, J.-D. 1998. Hypoxia tolerance in Atlantic cod. J. Fish Biol. 53: 1342–1356.

Plourde, S., Dodson, J. J., Runge, J. A., and Therriault, J.-C. 2002. Spatial and temporal variations in copepod community structure in the lower St. Lawrence Estuary, Canada. Mar. Ecol. Prog. Ser. 230: 221–224.

Plourde, S., Joly, P., Runge, J.A., Dodson, J., and Zakardjian B. 2003. Life cycle of *Calanus hyperboreus* in the lower St. Lawrence Estuary and its relationship to local environmental conditions. Mar. Ecol. Prog. Ser. 255: 219–233.

Plourde, S., Maps, F., and Joly, P. 2009. Mortality and survival in early stages control recruitment in *Calanus finmarchicus*. J. Plankton Res. 31(4): 371–388.

Plourde, S., Lehoux, C., Johnson, C. L., Perrin, G., and Lesage, V. 2019. North Atlantic right whale (*Eubalaena glacialis*) and its food: (I) a spatial climatology of *Calanus* biomass and potential foraging habitats in Canadian waters. J. Plankton Res. 41(5): 667–685.

Redfield A. C. 1958. The biological control of chemical factors in the environment. Am. Sci. 46, 205–221.

Runge, J. A., Castonguay, M., de Lafontaine, Y., Ringuette, M., and Beaulieu, J. L. 1999. Covariation of climate, zooplankton biomass and mackerel recruitment in the southern Gulf of St. Lawrence. Fish. Oceanogr. 8(2): 139–149.

Sathyendranath, S., Brewin, R. J. W., Brockmann, C., Brotas, V., Calton, B., Chuprin, A., Cipollini, P., Couto, A. B., Dingle, J., Doerffer, R., Donlon, C., Dowell, M., Farman, A., Grant, M., Groom, S., Horseman, A., Jackson, T., Krasemann, H., Lavender, S., Martinez-Vicente, V., … Platt, T. (2019). An Ocean-Colour Time Series for Use in Climate Studies: The Experience of the Ocean-Colour Climate Change Initiative (OC-CCI). Sensors (Basel, Switzerland), 19(19), 4285. https://doi.org/10.3390/s19194285

Shaw, J.-L. and Galbraith, P.S.. 2023. Climatology of Transport in the Strait of Belle Isle. J. Geophys. Res. Oceans, 128, e2022JC019084. https://doi.org/10.1029/2022JC019084

Sommer, U., and Lengfellner, K. 2008. Climate change and the timing, magnitude, and composition of the phytoplankton spring bloom. Global Change Biol. 14: 1199–1208.

Therriault, J.-C., Petrie, B., Pépin, P., Gagnon, J., Gregory, D., Helbig, J., Herman, A., Lefaivre, D., Mitchell, M., Pelchat, B., Runge, J., and Sameoto, D. 1998. Proposal for a Northwest Atlantic zonal monitoring program. Can. Tech. Rep. Hydrogr. Ocean Sci. 194: vii + 57 pp.

Ward, B. A., Dutkiewicz, S., Jahn, O., and Follows, M.J. 2012. A size-structured food-web model for the global ocean. Limnol. Oceanogr. 57: 1877–1891. doi:10.4319/lo.2012.57.6.1877.

Zakardjian, B.A., Gratton, Y., Vézina, A.F. 2000. Late spring phytoplankton bloom in the Lower St. Lawrence Estuary: the flushing hypothesis revisited. Mar. Ecol. Prog. Ser. 192: 31–48.

Zhai, L., Platt, T., Tang, C., Sathyendranath, S., and Hernández Walls, R. 2011. Phytoplankton phenology on the Scotian Shelf. ICES J. Mar. Sci. 68: 781–791, doi:10.1093/icesjms/fsq175.

TABLES

Table 1. List of oceanographic surveys with dates and sampling activities for each Gulf region/subregion. While numbers of CTD/bottle are indicated for each subregion, numbers of nets are only indicated for main regions (see region vs. subregion in Figure 1).

High Frequency Monitoring Stations

Dates (2024)	Vessel	Station	CTD/Bottle	Net
Mar. 4–Nov. 26	*Beluga II* (+ others)	Rimouski	24	22
Mar. 14–Oct. 25	Multiple	Shediac Valley	6	5

Surveys

Survey	Dates (2024)	Vessel	Region/subregion	CTD/Bottle	Net
Winter	Mar. 4–15	GC-945 Helicopter	Estuary	5	0
			Northwest Gulf	9	
			Northeast Gulf	21	0
			Central Gulf	9	0
			Cabot Strait	7	
			Magdalen Shallows	30	0
			Total	**81**	**0**
Early summer	Jun. 6–29	Coriolis II	Estuary	16	18
			Northwest Gulf	14	
			Northeast Gulf	13	6
			Central Gulf	16	11
			Cabot Strait	5	
			Magdalen Shallows	42	61
			Total	**106**	**96**
Late summer	Aug. 3–20 Sep.	Teleost	Estuary	10	15
			Northwest Gulf	5	
			Northeast Gulf	11	18
			Central Gulf	19	8
			Cabot Strait	5	
			Magdalen Shallows	108	12
			Total	**158**	**50**
Fall	Oct. 16– 3 Nov.	Coriolis II	Estuary	16	17
			Northwest Gulf	14	
			Northeast Gulf	14	7
			Central Gulf	11	8
			Cabot Strait	5	
			Magdalen Shallows	19	12
			Total	**79**	**44**

FIGURES

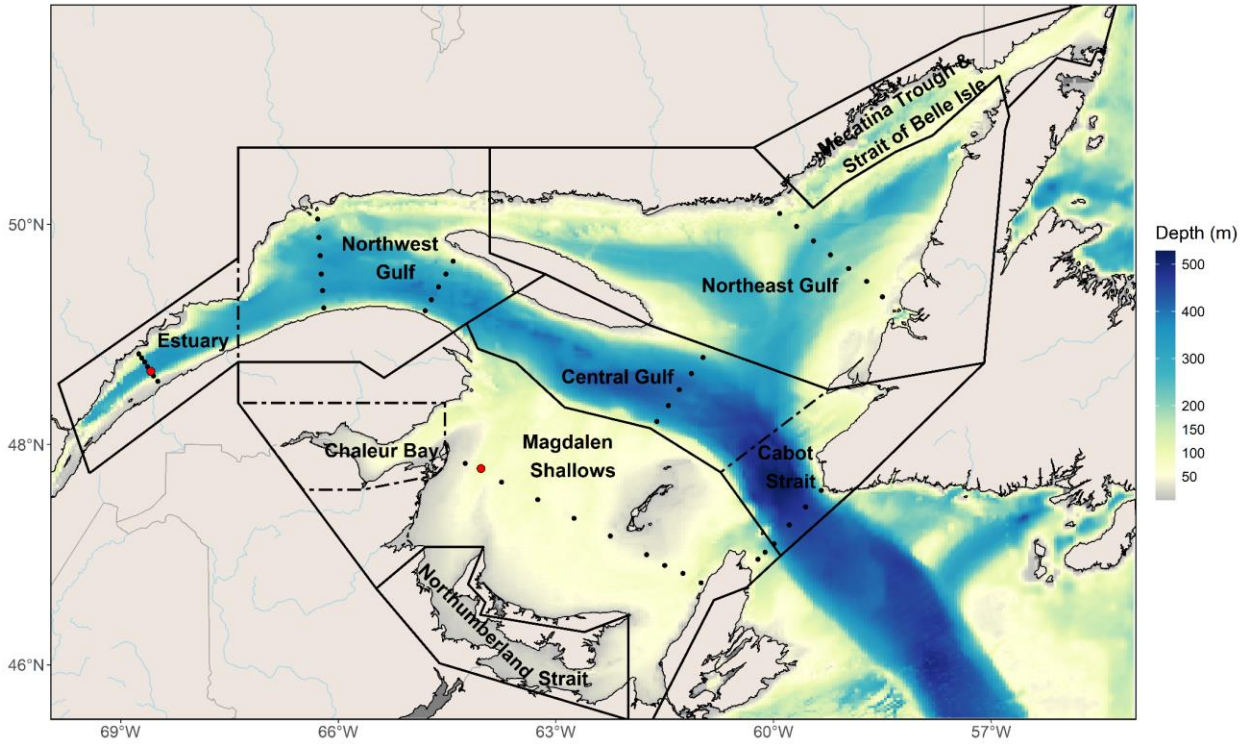

Figure 1. Bathymetric map of the Estuary and Gulf of St. Lawrence showing core AZMP sampling stations on the different sections (black circles), and high-frequency Rimouski and Shediac Valley stations (red circles). Dashed lines indicate region subdivisions.

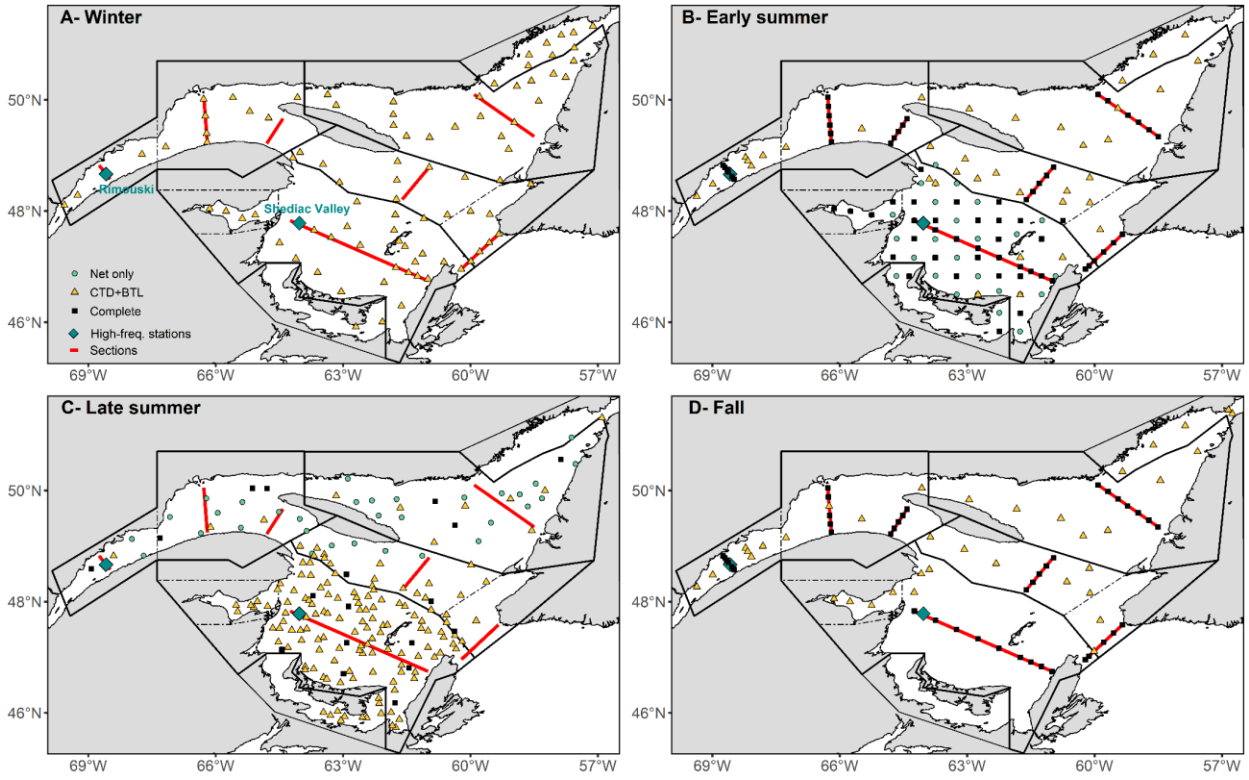

Figure 2. Locations of stations sampled during winter (A), early summer (B), late summer (C), and fall (D) 2024 (see Figure 1 caption for region and subregion descriptions). A complete station indicates that a CTD profile, water collection, and zooplankton net tows were performed.

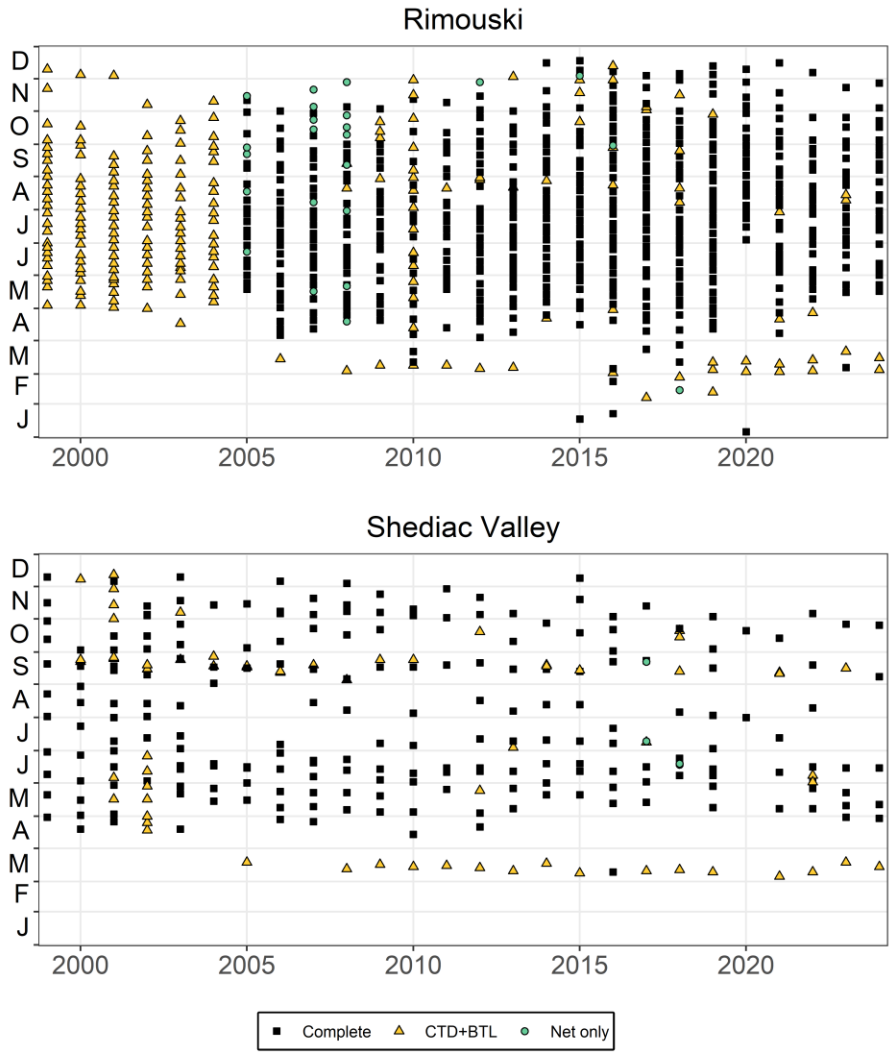

Figure 3. Sampling frequency at Rimouski and Shediac Valley stations from 1999 to 2024. Sampling included CTD/bottle as well as plankton net tows most of the time (weather permitting).

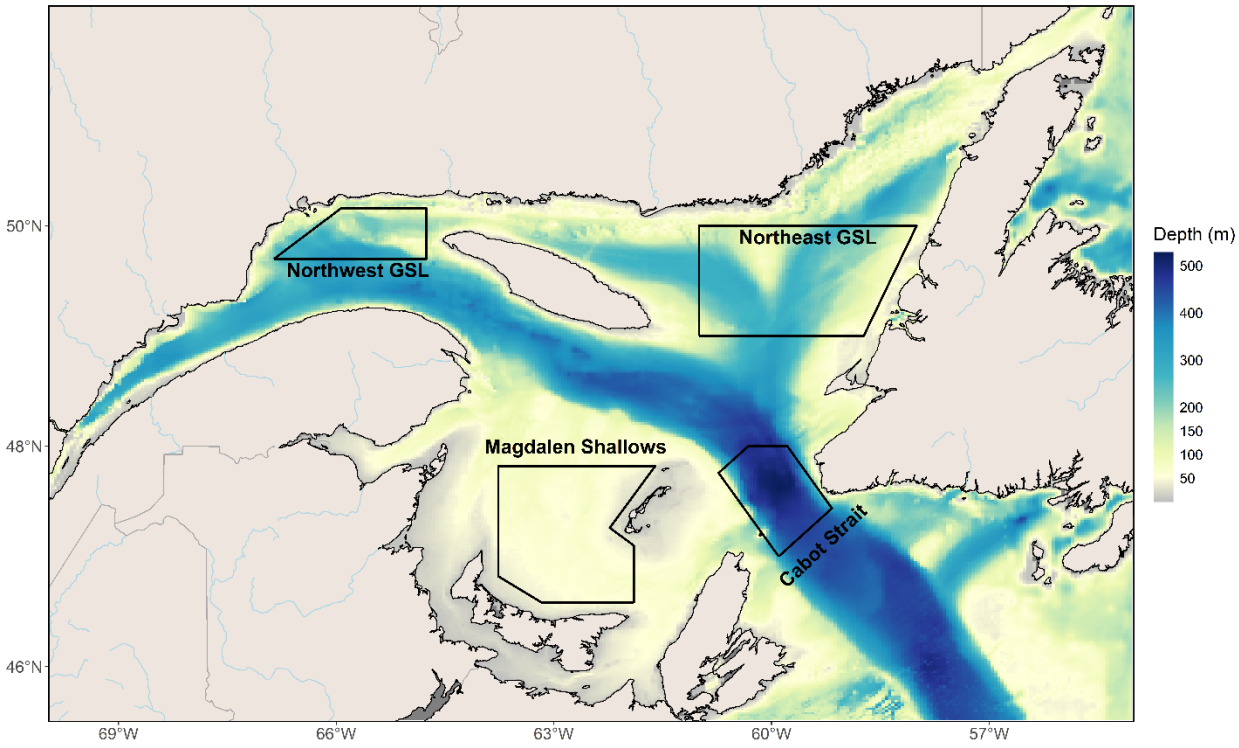

Figure 4. Ocean colour polygons used for the spatial/temporal analysis of satellite ocean colour data.

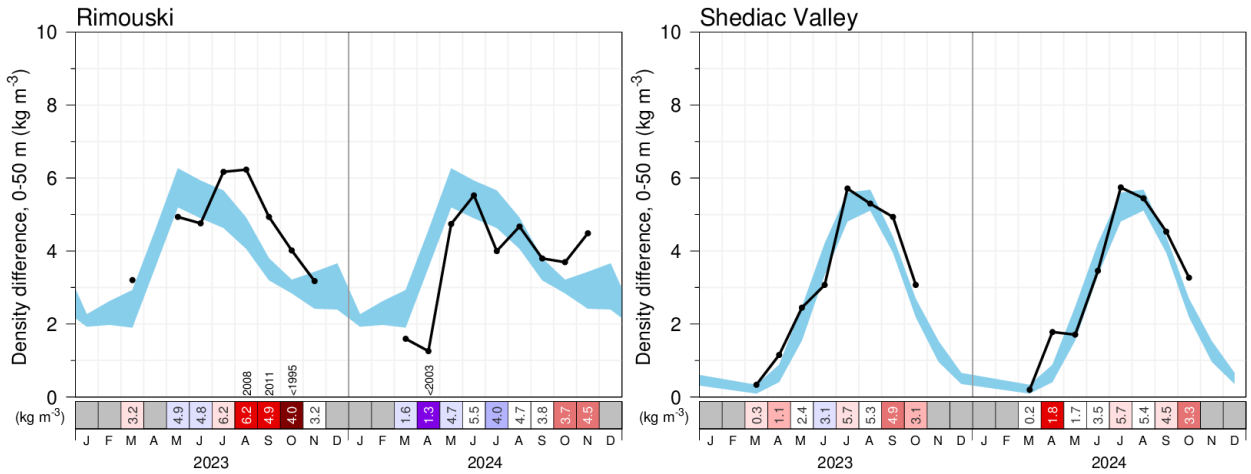

Figure 5. Seasonal stratification index during 2023 and 2024 at Rimouski and Shediac Valley stations. The blue area represents the climatological monthly mean ± 0.5 SD (1991–2020). Numbers in the scorecard are monthly density differences in kg m^{-3}. Blue colours indicate weaker-than-normal stratification (negative anomaly), reds are stronger-than-normal levels (positive anomaly), and white represents normal levels. For anomalies greater than 2 SD from normal, the prior year with a greater anomaly is indicated, with the less-than symbol (<) indicating a series record since that first year of observations. Grey boxes indicate no monthly data is available. This figure is adapted from Figure 68 of Galbraith et al. 2025b.

	2023				2024			
	Mar	June	Aug	Oct	Mar	June	Aug	Oct
Estuary	3.27	4.3	5.5	3.9	2.43	5.1	3.8	3.4
Northwest Gulf	0.92	2.5	3.4	2.7	0.98	3.3	4.2	2.0
Northeast Gulf	0.10	0.8	3.5	1.6	0.04	1.6	2.9	1.5
Mécatina	0.48	0.5		0.7	0.14	1.0	2.3	0.4
Centre	0.22	1.4	3.9	2.3	0.35	2.0	4.1	1.7
Cabot Strait	0.08	1.2	4.1	3.0	0.39	1.7	3.7	1.3
Magdalen Shallows	0.29	2.7	4.9	4.0	0.56	3.6	4.5	2.0

Figure 6. Monthly averaged stratification for the Gulf-wide oceanographic surveys in 2023 and 2024. Blue colours indicate weaker-than-normal stratification levels (negative anomalies), reds are stronger-than-normal levels (positive anomalies), and white represents normal levels (± 0.5 SD 1991–2020 climatology). This figure is adapted from Figure 58 of Galbraith et al. 2025b.

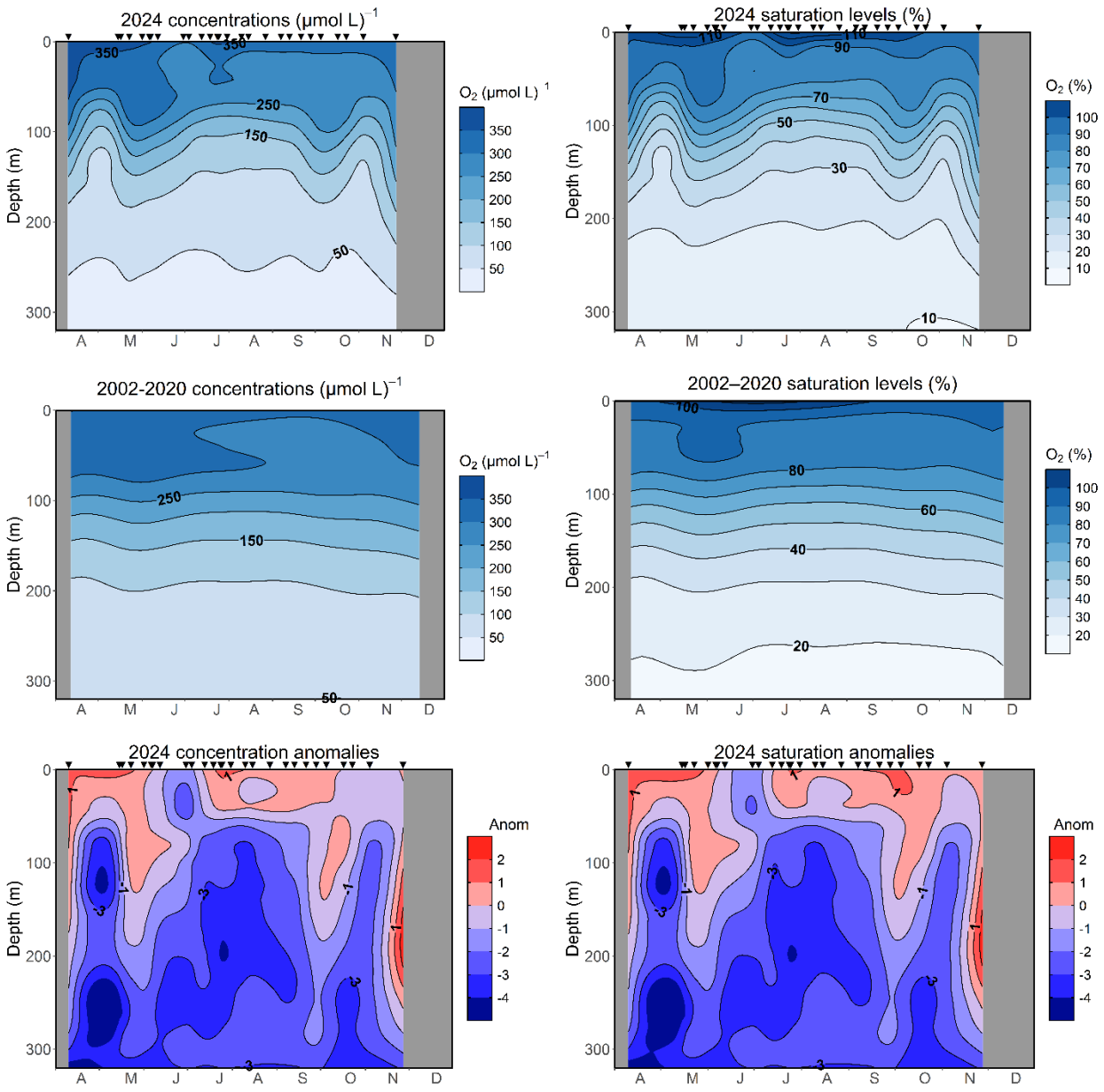

Figure 7. Vertical profiles of oxygen concentration (left panels) and saturation (right panels) at Rimouski station in 2024 (upper panels), climatology 2002–2020 (middle panels), and normalized anomalies for 2024 (bottom panels). For anomalies, blue colours indicate below-normal levels (negative anomalies), reds are above-normal levels (positive anomalies), and white represents normal levels. Black triangles indicate the timing of the station occupation.

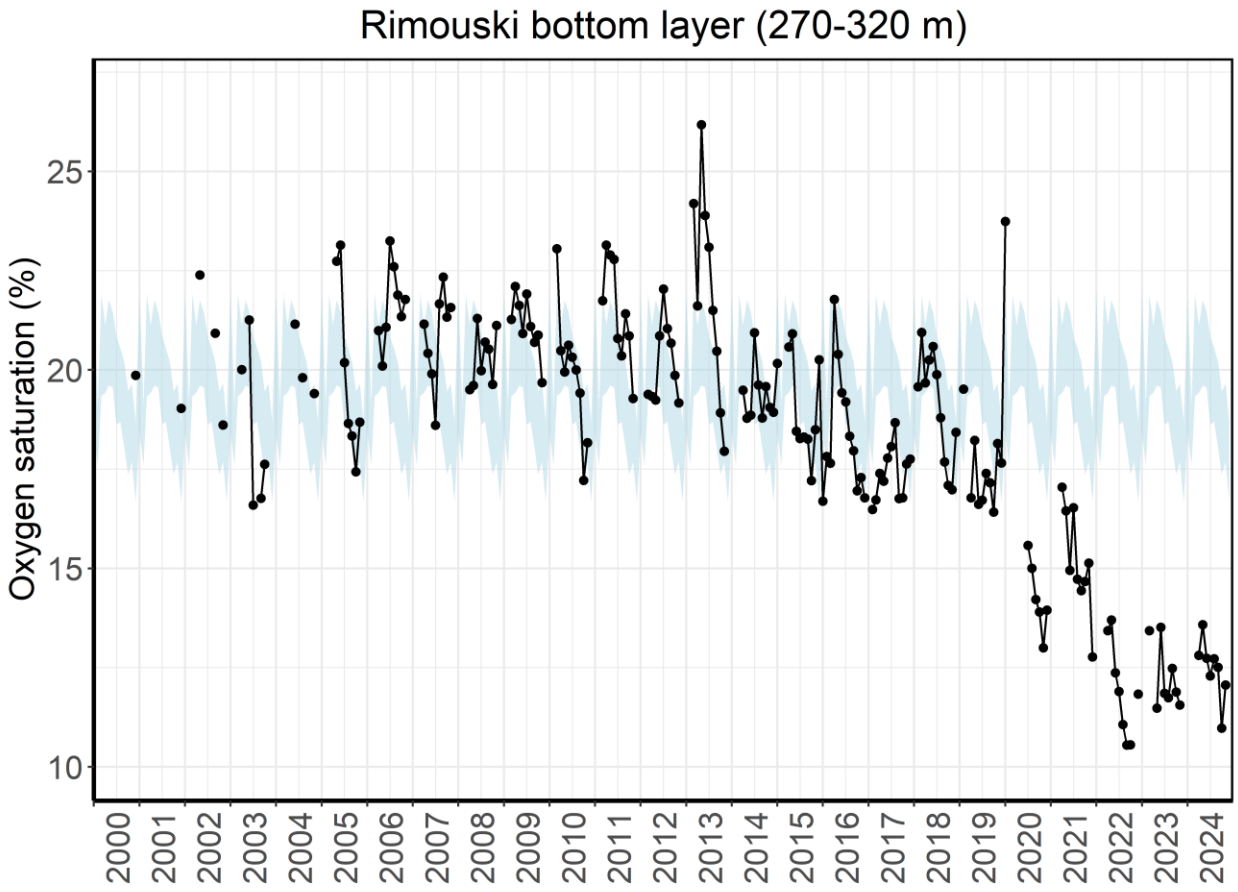

Figure 8. Time series of the monthly average oxygen saturation in the deep waters (> 270 m) of Rimouski station. The blue shading shows the monthly climatology for the 2002–2020 period.

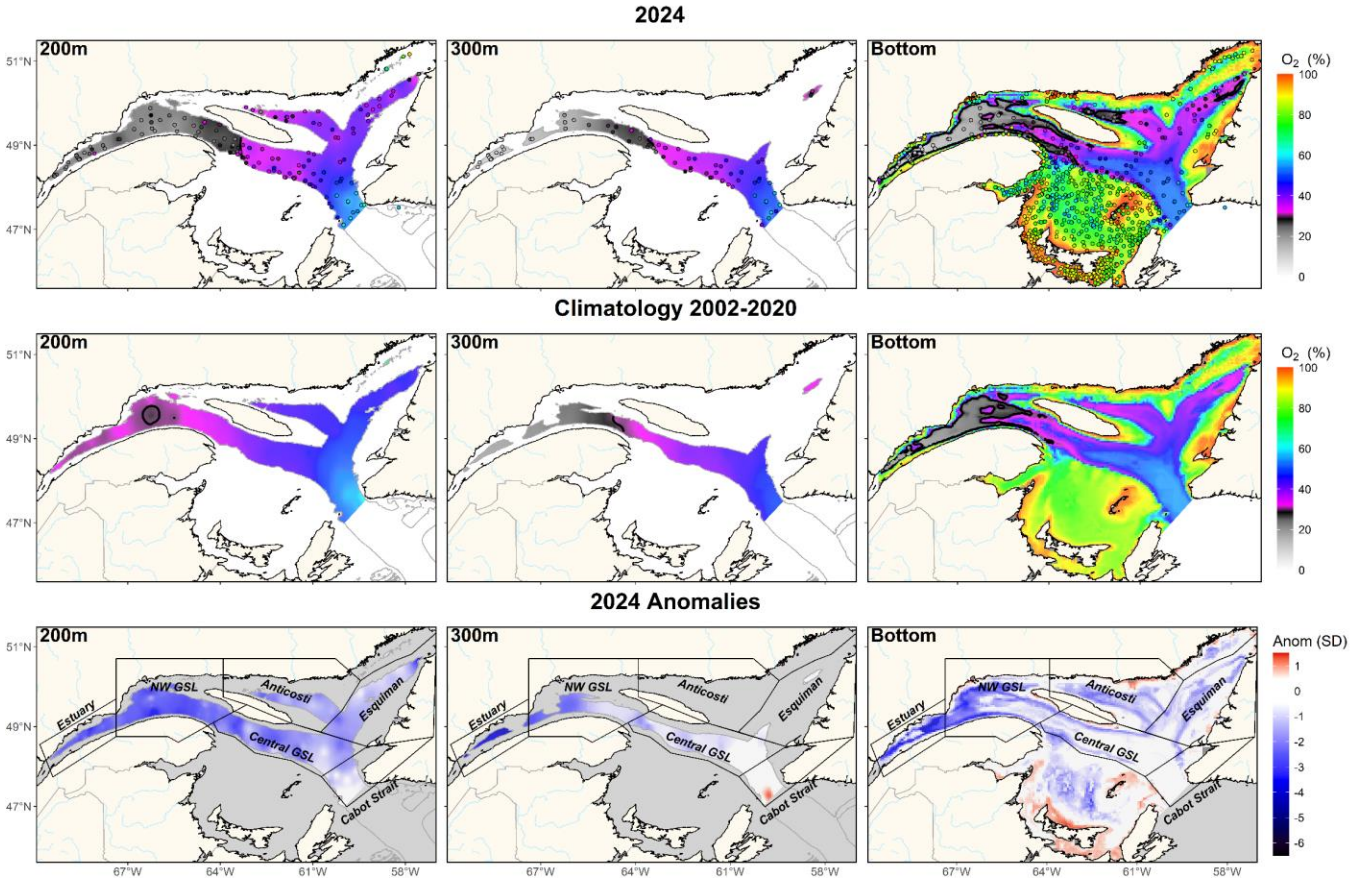

Figure 9. Annual averaged distribution of dissolved oxygen saturation at depths of 200 m, 300 m, and at the bottom in the Estuary and Gulf of St. Lawrence during 2024 (upper panel). The climatology (2002–2020; middle panel), and anomalies (lower panel) are also shown. The black contour lines identify areas associated with hypoxic waters (<30%). In the bottom panels, blue colours indicate below-normal levels (negative anomalies), reds are above-normal levels (positive anomalies), and white represents normal levels. Open circles show station locations in 2024.

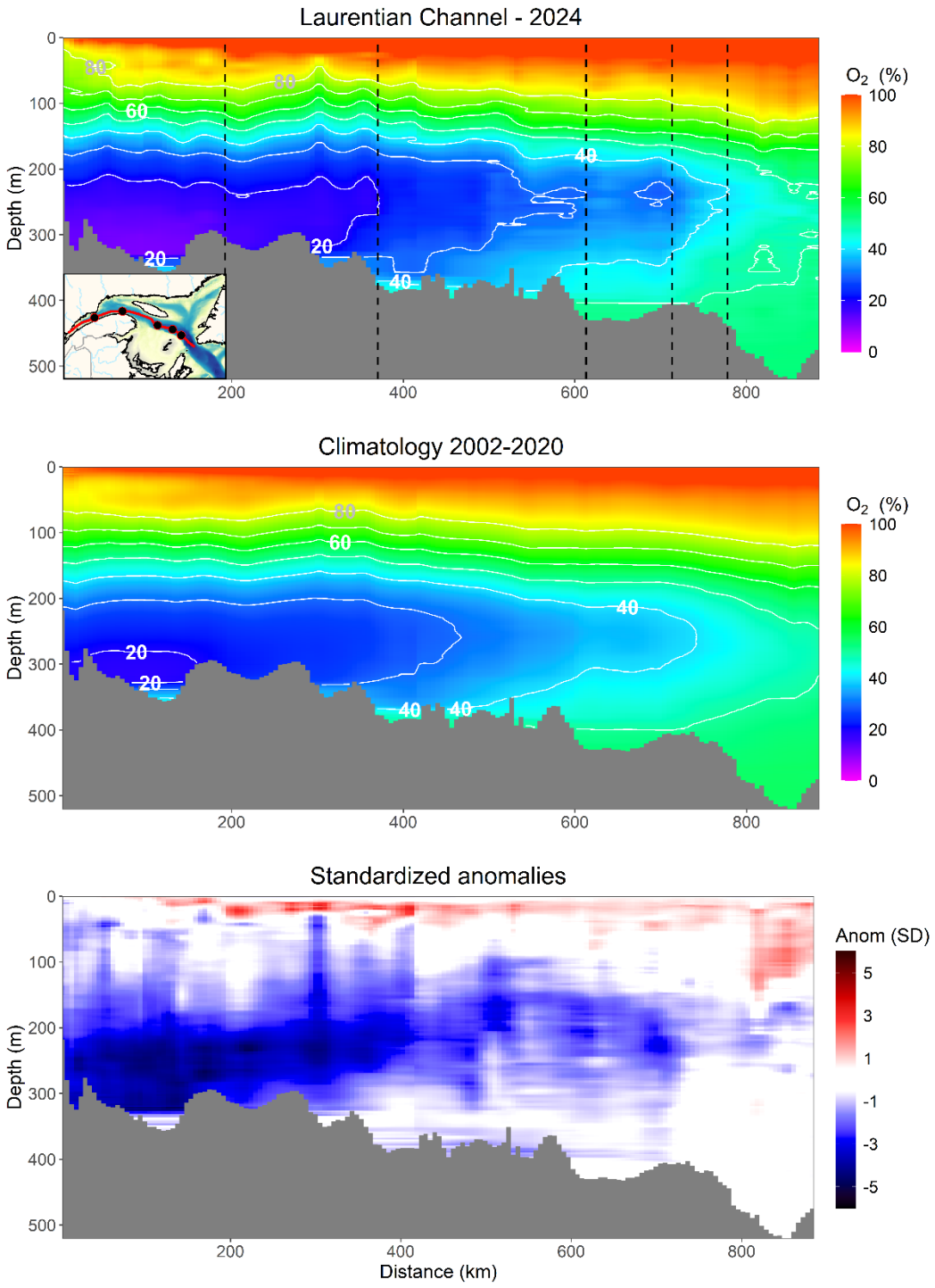

Figure 10. Mean annual vertical distribution of oxygen saturation along the Laurentian Channel in 2024 (upper panel), and for climatology (2002–2020; middle panel). Standardized anomalies are presented in the bottom panel where blue colours indicate below-normal levels (negative anomalies), reds are above-normal levels (positive anomalies), and white represents normal levels. Section is presented from the head of the Laurentian Channel (Estuary) to Cabot Strait. The dashed black vertical lines on the upper panel are geographical markers corresponding to the black points on the map (left bottom corner of the upper panel).

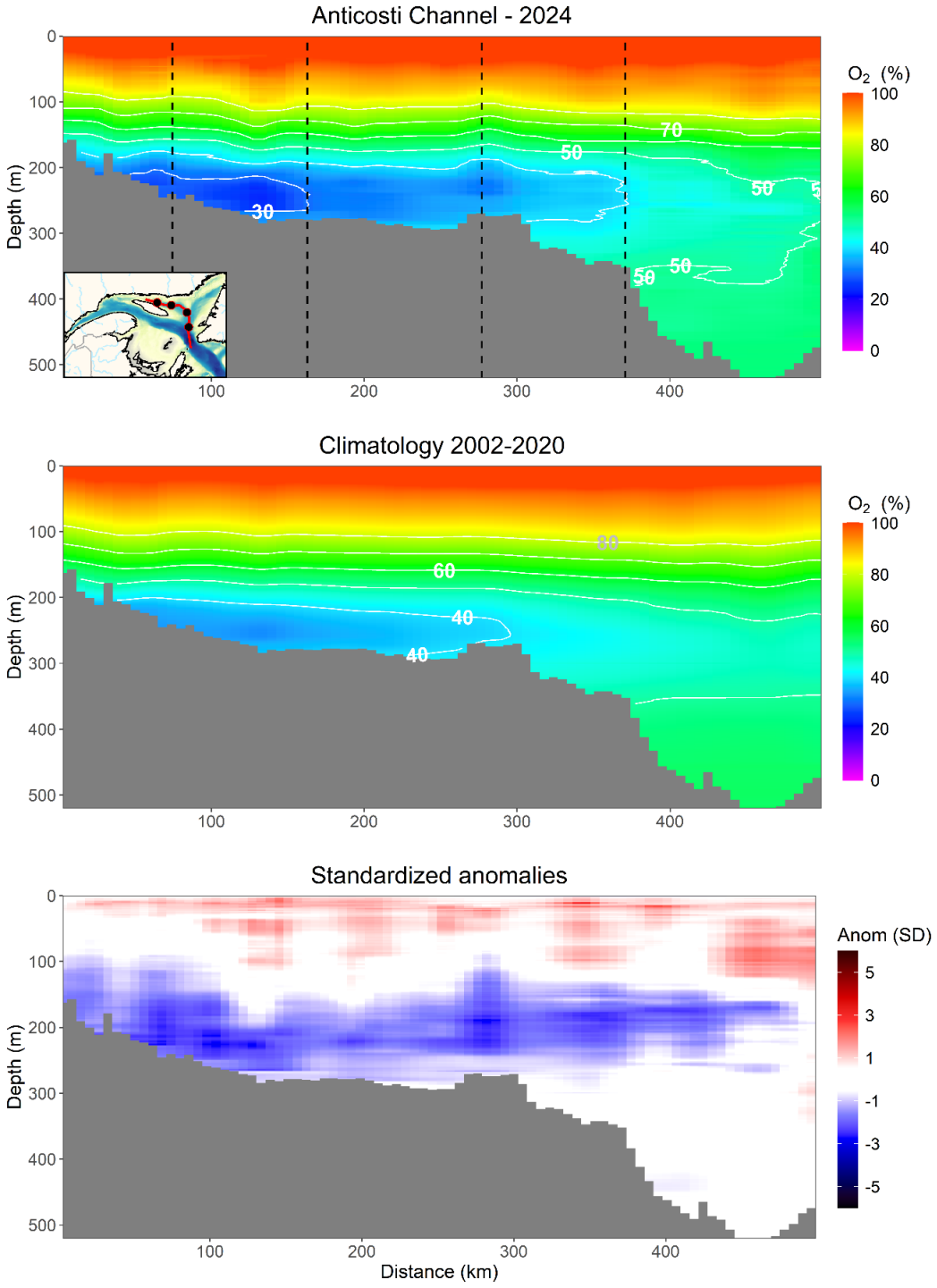

Figure 11. Mean annual vertical distribution of oxygen saturation along the Anticosti Channel in 2024 (upper panel), and for climatology (2002–2020; middle panel). Standardized anomalies are presented in the bottom panel where blue colours indicate below-normal levels (negative anomalies), reds are above-normal levels (positive anomalies), and white represents normal levels. Section is presented from the head of the Anticosti Channel to Cabot Strait. The dashed black vertical lines on the upper panel are geographical markers corresponding to the black points on the map (left bottom corner of the upper panel).

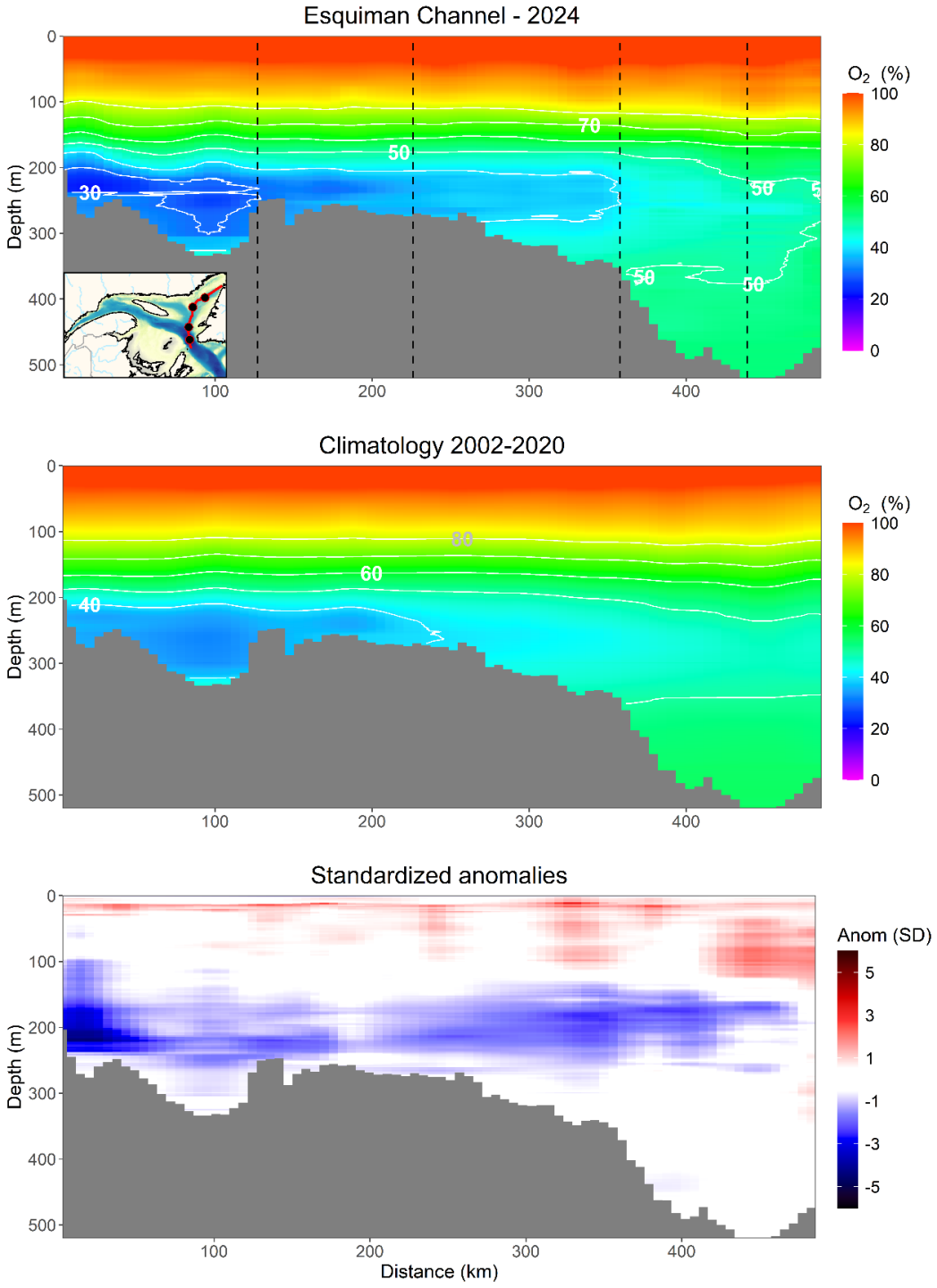

Figure 12. Mean annual vertical distribution of oxygen saturation along the Esquiman Channel in 2024 (upper panel), and for climatology (2002–2020; middle panel). Standardized anomalies are presented in the bottom panel where blue colours indicate below-normal levels (negative anomalies), reds are above-normal levels (positive anomalies), and white represents normal levels. Section is presented from the head of the Esquiman Channel to Cabot Strait. The dashed black vertical lines on the upper panel are geographical markers corresponding to the black points on the map (left bottom corner of the upper panel).

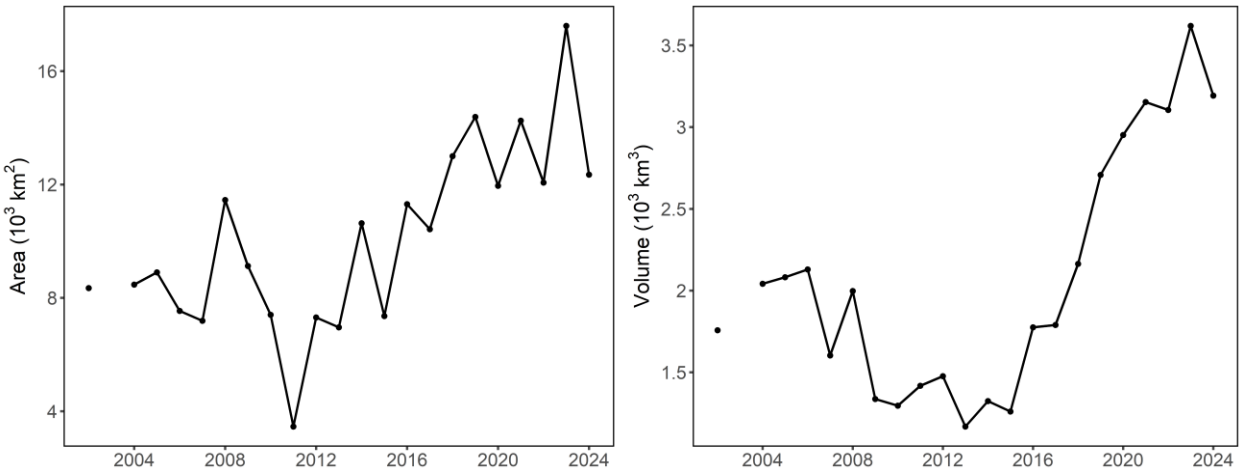

Figure 13. Area at 300 m and volume covered by hypoxic waters (<30% of oxygen saturation) in the Estuary and Gulf of St. Lawrence over the 2002–2024 time series.

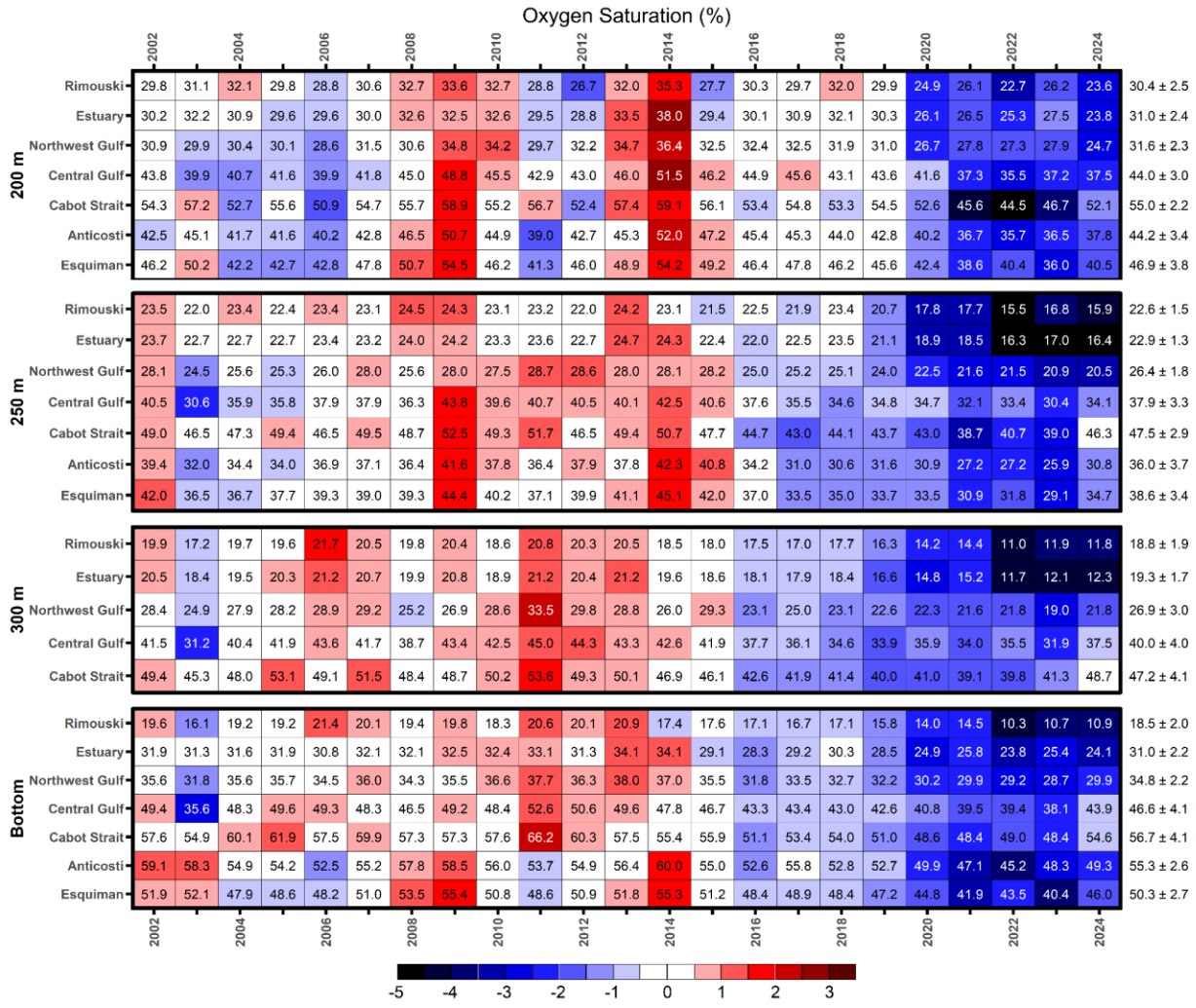

Figure 14. Annual averages of deep-layer dissolved oxygen saturation (%) at 200 m, 250 m, and 300 m, and at the bottom (for locations deeper than 100 m). The numbers on the right are the 2002–2020 climatological means and standard deviations, and the numbers in the boxes are the oxygen saturation levels. Blue colours indicate below-normal levels (negative anomalies), reds are above-normal levels (positive anomalies), and white cells represent normal levels. White text is used for readability purposes when anomalies are higher (lower) than +2 SD (-2 SD) throughout this document.

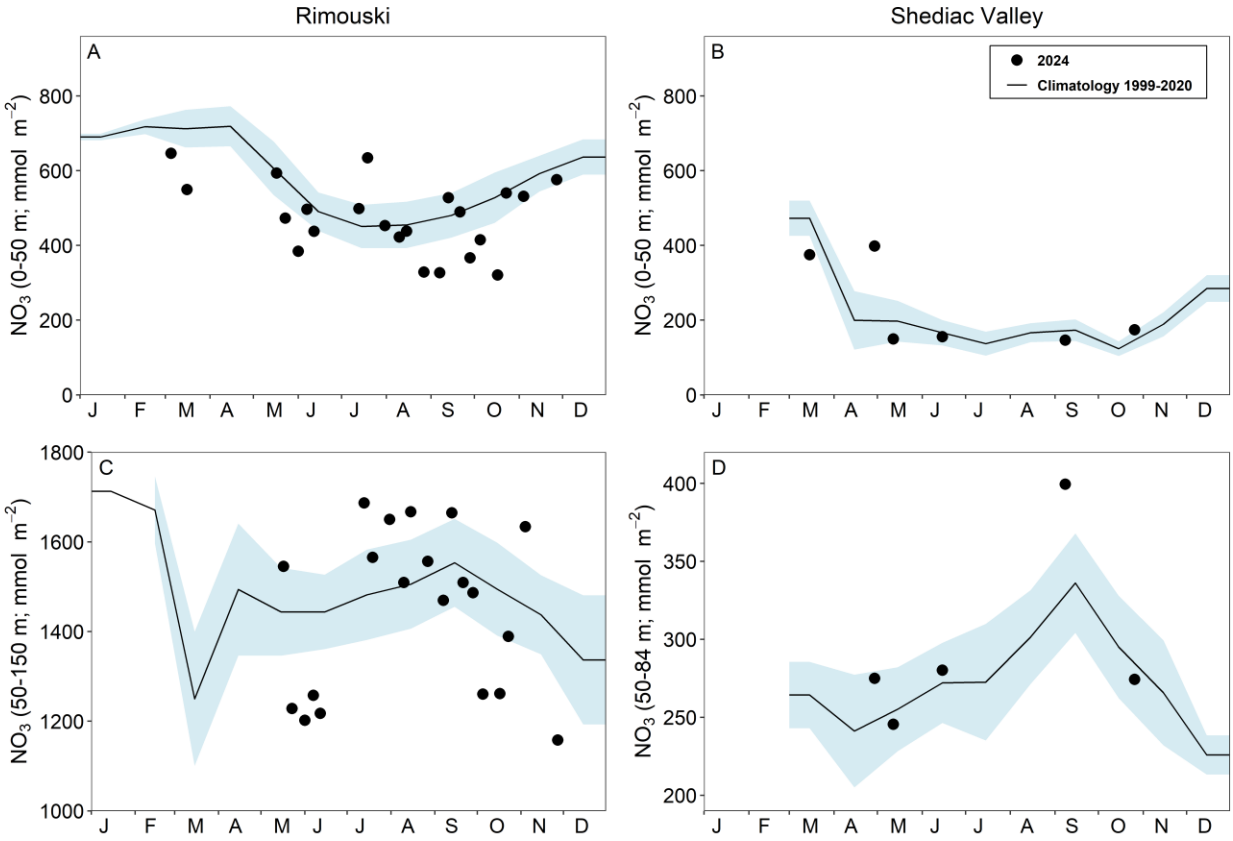

Figure 15. Surface nitrate inventories (0–50 m; top panels), and mid-layer nitrate inventories (50–150 m for Rimouski and 50–84 m for Shediac Valley; bottom panels) in 2024 (black circles) with monthly mean conditions (± 0.5 SD) for the 1999–2020 climatology (black line with blue shading) at Rimouski and Shediac Valley stations.

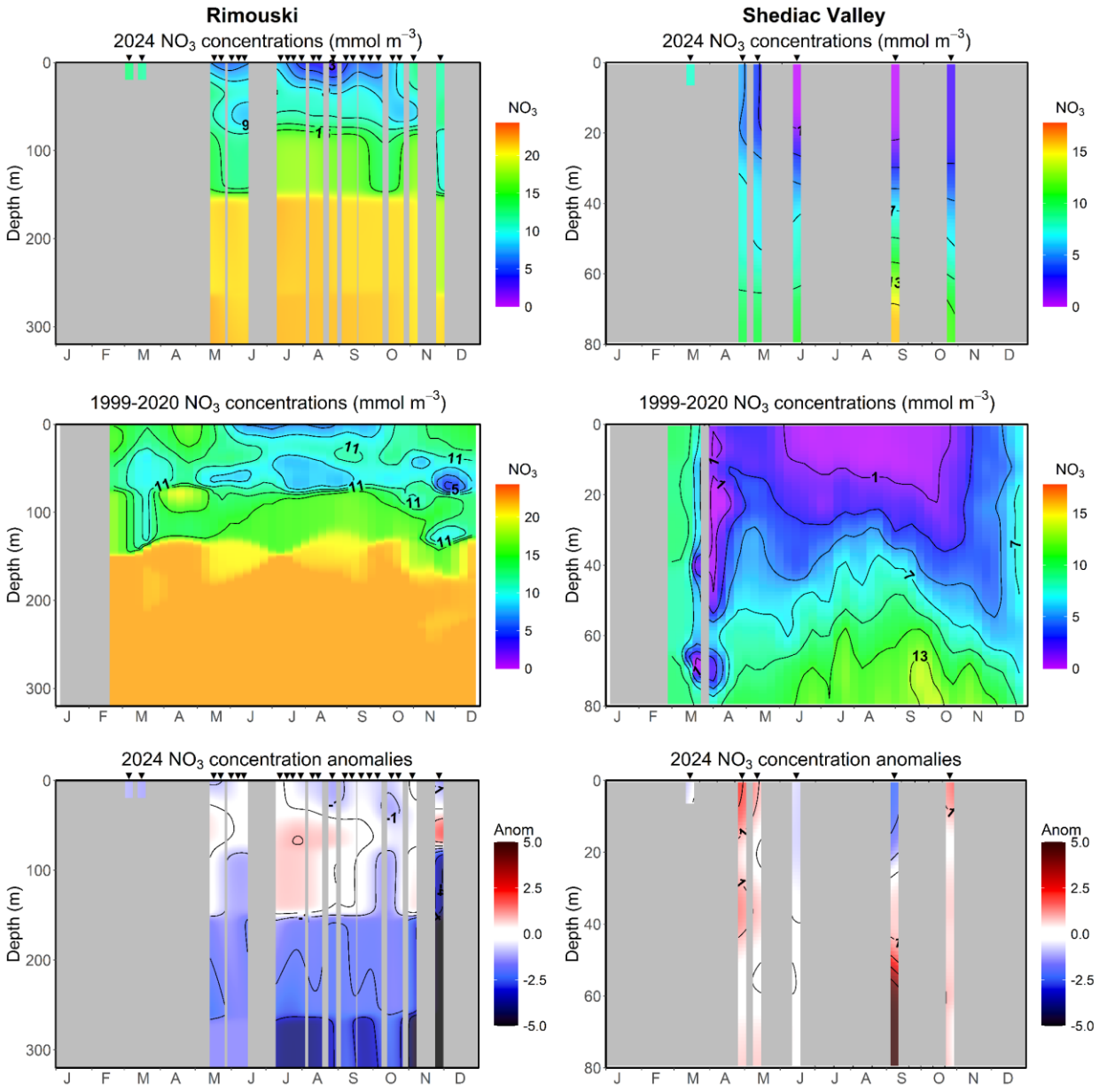

Figure 16. Vertical profiles of nitrate concentrations (mmol m^{-3}) at Rimouski and Shediac Valley stations in 2024 (upper panels), and for the 1999–2020 climatology (middle panels). Bottom panels show the vertical profiles of nitrate standardized anomalies. Blue colours indicate below-normal levels (negative anomalies), reds are above-normal levels (positive anomalies), and white represents normal levels.

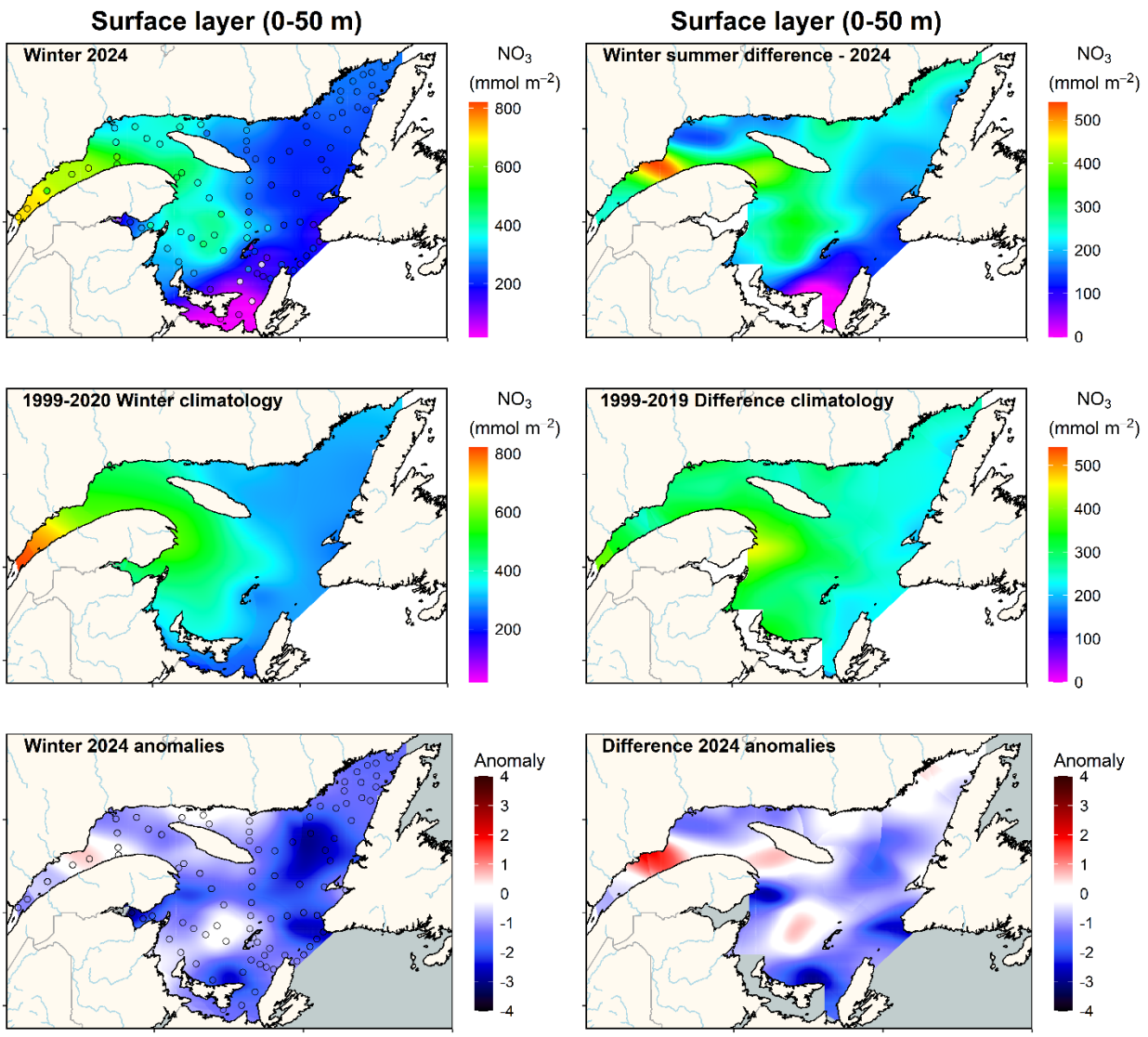

Figure 17. Nitrate inventories (mmol m^{-2}) in the surface layer (0–50 m) of the Estuary and Gulf of St. Lawrence during early March 2024 (upper left panel). Difference in nitrate inventories (mmol m^{-2}) in the surface layer of the Estuary and Gulf of St. Lawrence between winter and early summer (upper right panel). The climatology (1999–2020 for winter, 1999–2019 for difference; middle panels), and anomalies (lower panels) are shown. Blue colours indicate below-normal levels (negative anomalies), reds are above-normal levels (positive anomalies), and white represents normal levels. Open circles show station locations in 2024.

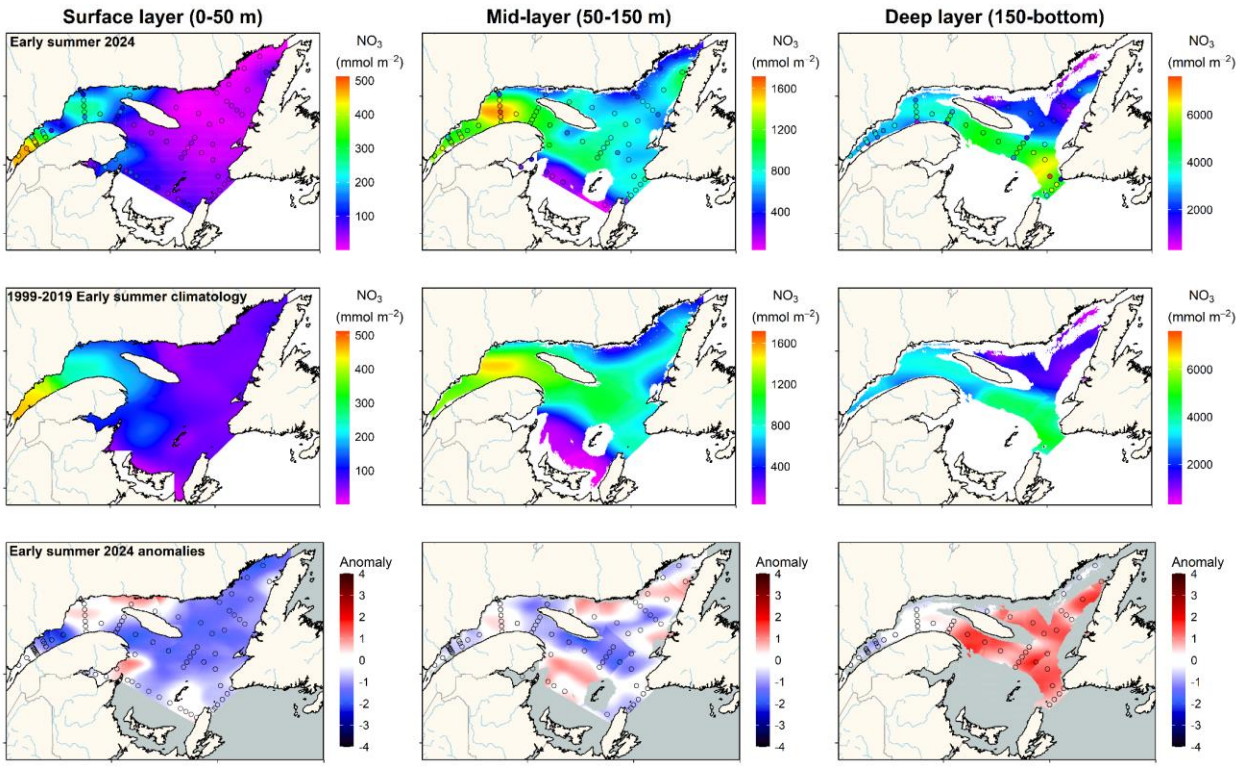

Figure 18. Nitrate inventories (mmol m^{-2}) in the surface (left panels), mid (middle panels), and deep (right panels) layers of the Estuary and Gulf of St. Lawrence during early summer 2024 (upper panels). The climatology (1999–2019; middle panels), and anomalies (lower panels) are shown for each layer. Blue colours indicate below-normal levels (negative anomalies), reds are above-normal levels (positive anomalies), and white represents normal levels. Open circles show station locations in 2024.

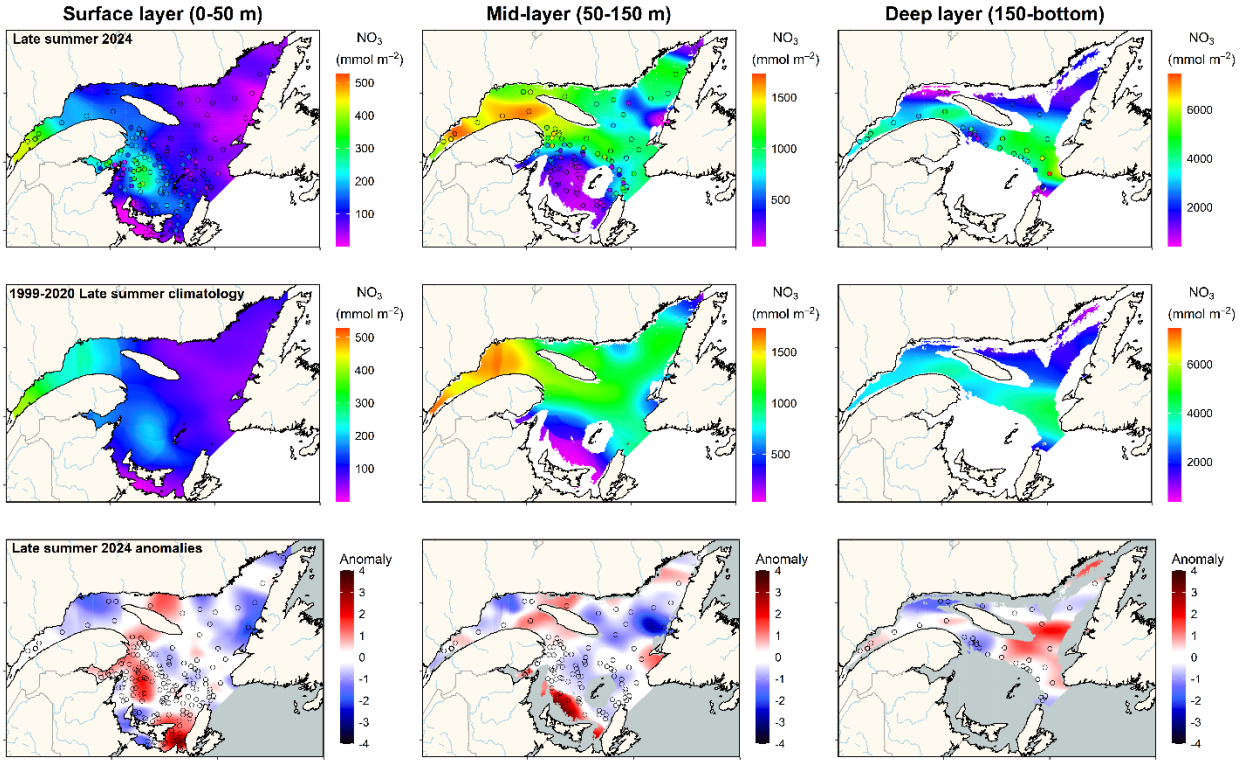

Figure 19. Nitrate inventories (mmol m^{-2}) in the surface (left panels), mid (middle panels), and deep (right panels) layers of the Estuary and Gulf of St. Lawrence during late summer 2024 (upper panels). The climatology (1999–2019; middle panels), and anomalies (lower panels) are shown for each layer. Blue colours indicate below-normal levels (negative anomalies), reds are above-normal levels (positive anomalies), and white represents normal levels. Open circles show station locations in 2024.

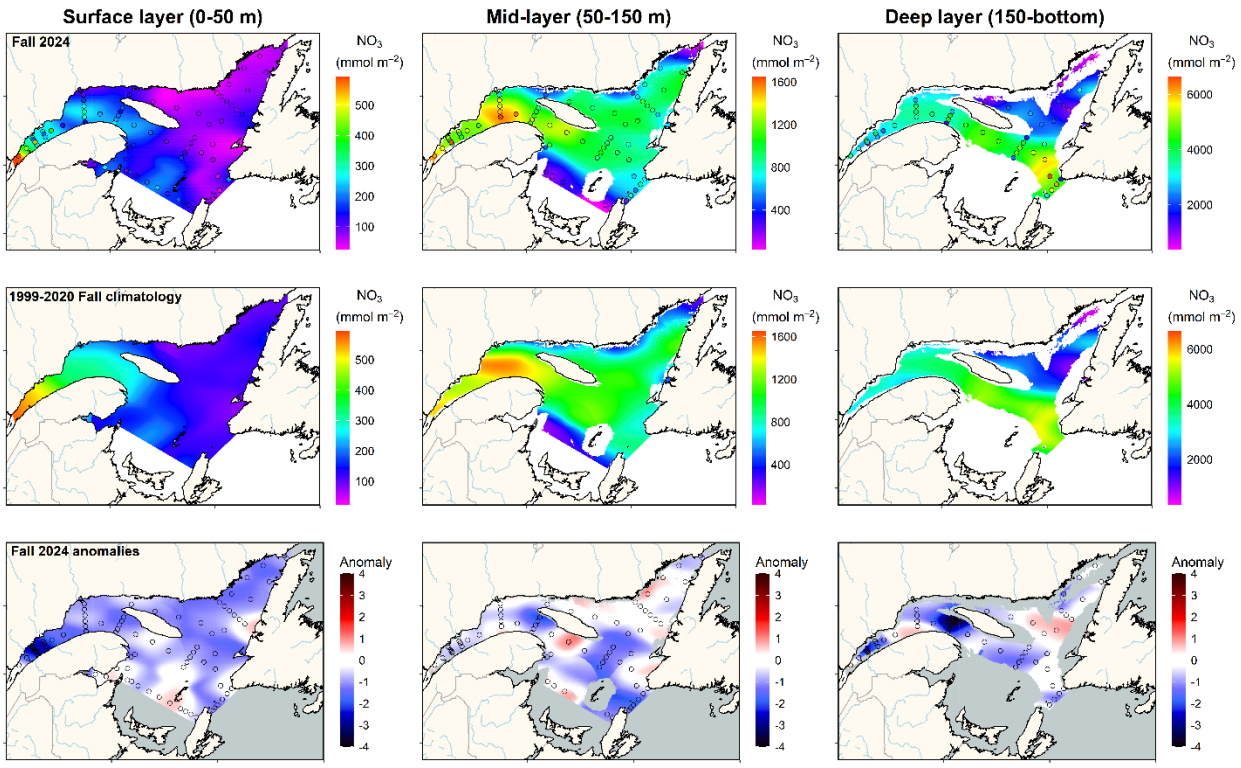

Figure 20. Nitrate inventories (mmol m^{-2}) in the surface (left panels), mid (middle panels), and deep (right panels) layers of the Estuary and Gulf of St. Lawrence during fall 2024 (upper panels). The climatology (1999–2019; middle panels), and anomalies (lower panels) are shown for each layer. Blue colours indicate below-normal levels (negative anomalies), reds are above-normal levels (positive anomalies), and white represents normal levels. Open circles show station locations in 2024.

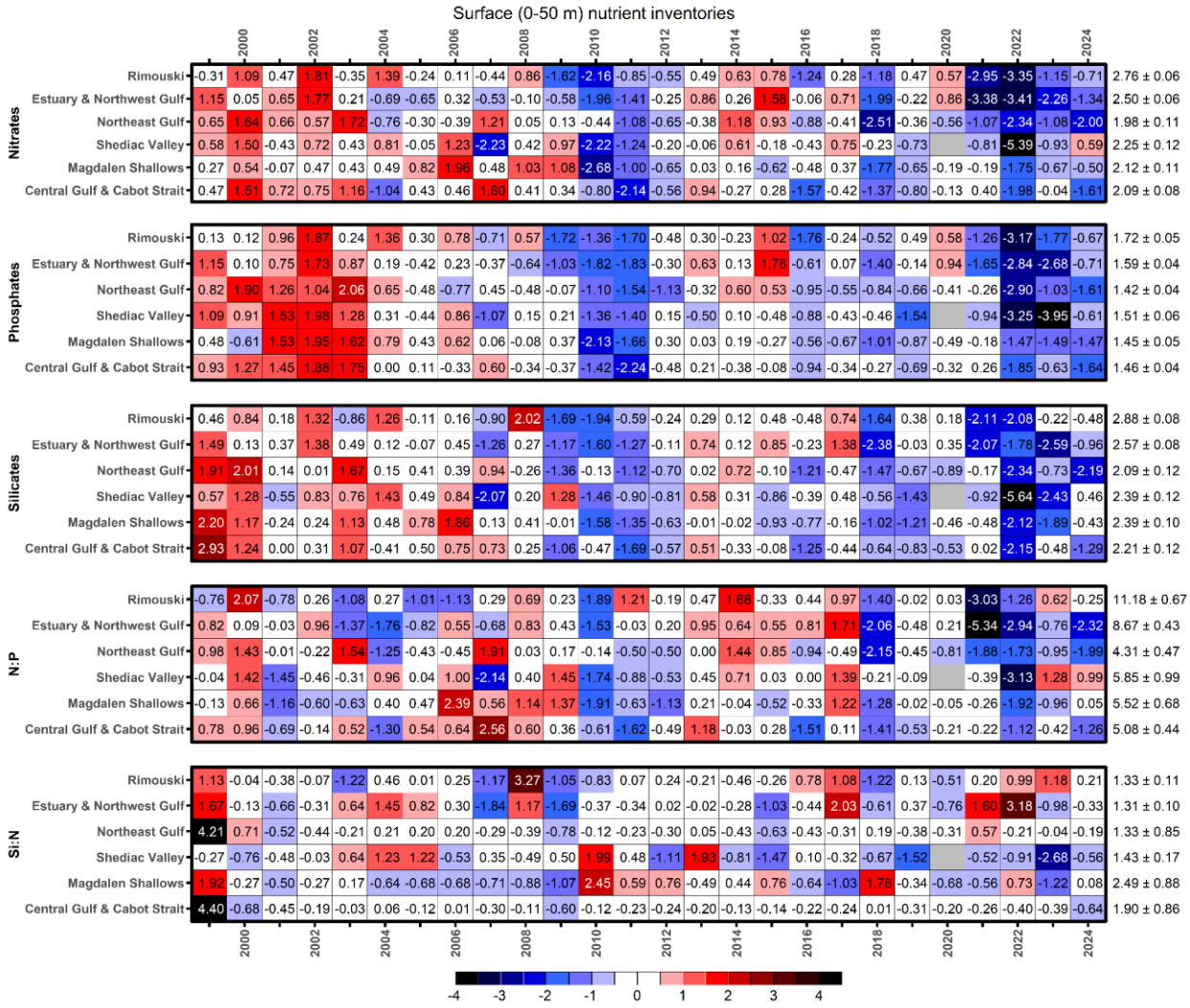

Figure 21. Time series of normalized annual anomalies for nutrient inventories and ratios in the surface layer (0–50 m) for high-frequency monitoring stations and Gulf regions. The numbers on the right are the 1999–2020 climatological means and standard deviations in units of $\log_{10}$(mmol m^{-2}) for nutrient inventories; nutrient ratios are dimensionless and have not been log-transformed. Blue colours indicate below-normal levels (negative anomalies), reds are above-normal levels (positive anomalies), and white represents normal levels.

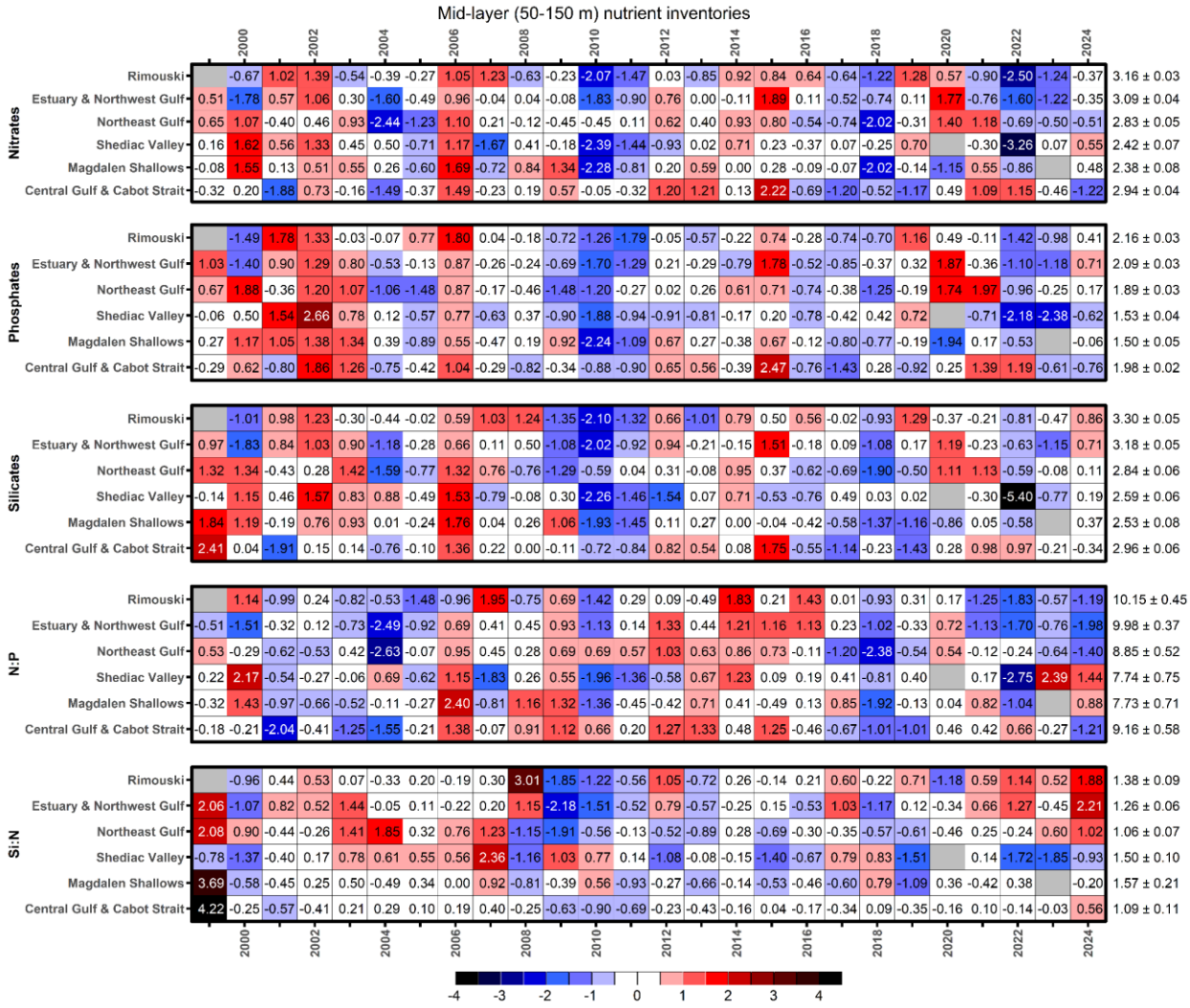

Figure 22. Time series of normalized annual anomalies for nutrient inventories and ratios in the mid-layer (50–150 m) for high-frequency monitoring stations and Gulf regions. The numbers on the right are the 1999–2020 climatological means and standard deviations in units of $\log_{10}$(mmol m^{-2}) for nutrient inventories; nutrient ratios are dimensionless and have not been log-transformed. Blue colours indicate below-normal levels (negative anomalies), reds are above-normal levels (positive anomalies), and white represents normal levels.

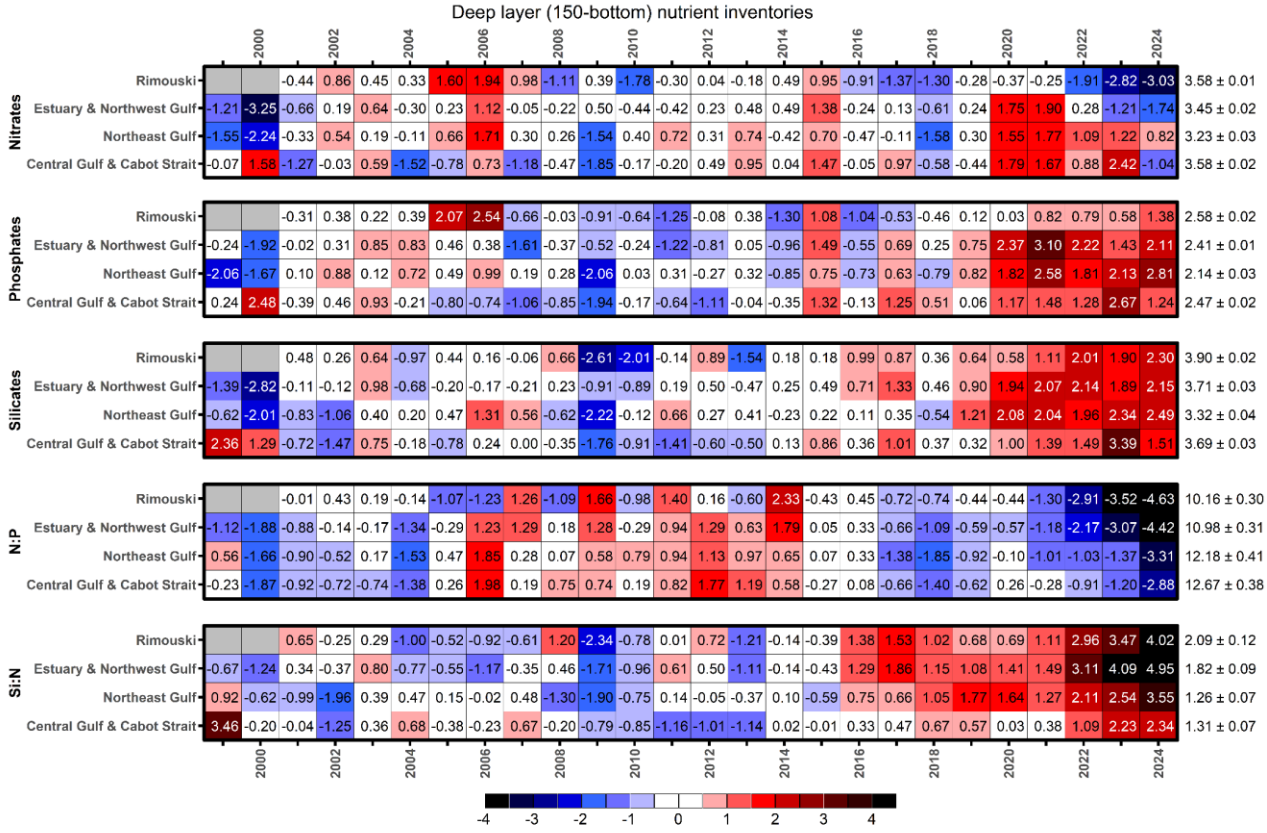

Figure 23. Time series of normalized annual anomalies for nutrient inventories and ratios in the deep layer (150—bottom) for high-frequency monitoring stations and Gulf regions. The numbers on the right are the 1999–2020 climatological means and standard deviations in units of $\log_{10}$(mmol m^{-2}) for nutrient inventories; nutrient ratios are dimensionless and have not been log-transformed. Blue colours indicate below-normal levels (negative anomalies), reds are above-normal levels (positive anomalies), and white represents normal levels.

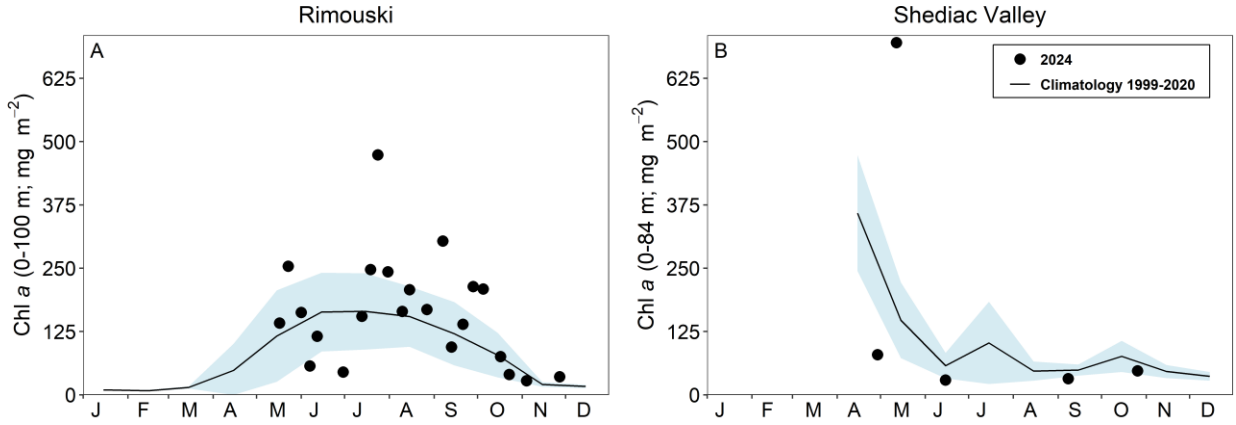

Figure 24. Chlorophyll *a* inventories (0–100 m for Rimouski and 0–84 m for Shediac Valley) in 2024 (black circles) with monthly mean conditions (± 0.5 SD) for the 1999–2020 climatology (black line with blue shading) at Rimouski and Shediac Valley stations.

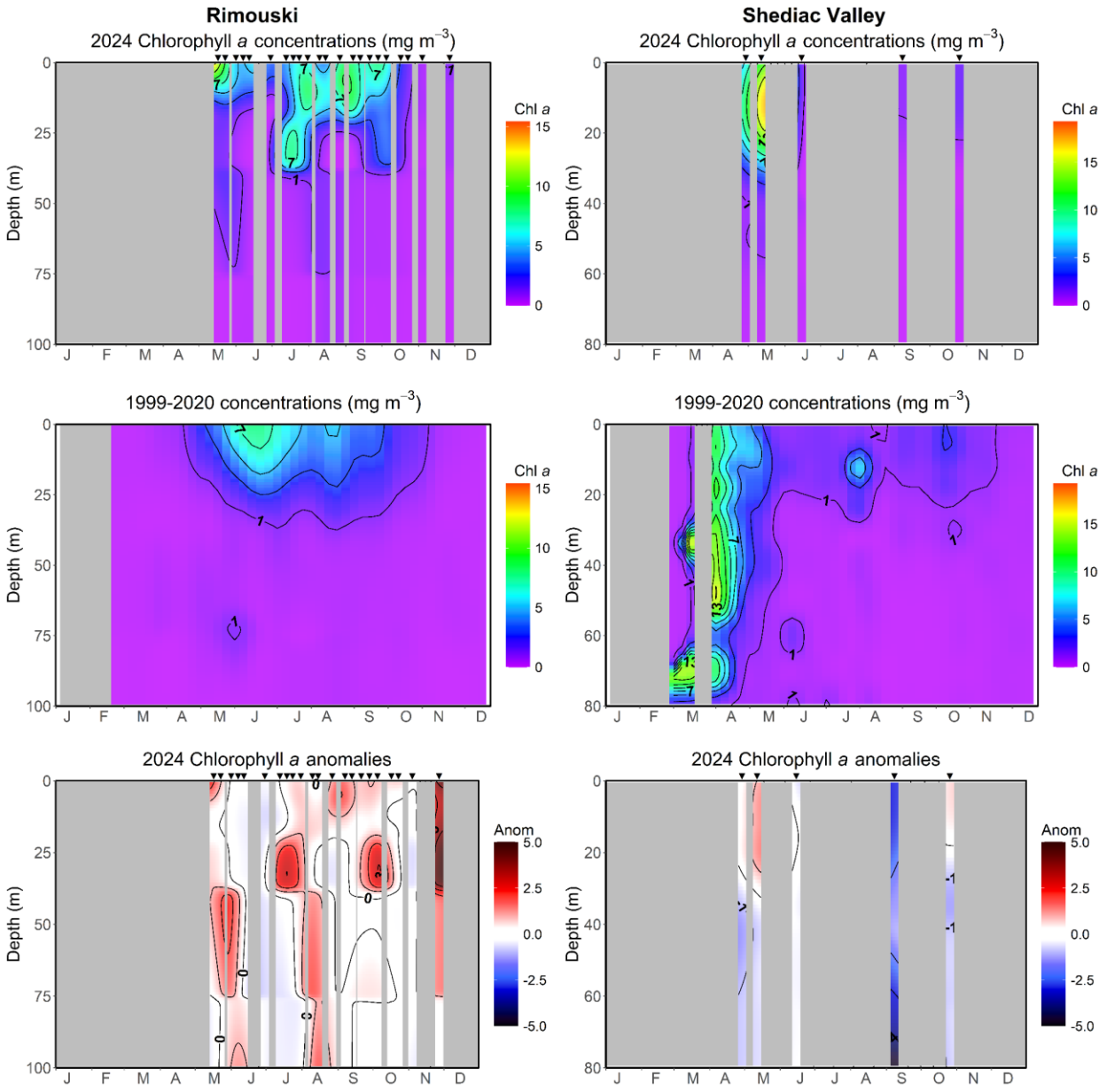

Figure 25. Vertical profiles of chlorophyll *a* concentrations (mg m^{-3}) at Rimouski and Shediac Valley stations in 2024 (upper panels), and for the 1999–2020 climatology (middle panels). Bottom panels show the vertical profiles of chlorophyll *a* standardized anomalies. Blue colours indicate below-normal levels (negative anomalies), reds are above-normal levels (positive anomalies), and white represents normal levels.

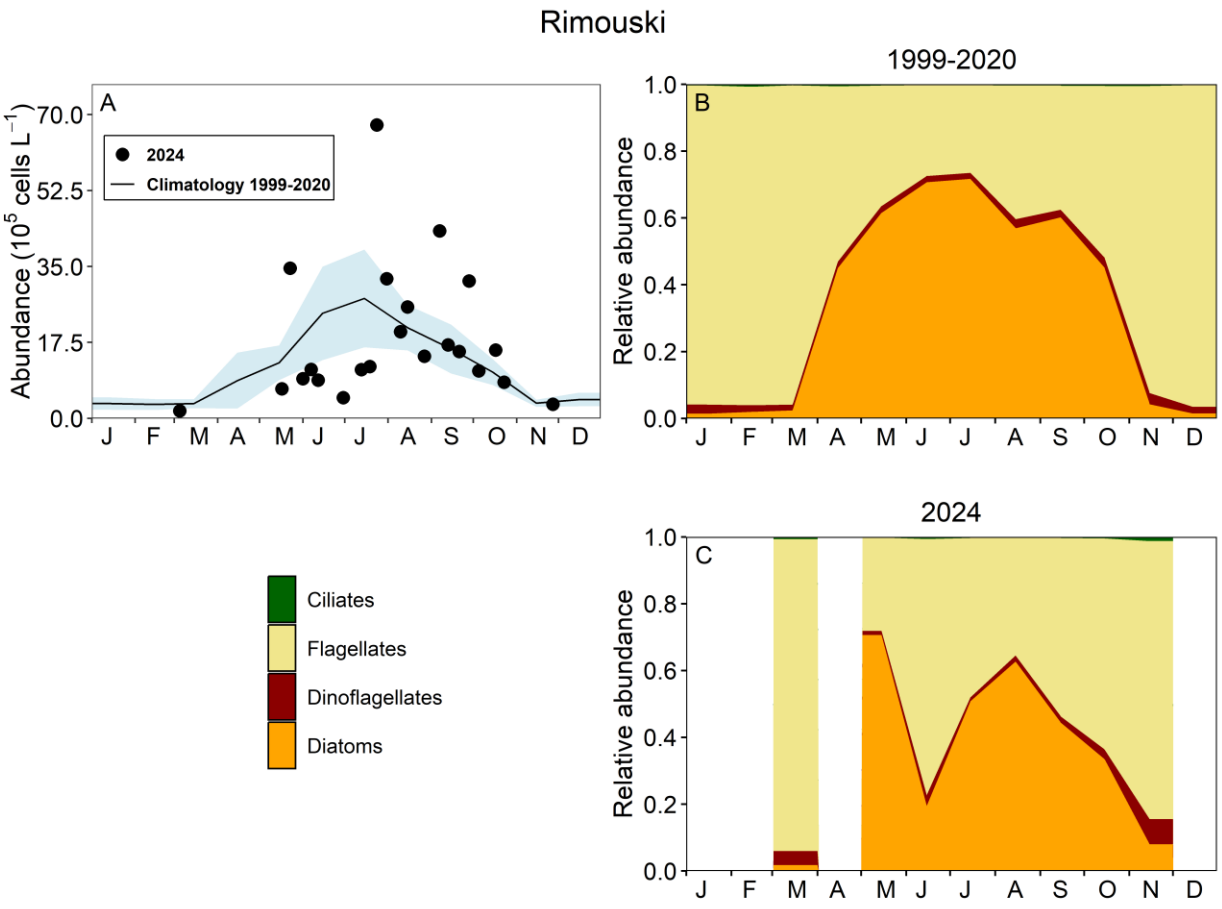

Figure 26. Phytoplankton abundance (A) and community composition at Rimouski station for the 1999–2020 climatology (B), and for 2024 (C). Blue shading on panel (A) represents ± 0.5 SD of the monthly mean phytoplankton abundance for the climatology. While ciliate abundances were included in the graphics, they are barely visible because they represent <1% of phytoplankton cells each month for the climatology.

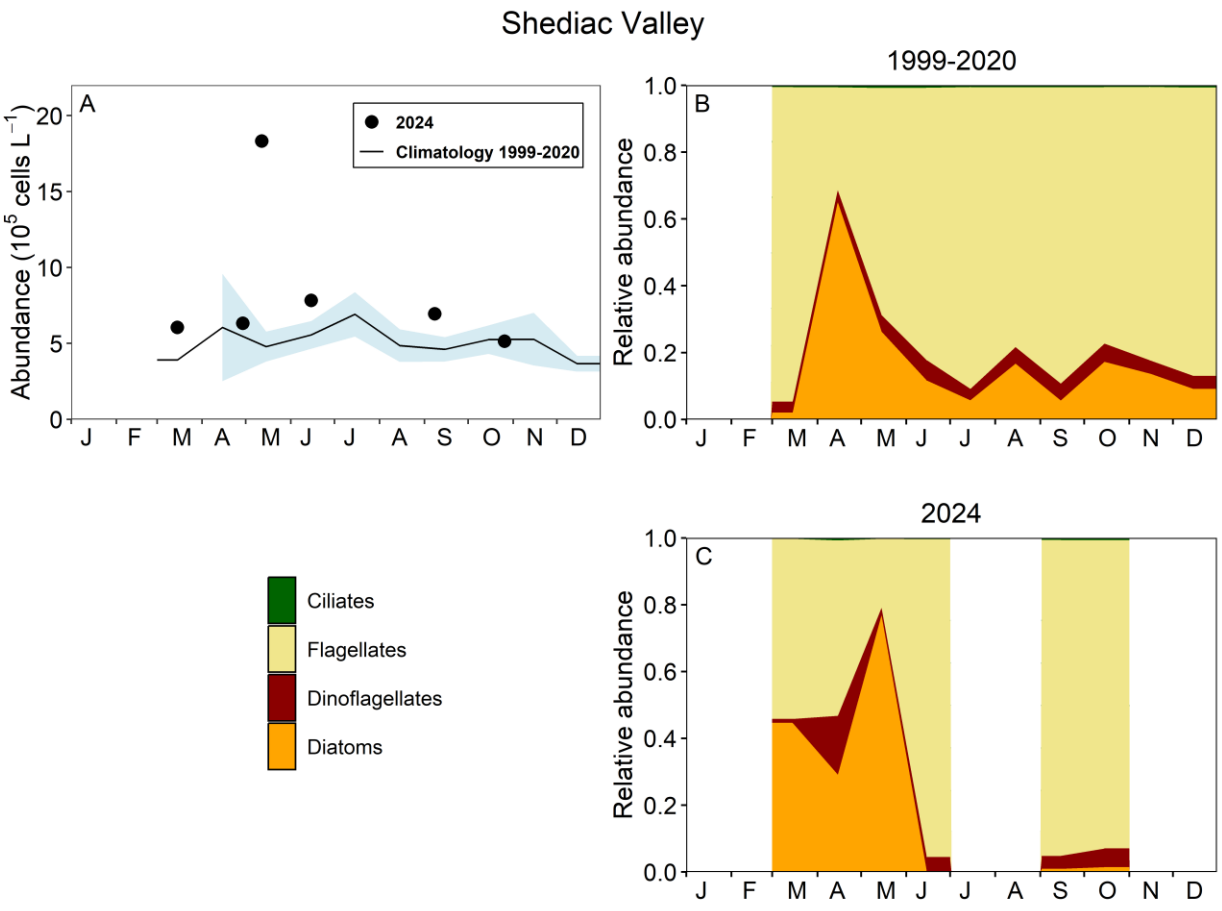

Figure 27. Phytoplankton abundance (A) and community composition at Shediac Valley station for the 1999–2020 climatology (B), and for 2024 (C). Blue shading on panel (A) represents ± 0.5 SD of the monthly mean phytoplankton abundance for the climatology.

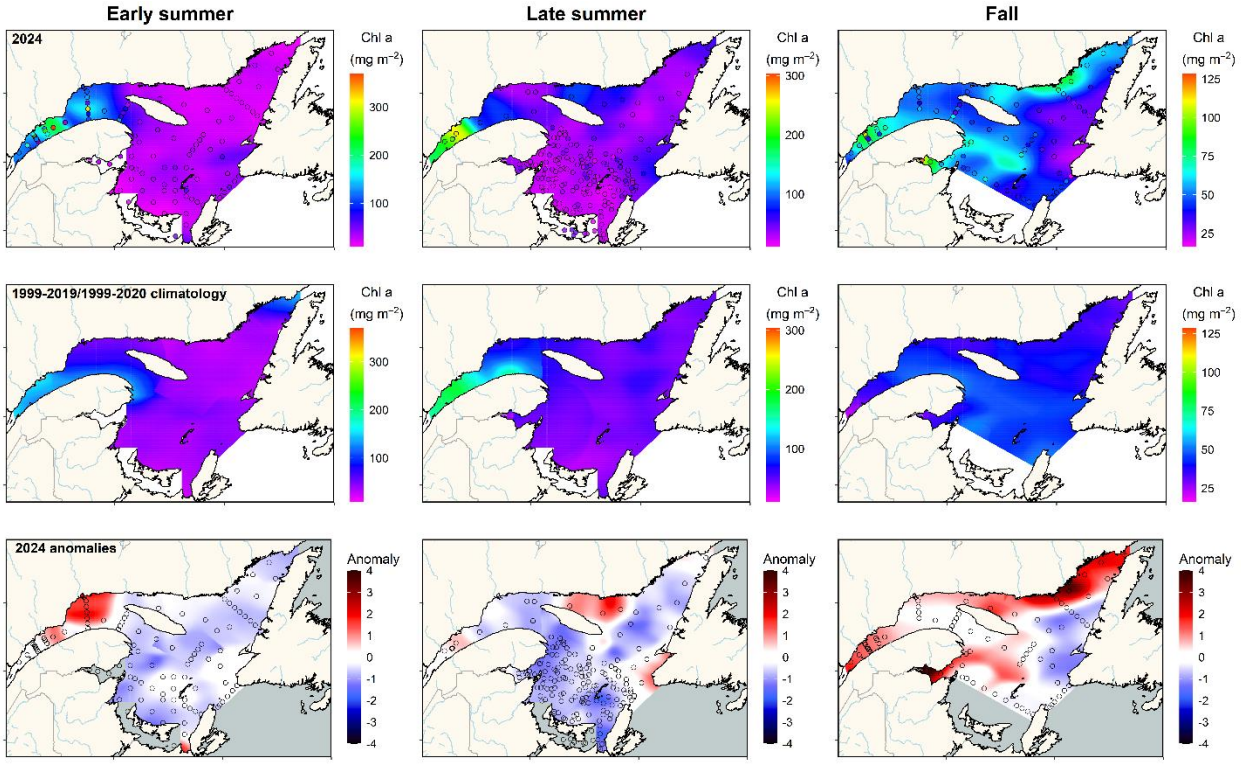

Figure 28. Vertically integrated (0–100 m) chlorophyll *a* inventory (mg m^{-2}) in the Estuary and Gulf of St. Lawrence during early summer (left panels), late summer (middle panels), and fall (right panels) 2024. The climatology (1999–2019 for early summer and 1999–2020 for the other seasons; middle panels) and anomalies (lower panels) are shown for each season. Blue colours indicate below-normal levels (negative anomalies), reds are above-normal levels (positive anomalies), and white represents normal levels. Open circles show station locations in 2024.

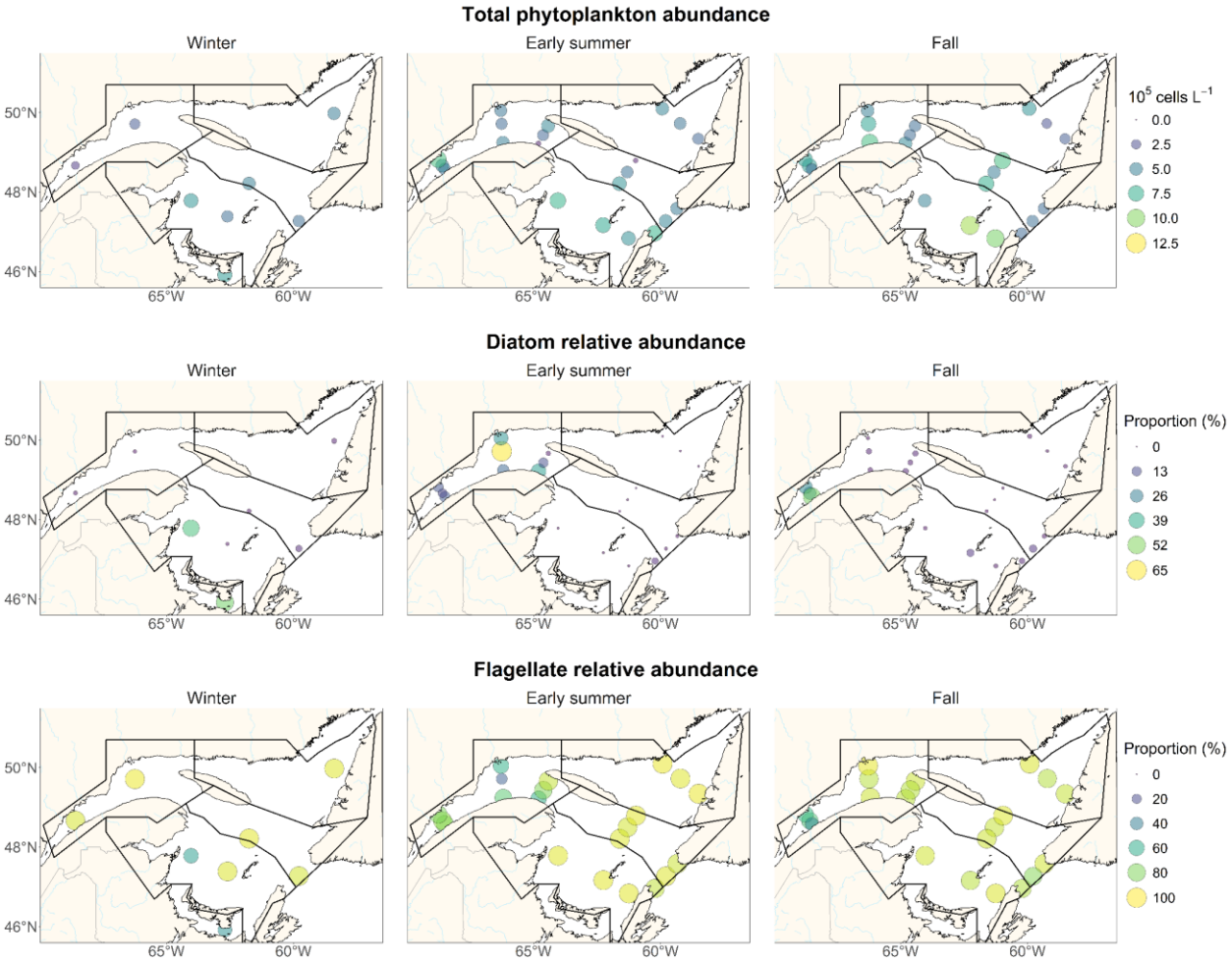

Figure 29. Total phytoplankton abundance (10^5 cells m^{-2}; top panels) and proportion (%) of diatoms (mid-panels) and flagellates (bottom panels) in the upper 100 m of the Estuary and Gulf of St. Lawrence during winter, early summer and fall 2024.

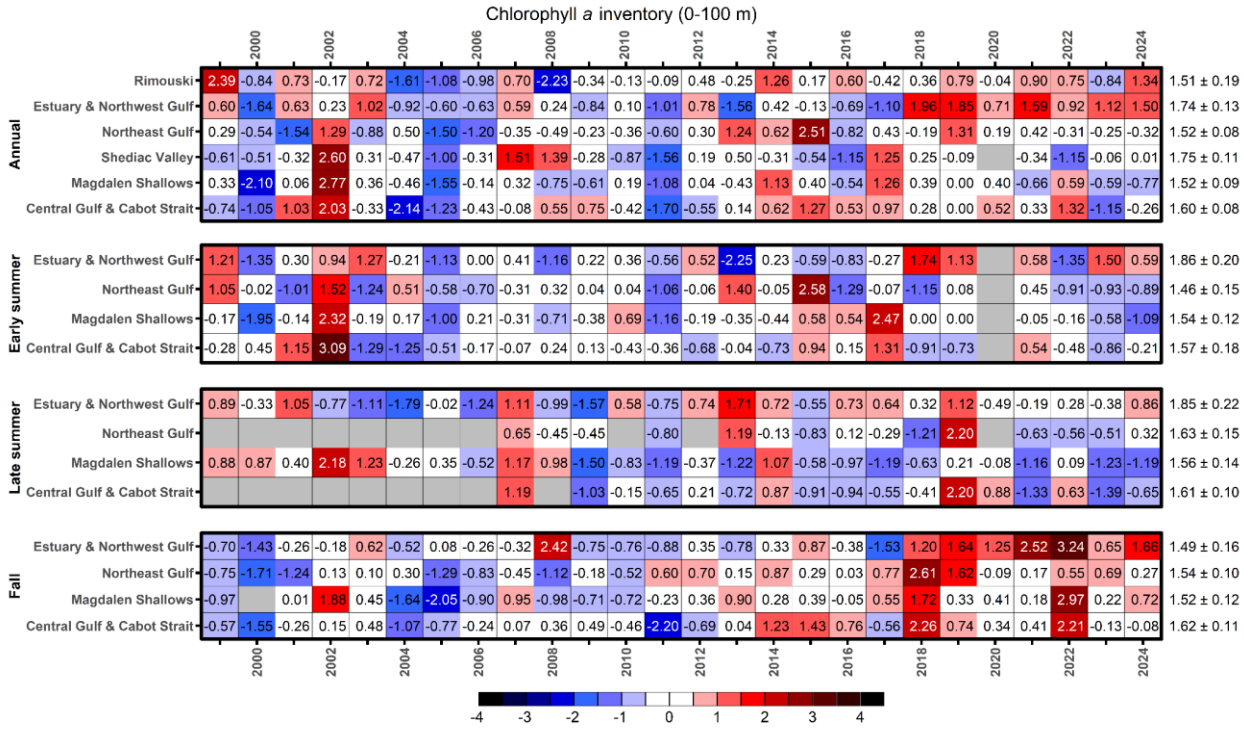

Figure 30. Time series of normalized annual and seasonal anomalies for chlorophyll *a* inventories (0–100 m) for high-frequency monitoring stations and Gulf regions. The numbers on the right are the 1999–2020 (1999–2019 for early summer) climatological means and standard deviations in units of $\log_{10}(\text{mg m}^{-2})$. Blue colours indicate below-normal levels (negative anomalies), reds are above-normal levels (positive anomalies), and white represents normal levels. Gray cells indicate missing data.

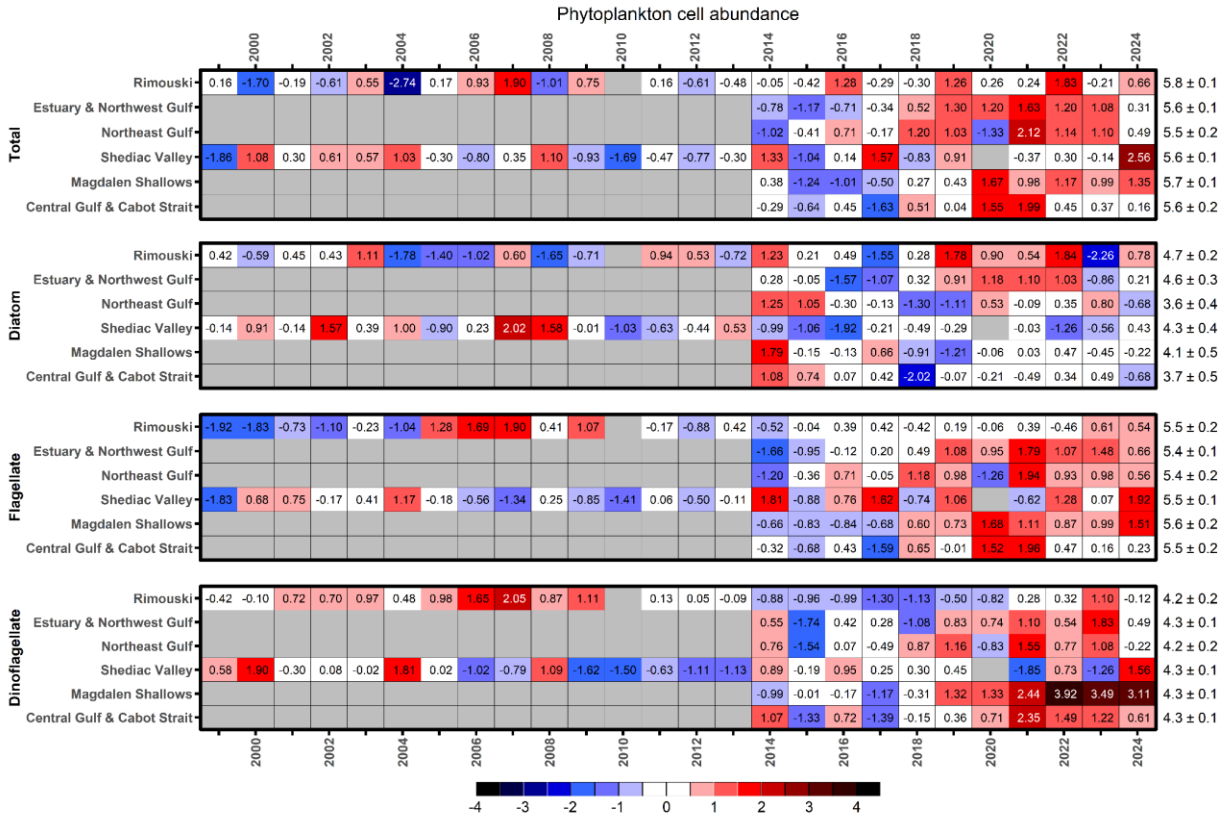

Figure 31. Time series of normalized annual anomalies for total phytoplankton abundance and the abundance of the main phytoplankton taxonomic groups at high-frequency monitoring stations and in Gulf regions. The numbers on the right are the 1999–2020 climatological means and standard deviations in units of $\log_{10}$(cells L^{-1}). Blue colours indicate below-normal levels (negative anomalies), reds are above-normal levels (positive anomalies), and white represents normal levels. Gray cells indicate missing data.

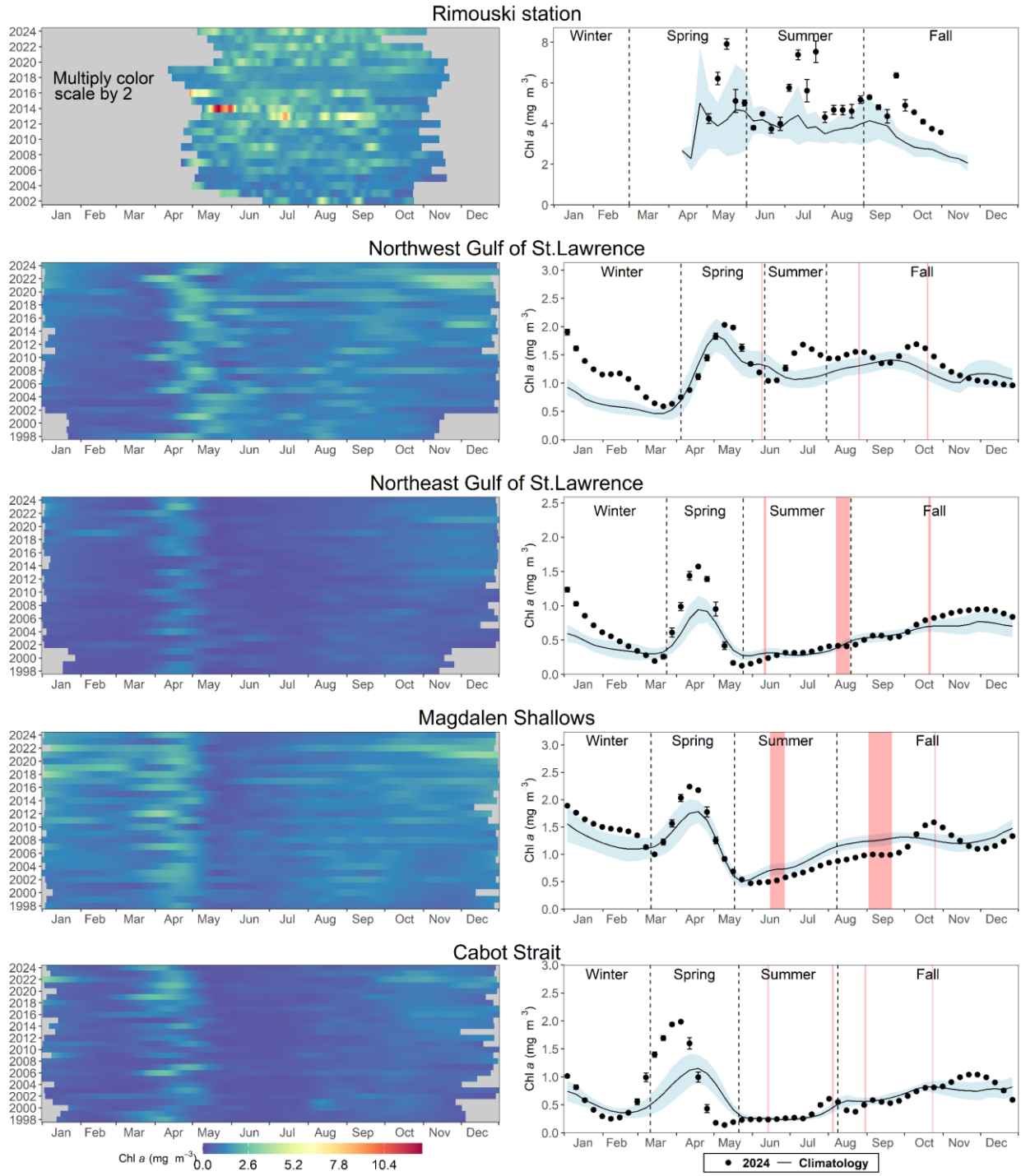

Figure 32. Left panels: LOESS-smoothed time series of daily surface chlorophyll *a* concentrations derived from data recorded by a fluorescence sensor fixed on the oceanographic buoy at Rimouski station (1st row panels), and from OC-CCI ocean-colour data in the ocean colour polygons (see Figure 4 for polygon locations). Right panels: comparison of weekly mean (± 0.5 SD) of surface chlorophyll *a* estimates in 2024 (black circles) with average (± 0.5 SD) conditions from the 1999–2020 climatology (2002–2020 for Rimouski station; solid line with blue shading) for the same ocean-colour polygons. Red shadings indicate sampling times of the main surveys. Vertical dashed lines represent the season boundaries used to compute chl *a* seasonal average.

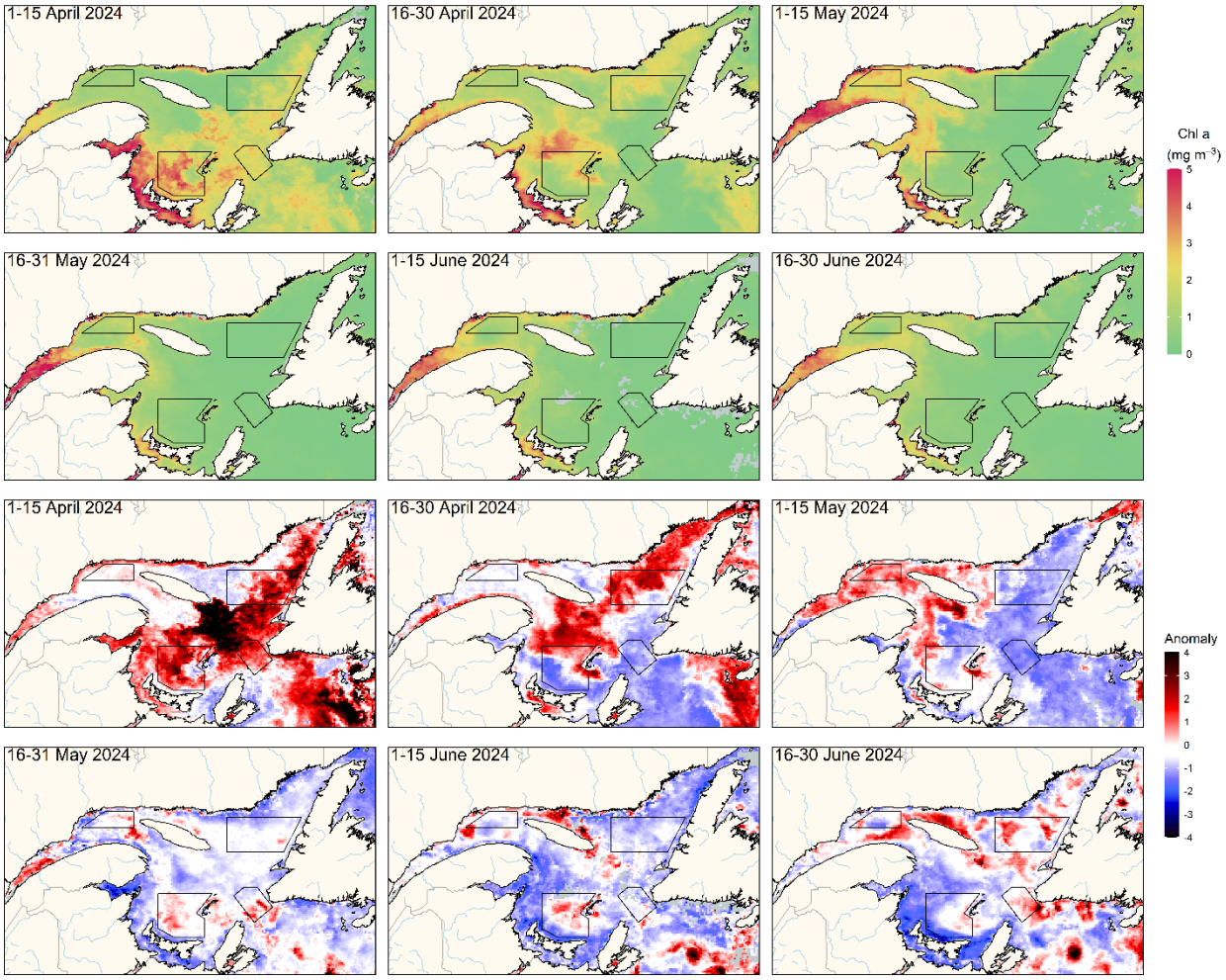

Figure 33. OC-CCI composite images of surface chlorophyll *a* (upper panels) and chlorophyll *a* normalized anomaly based on the 1999–2020 climatology (lower panels) in the Gulf of St. Lawrence during spring/early summer 2024. Grey colour indicates the absence of data. Blue colours indicate below-normal levels (negative anomalies), reds are above-normal levels (positive anomalies), and white represents normal levels. Ocean colour polygons shown for reference (see Figure 4).

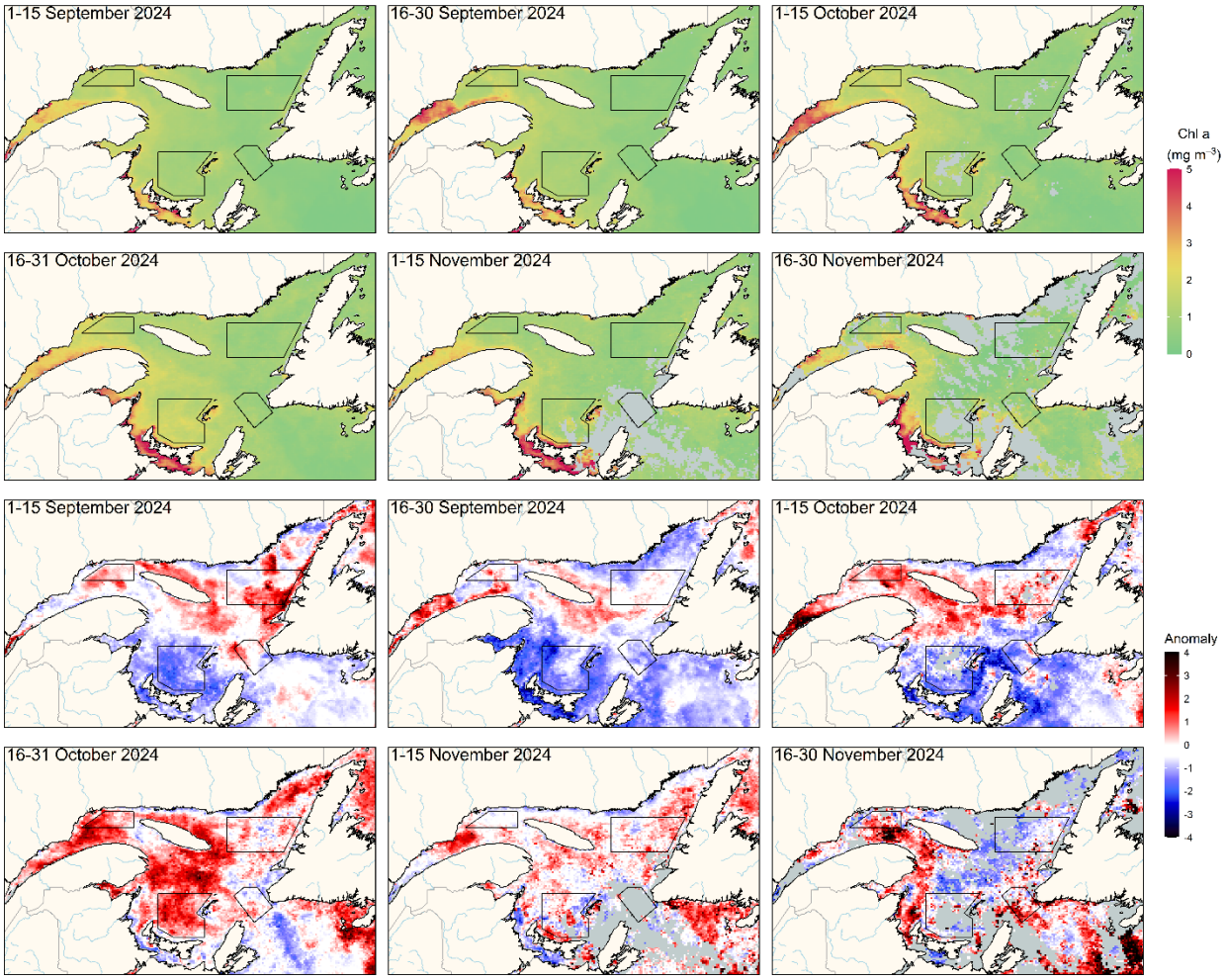

Figure 34. OC-CCI composite images of surface chlorophyll *a* (upper panels) and chlorophyll *a* normalized anomaly based on the 1999–2020 climatology (lower panels) in the Gulf of St. Lawrence during fall 2024. Grey colour indicates the absence of data. Blue colours indicate below-normal levels (negative anomalies), reds are above-normal levels (positive anomalies), and white represents normal levels. Ocean colour polygons shown for reference (see Figure 4).

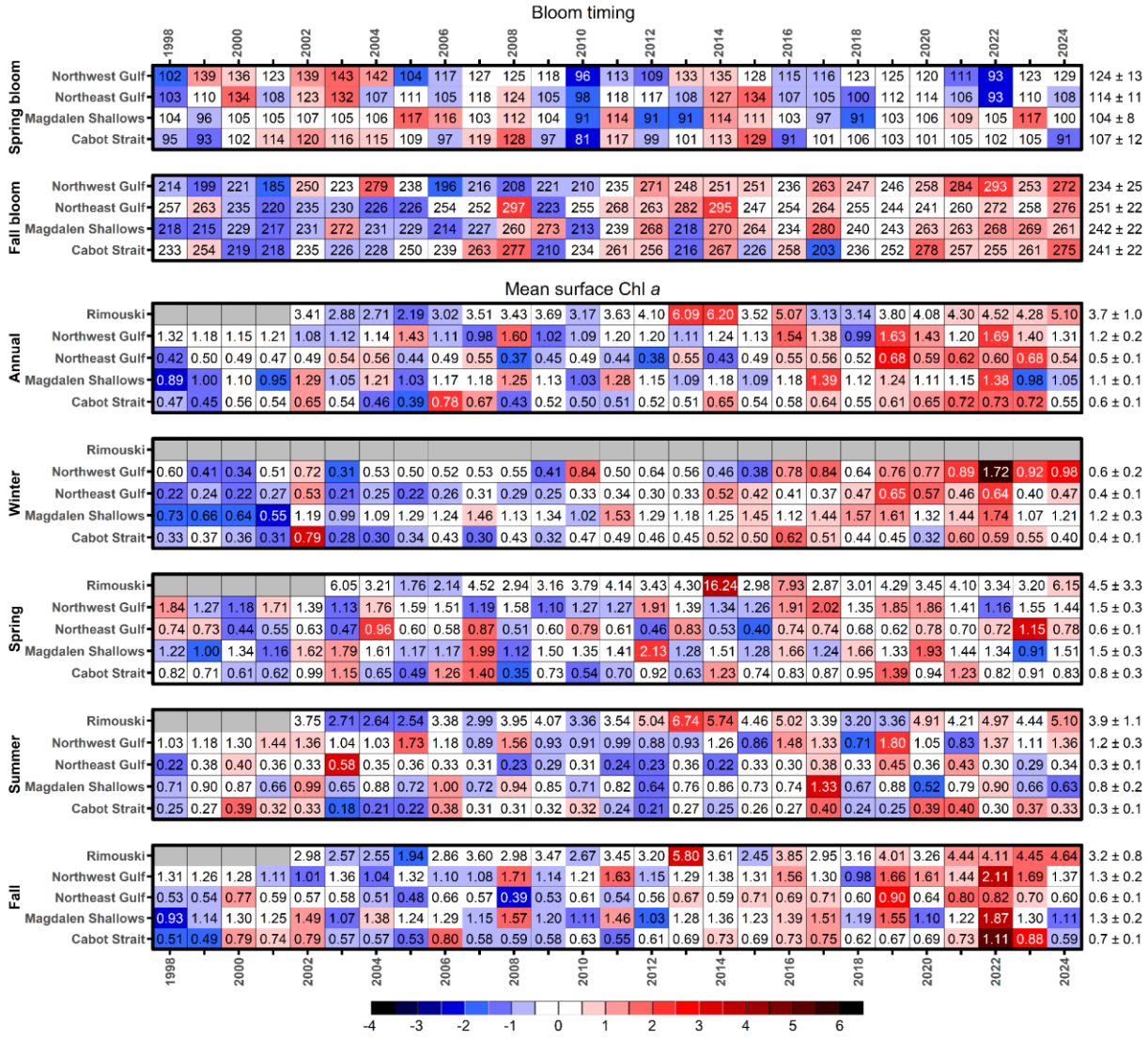

Figure 35. Time series of spring and fall bloom timings (upper section), and annual/seasonal mean surface chlorophyll *a* (lower section; mg m^{-3}) estimated from satellite ocean colour data (OC-CCI) in the Gulf of St. Lawrence ocean-colour polygons (see Figure 4), and from the oceanographic buoy surface sensor at Rimouski station. The bloom timing indices are the spring bloom peak timing (day of the year), and the fall bloom start (day of the year). Variable means and standard deviations for the 1999–2020 climatology are shown to the right of the scorecard. Blue colours indicate below-normal levels (negative anomalies), reds are above-normal levels (positive anomalies), and white represents normal levels.

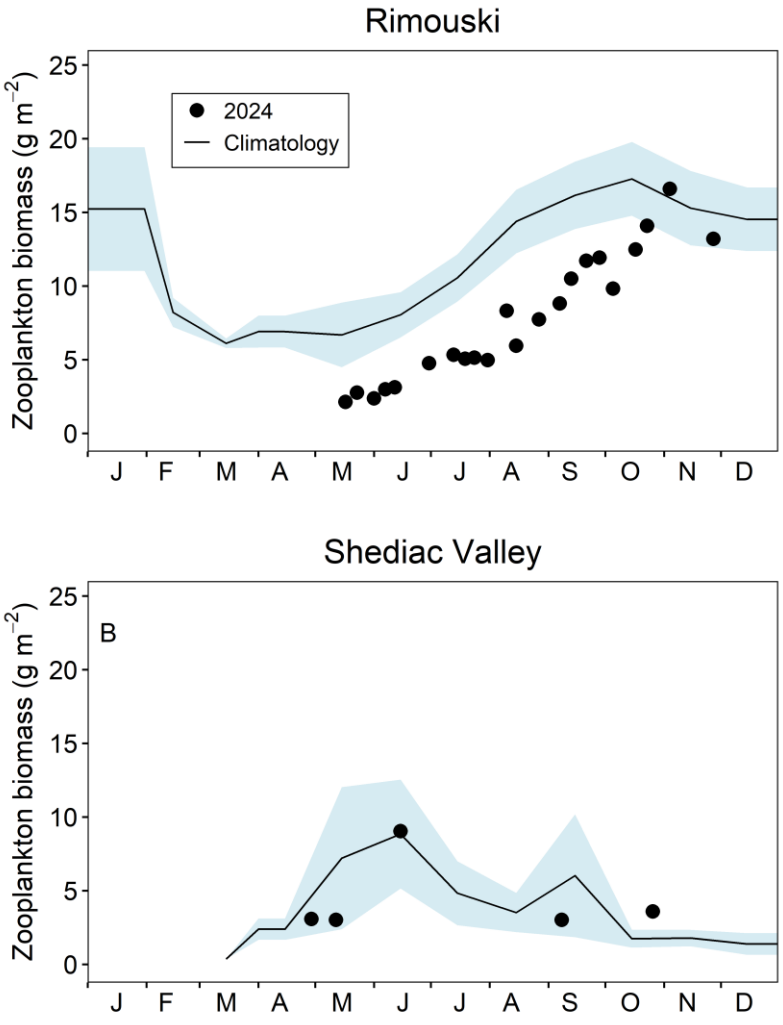

Figure 36. Comparison of total zooplankton biomass (dry weight) in 2024 (circles) with the monthly climatology from (A) Rimouski (2005–2020) and (B) Shediac Valley (1999–2020) stations (black line with blue shading). Blue shading represents ± 0.5 SD of the monthly means.

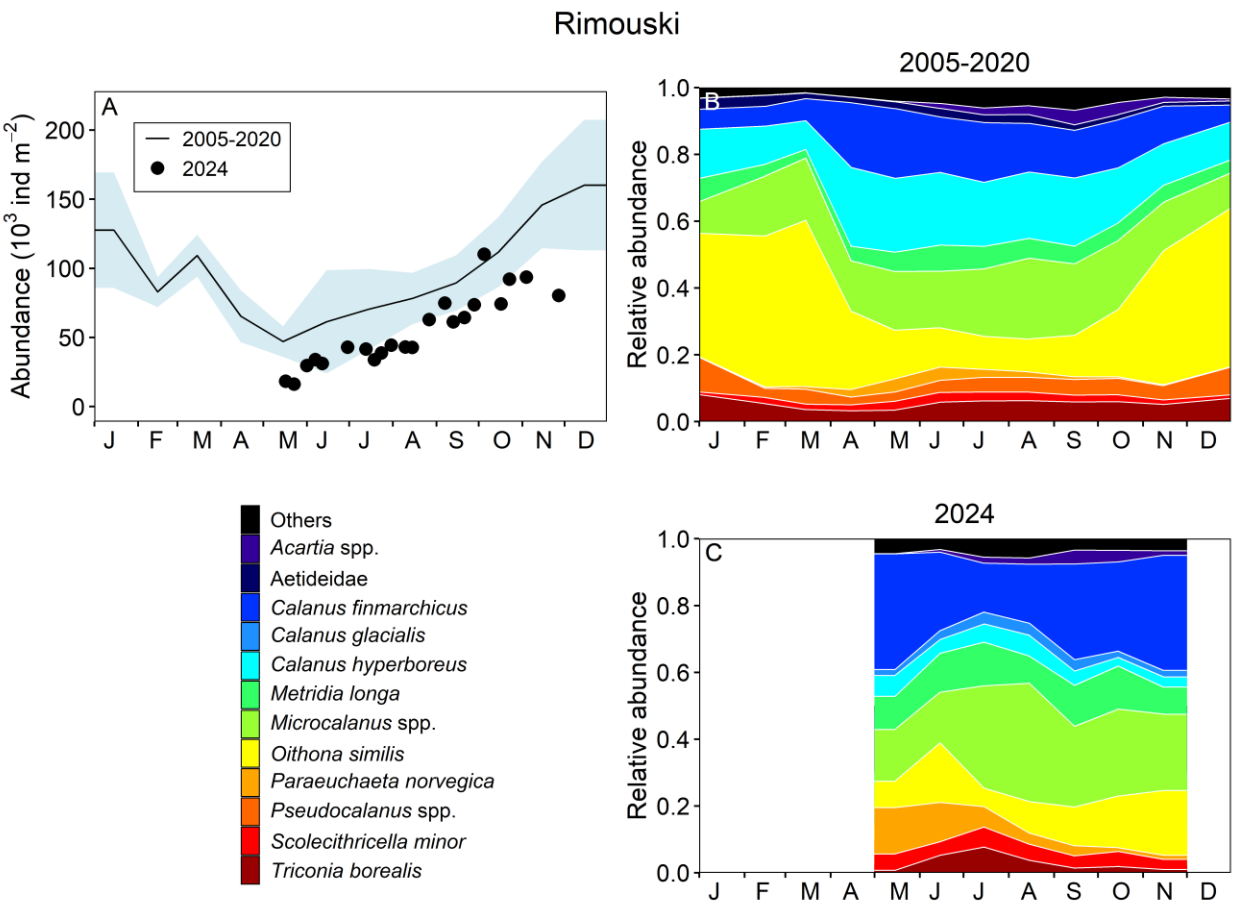

Figure 37. Seasonal variability of dominant copepods at Rimouski station. Climatology of copepod (copepodite stages only) abundance (10^3 individuals m^{-2}; black line with blue shading indicating ± 0.5 SD), and in 2024 (circles) (A); climatology of the relative abundance of the identified copepod taxa representing 95% of total copepod abundance during the 2005–2020 period (B), and in 2024 (C).

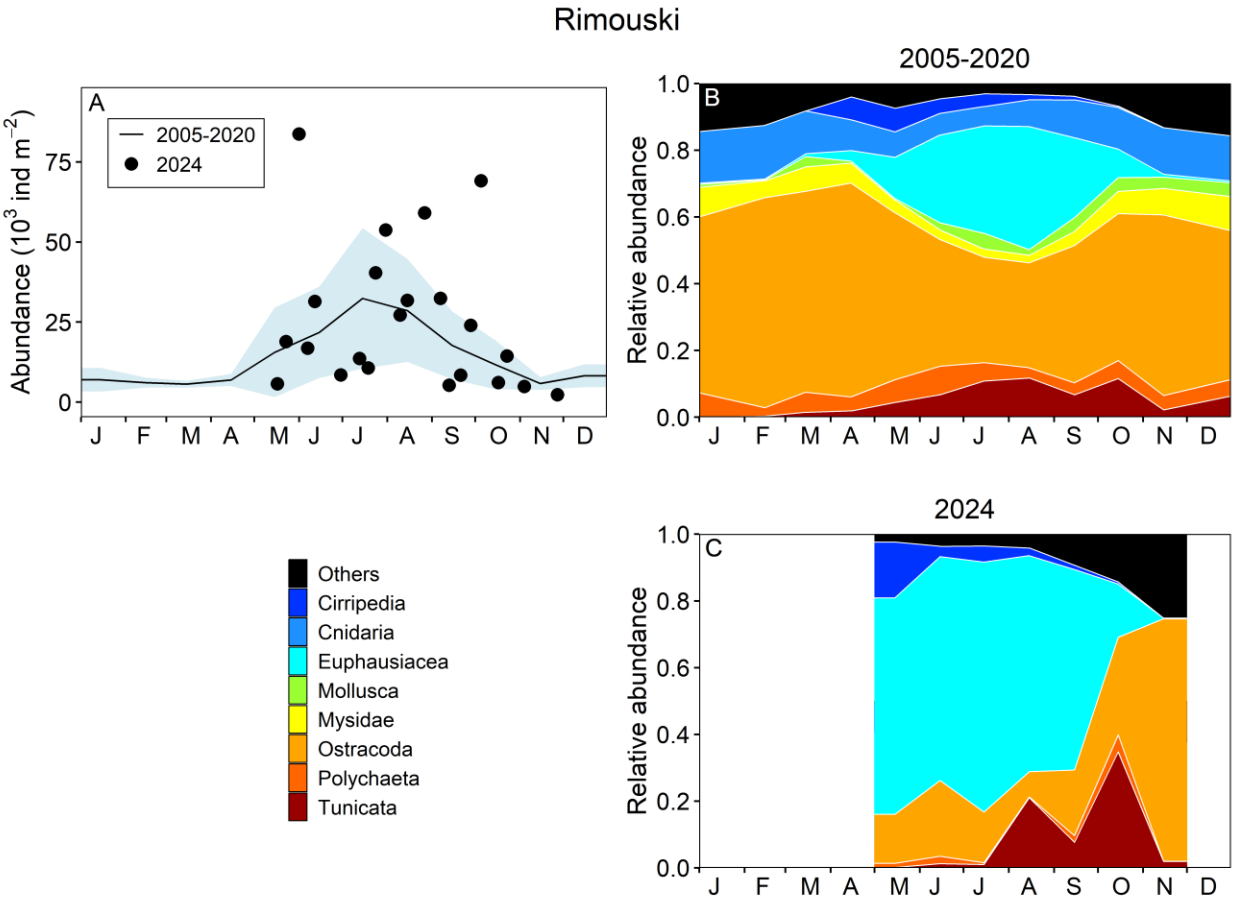

Figure 38. Seasonal variability of dominant non-copepod taxa at Rimouski station. Climatology of non-copepod abundance (10^3 individuals m^{-2}; black line with blue shading indicating ± 0.5 SD), and in 2024 (circles) (A); climatology of the relative abundance of the identified non-copepod taxa representing 95% of total non-copepod abundance during the 2005–2020 period (B), and in 2024 (C).

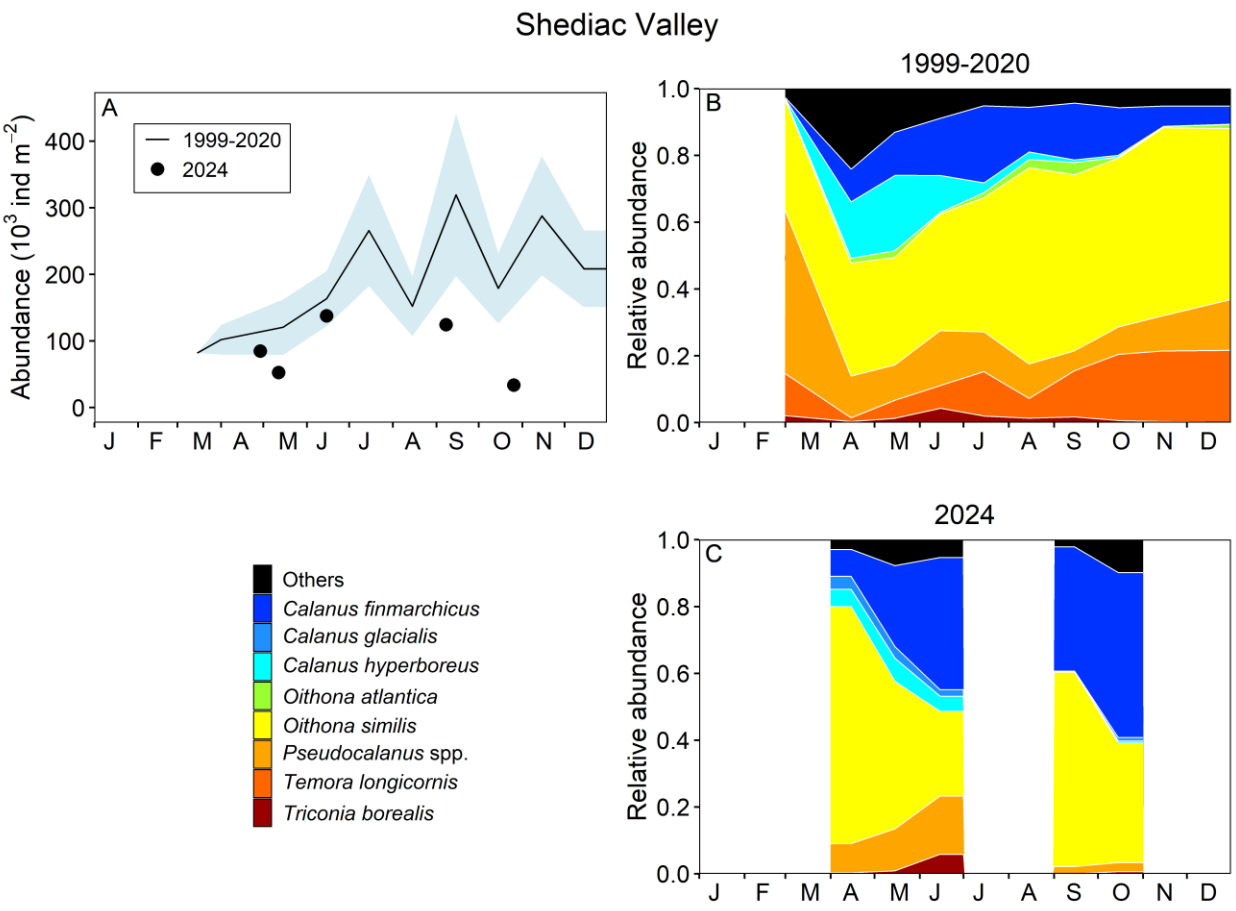

Figure 39. Seasonal variability of dominant copepods at Shediac Valley station. Climatology of copepod (copepodite stages only) abundance (10^3 individuals m^{-2}; black line with blue shading indicating ± 0.5 SD), and in 2024 (circles) (A); climatology of the relative abundance of the identified copepod taxa representing 95% of total copepod abundance during the 1999–2020 period (B), and in 2024 (C).

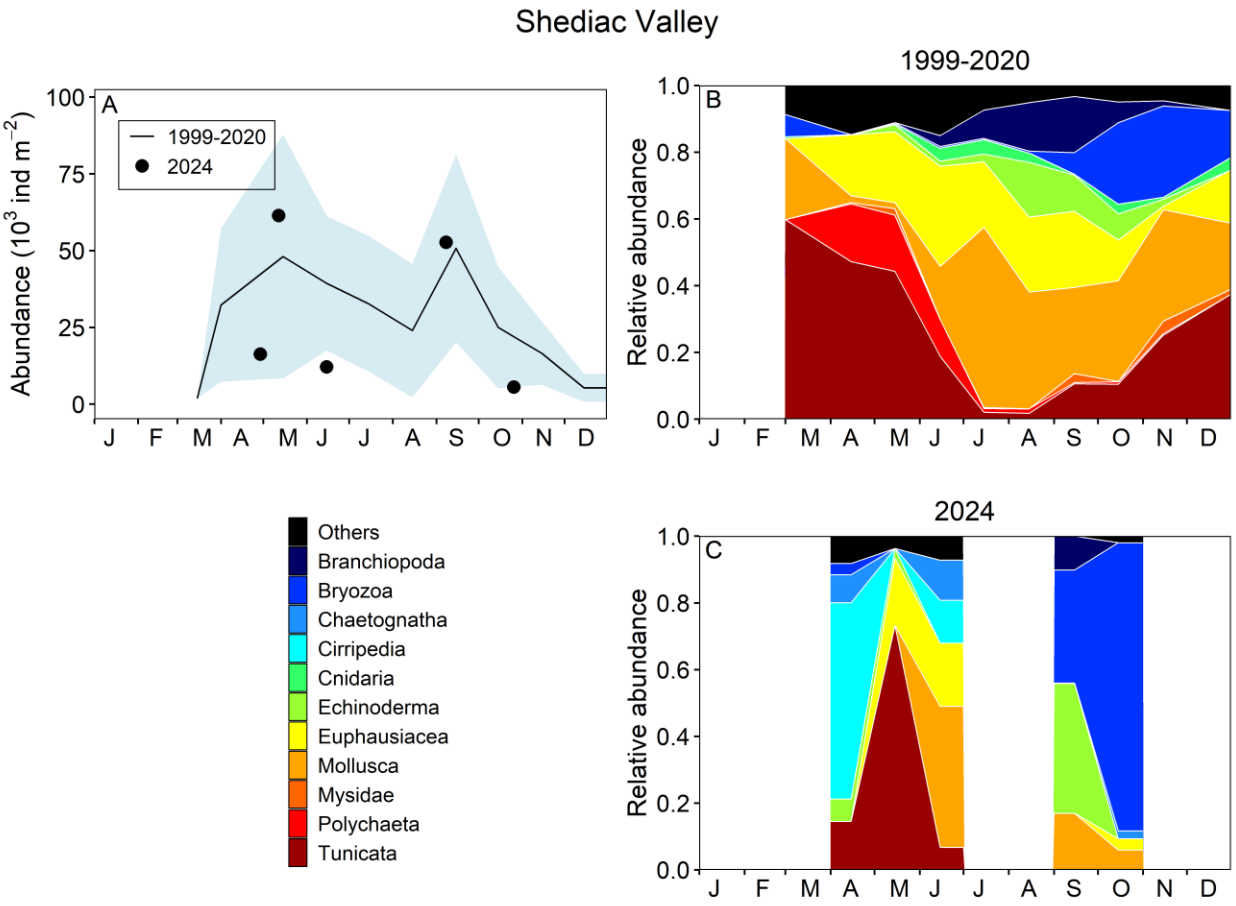

Figure 40. Seasonal variability of dominant non-copepod taxa at Shediac Valley station. Climatology of non-copepod abundance (10^3 individuals m^{-2}; black line with blue shading indicating ± 0.5 SD), and in 2024 (circles) (A); climatology of the relative abundance of the identified non-copepod taxa representing 95% of total non-copepod abundance during the 1999–2020 period (B), and in 2024 (C).

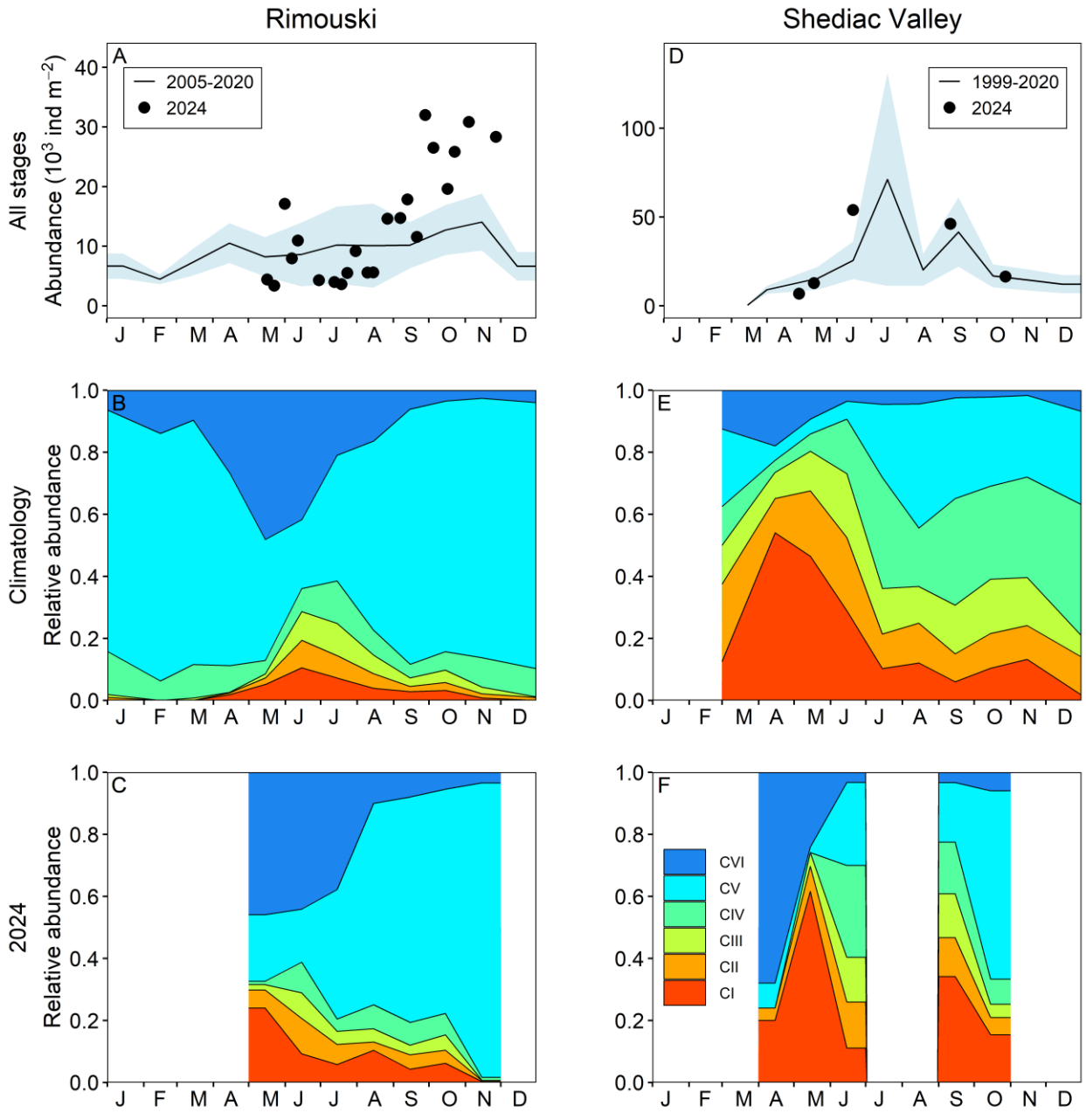

Figure 41. Seasonal variability in *Calanus finmarchicus* copepodite abundance (10^3 individuals m^{-2}) and stage composition at Rimouski (A–C) and Shediac Valley (D–F) stations. Climatology of *C. finmarchicus* abundance (black line with blue shading indicating ± 0.5 SD) with data from 2024 (circles) (A, D). Climatology of individual copepodite stages (B, E), and data for 2024 (C, F).

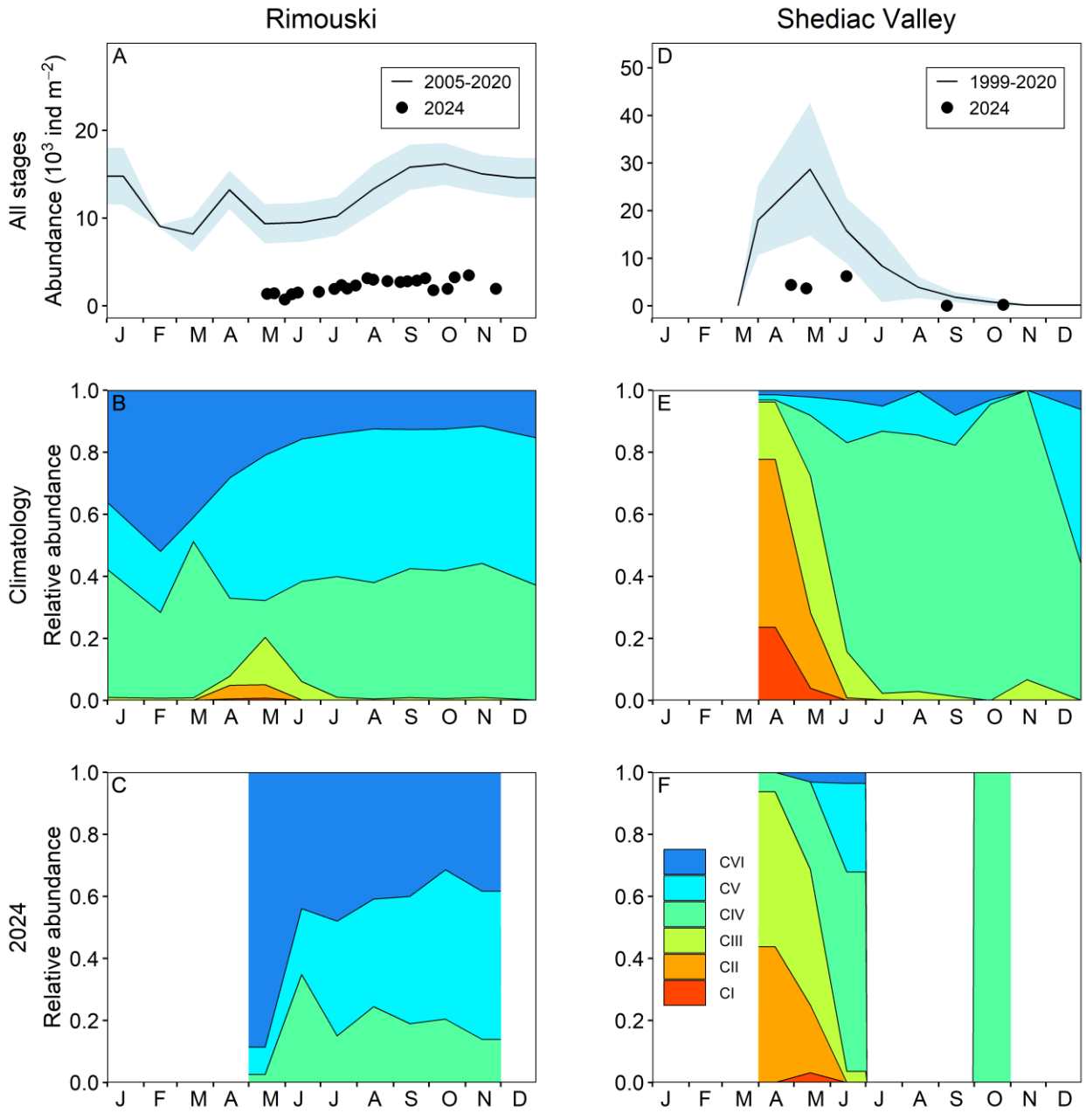

Figure 42. Seasonal variability in *Calanus hyperboreus* copepodite abundance (10^3 individuals m^{-2}) and stage composition at Rimouski (A–C) and Shediac Valley (D–F) stations. Climatology of *C. hyperboreus* abundance (black line with blue shading indicating ± 0.5 SD) with data from 2024 (circles) (A, D). Climatology of individual copepodite stages (B, E), and data for 2024 (C, F).

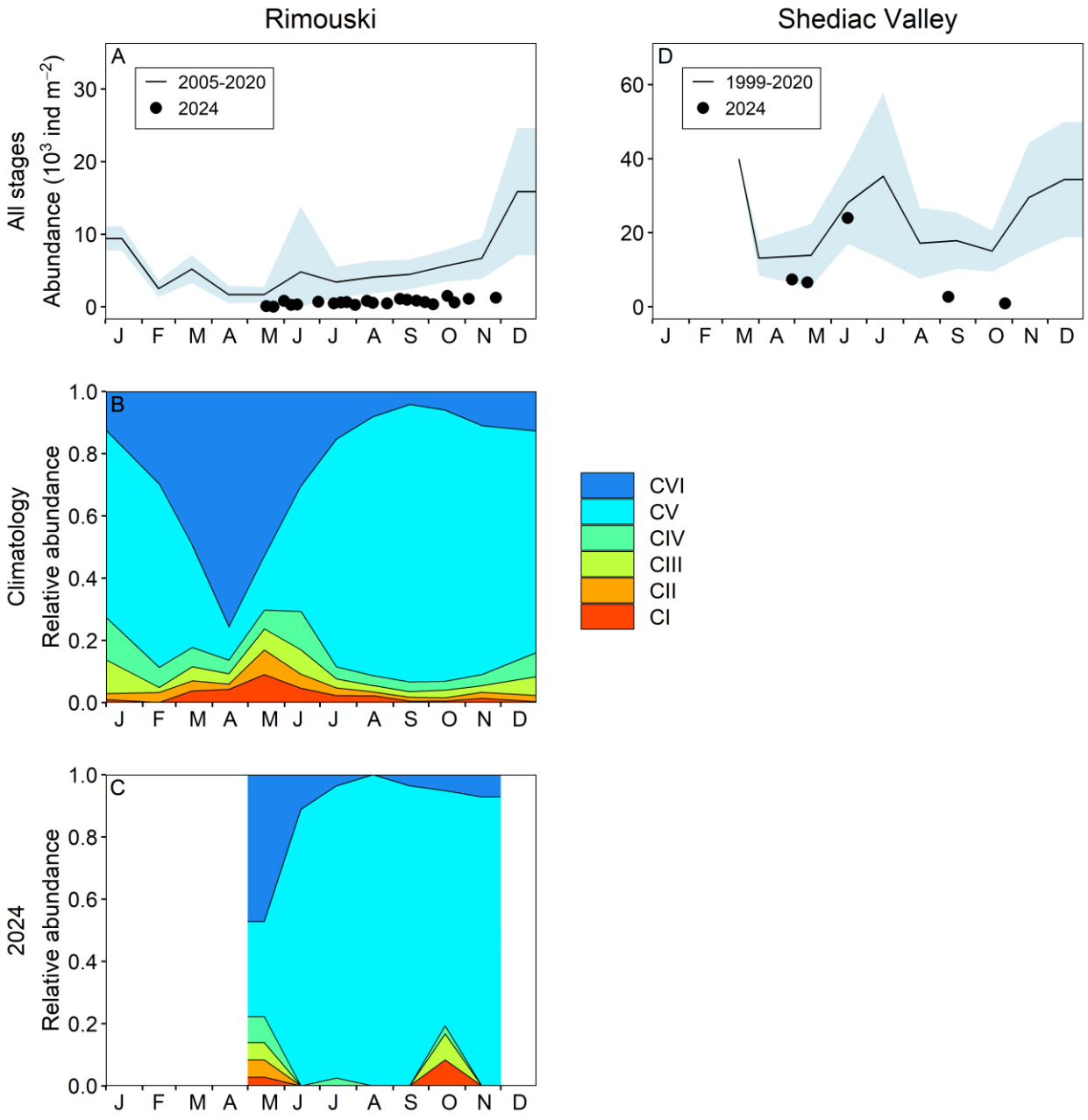

Figure 43. Seasonal variability in *Pseudocalanus* spp. copepodite abundance (10^3 individuals m^{-2}) and stage composition at Rimouski (A–C) and Shediac Valley (D) stations. Climatology of *Pseudocalanus* spp. abundance (black line with blue shading indicating ± 0.5 SD) with data from 2024 (circles) (A). Climatology of individual copepodite stages (B), and data for 2024 (C). Stage information is not available for Shediac Valley.

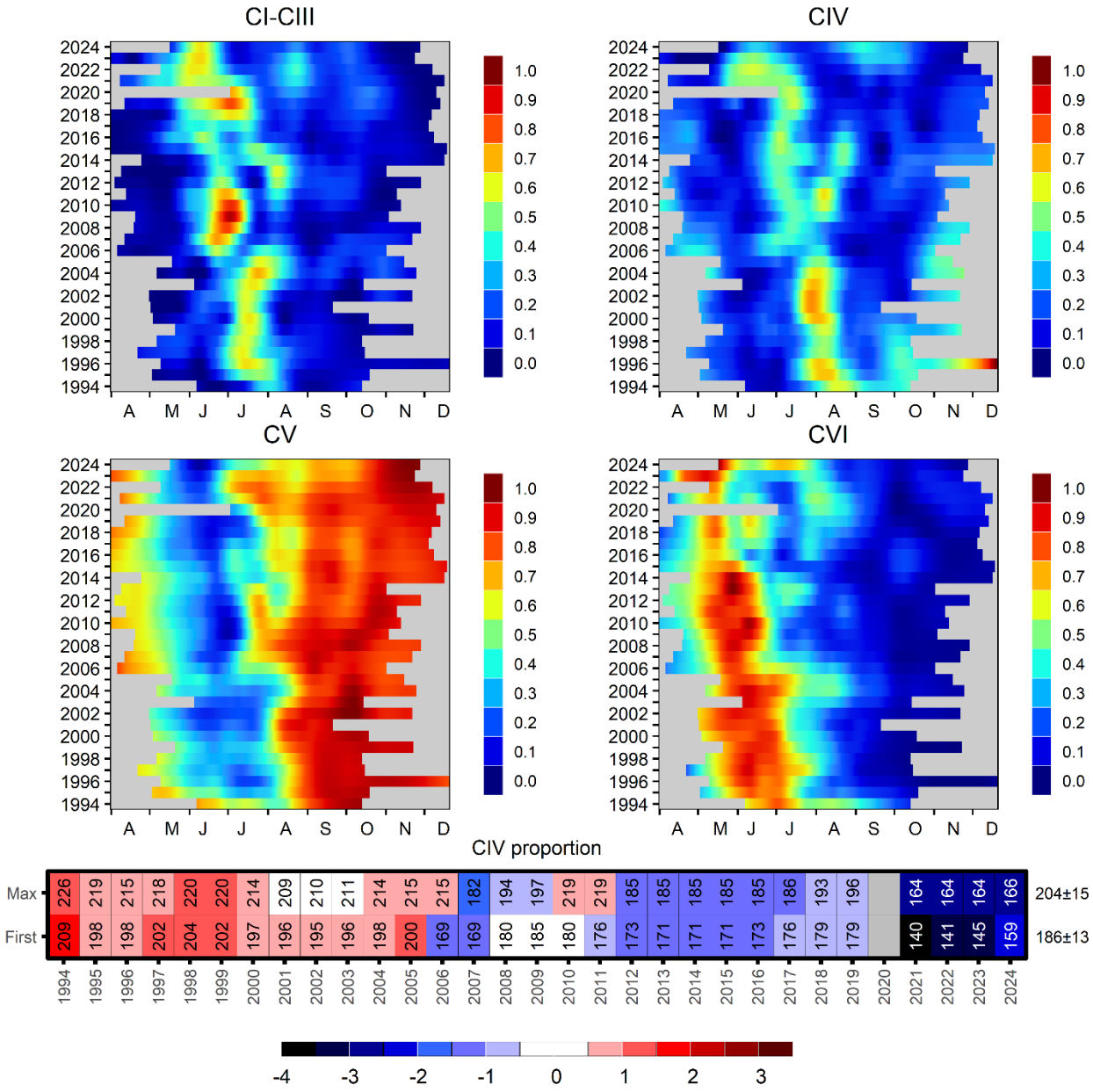

Figure 44. Time series of the seasonal cycle of relative proportion for *Calanus finmarchicus* copepodite stages at Rimouski station. Proportions are normalized by their annual maximum, and smoothed using a LOESS regression. Bottom scorecard shows the anomaly time series (climatology 1994–2020) associated with the day of maximum CIV proportion (Max), and the first day when the normalized proportion of CIV copepodite stage was higher than 35% (First). Variable means and standard deviations (in units of days) for the 1994–2020 climatology are shown to the right of the scorecard. Blue colours indicate below-normal levels (negative anomalies), reds are above-normal levels (positive anomalies), and white represents normal levels. Gray cells indicate unavailable data.

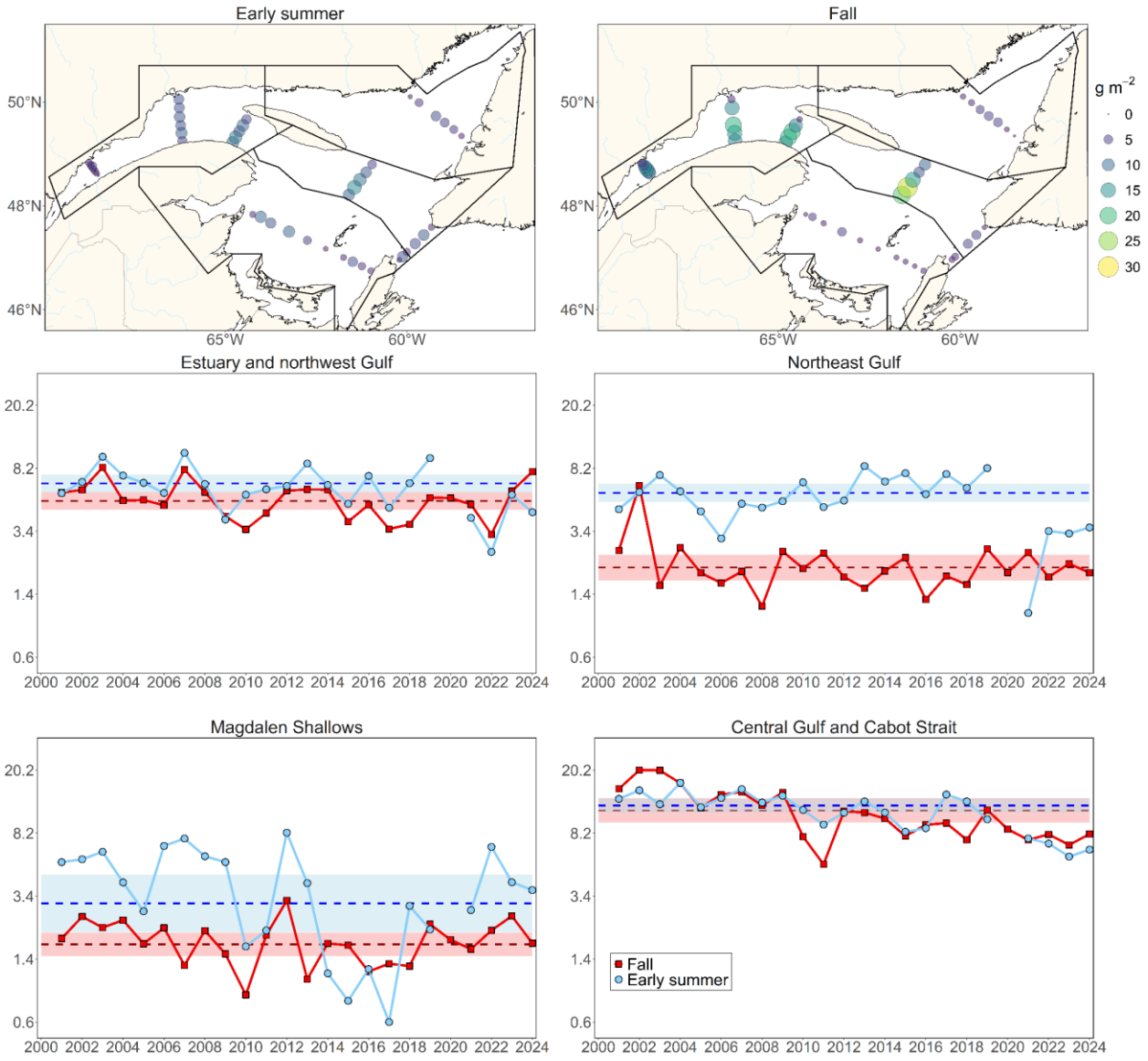

Figure 45. Zooplankton biomass (dry weight; g m^{-2}) spatial distribution during early summer and fall 2024 (upper panels), and regional seasonal time series of mean total zooplankton biomass (g m^{-2}; middle and bottom panels). Dashed blue and red lines represent the climatological (2001–2020) averages (blue and red shaded bands represent ± 0.5 SD) for early summer and fall, respectively.

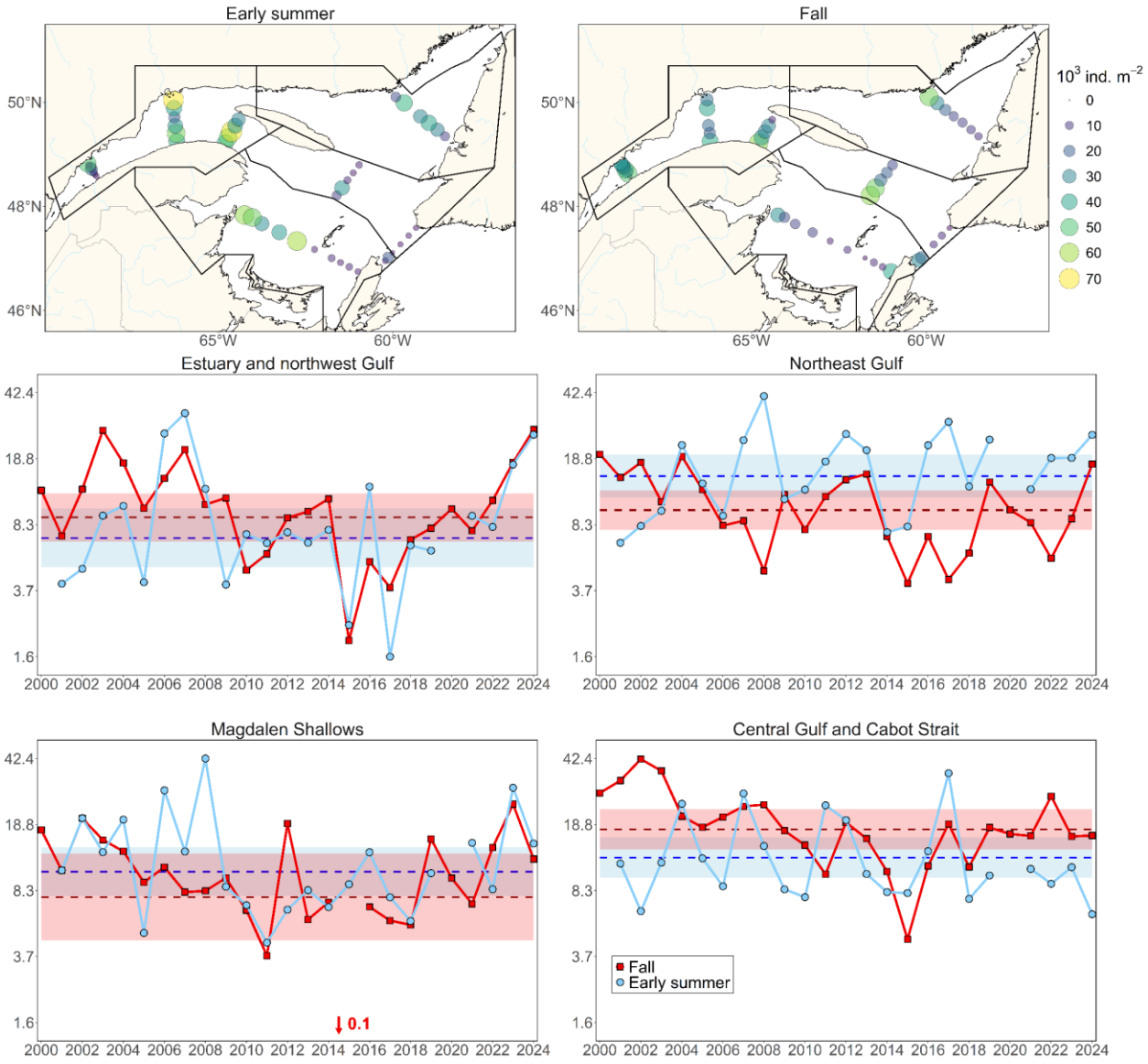

Figure 46. *Calanus finmarchicus* copepodite abundance (10^3 individuals m^{-2}) spatial distribution during early summer and fall 2024 (upper panels), and regional seasonal time series of mean total *C. finmarchicus* abundance (10^3 individuals m^{-2}; middle and bottom panels). In the Magdalen Shallows during 2015, the abundance of *C. finmarchicus* (100 individuals m^{-2}) is too low to be shown. Dashed blue and red lines represent the climatological (2000–2020) averages (blue and red shaded bands represent ± 0.5 SD) for early summer and fall, respectively.

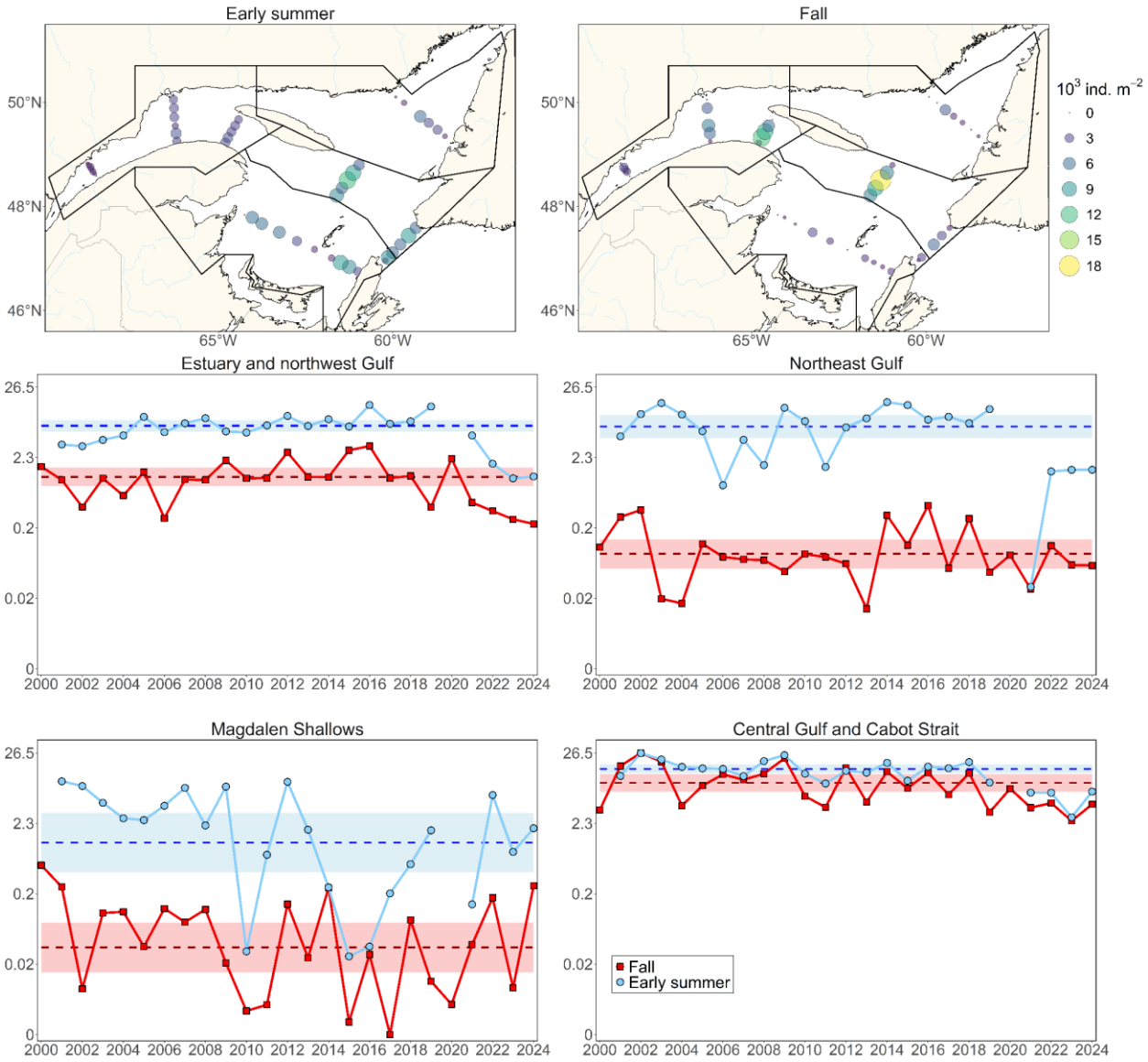

Figure 47. *Calanus hyperboreus* abundance (10^3 individuals m^{-2}) spatial distribution during early summer and fall 2024 (upper panels), and regional seasonal time series of mean total *C. hyperboreus* abundance (10^3 individuals m^{-2}; middle and bottom panels). Dashed blue and red lines represent the climatological (2000–2020) averages (blue and red shaded areas represent ± 0.5 SD) for early summer and fall, respectively.

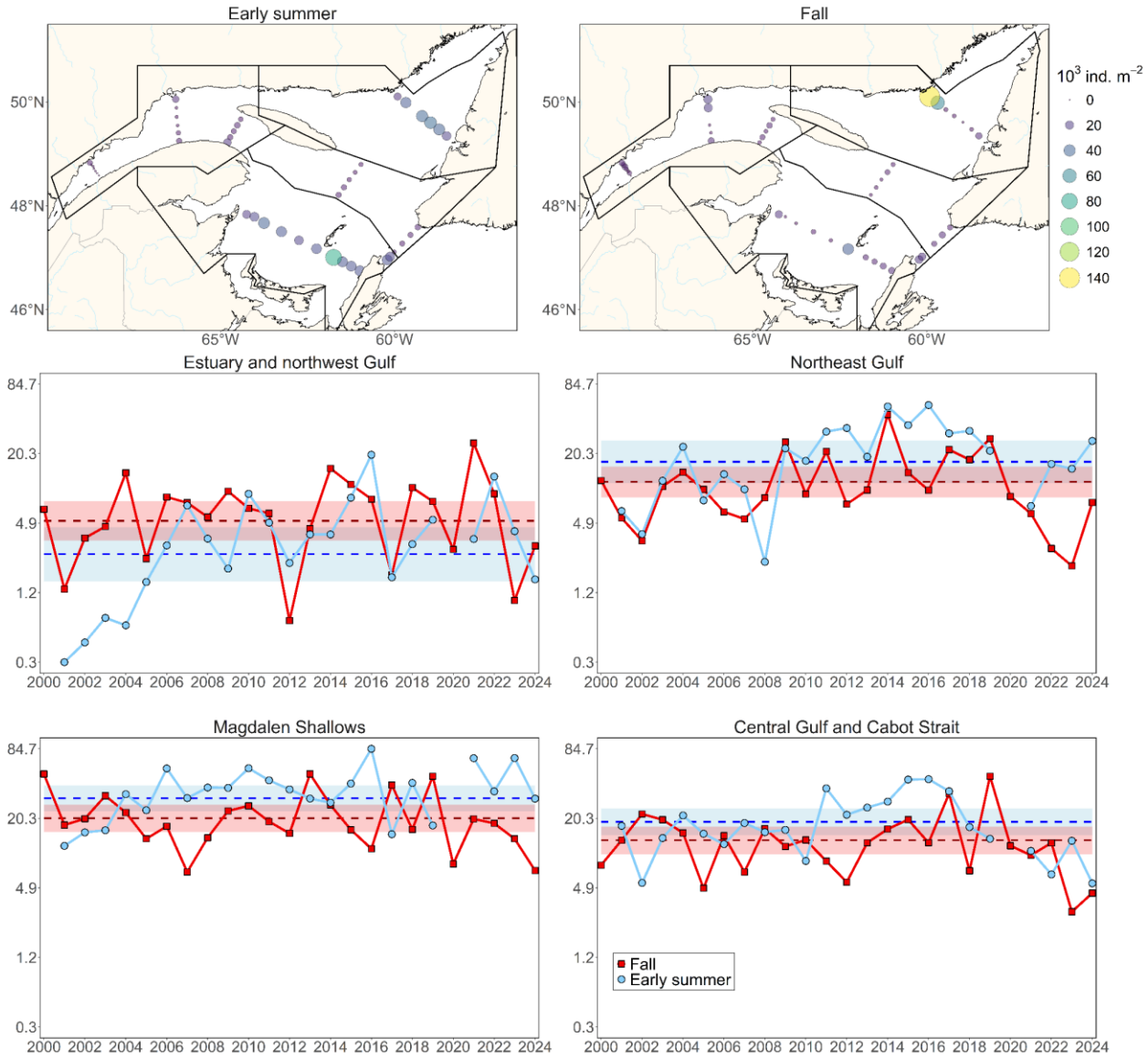

Figure 48. *Pseudocalanus* spp. abundance (10^3 individuals m^{-2}) spatial distribution during early summer and fall 2024 (upper panels), and regional seasonal time series of mean total *Pseudocalanus* spp. abundance (10^3 individuals m^{-2}; middle and bottom panels). Dashed blue and red lines represent the climatological (2000–2020) averages (blue and red shaded areas represent ± 0.5 SD) for early summer and fall, respectively.

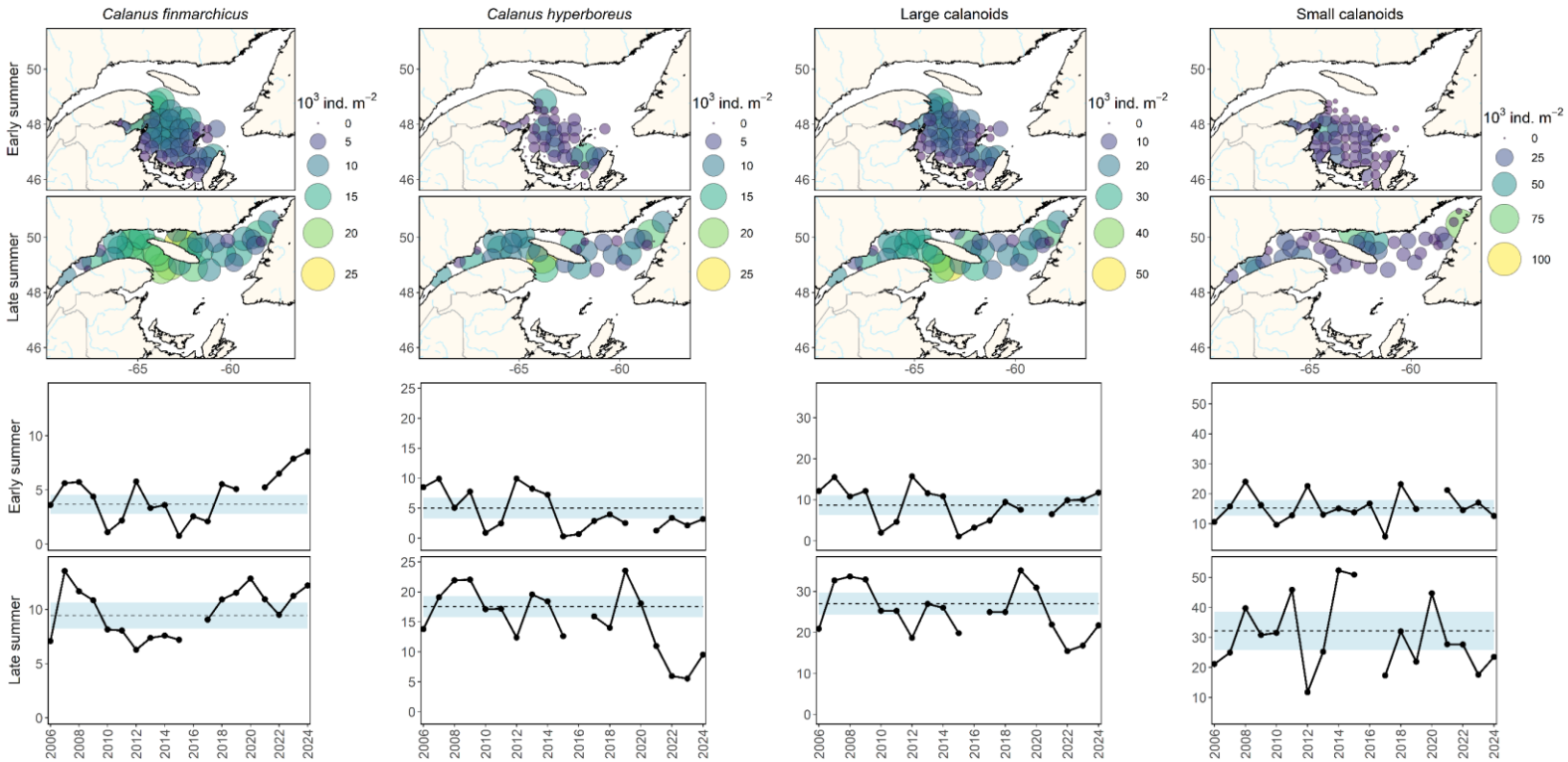

Figure 49. Abundances (10^3 individuals m^{-2}) of main taxa identified through automated numerical zooplankton images analysis (ZooImage) at each sampling station during early summer on the Magdalen Shallows, and late summer 2024 in the northern Gulf (upper panels). The annual time series of mean total abundances are also shown for these taxa (10^3 individuals m^{-2}; bottom panels). Dashed lines represent the climatology (2006–2020) averages (blue shading represents ± 0.5 SD). The abundances of *C. finmarchicus* and *C. hyperboreus* include copepodite stages CIV—CVI only. ZooImage does not distinguish between *C. finmarchicus* and *C. glacialis*, thus both species are included in the *C. finmarchicus* index. Large calanoid abundances correspond to the sum of these *C. finmarchicus* and *C. hyperboreus* indices; and small calanoid abundances correspond to the sum of the following taxa: *Temora* spp., *Eurytemora* spp., *Pseudocalanus* spp., *Microcalanus* spp. and *Scolecithricella* spp.

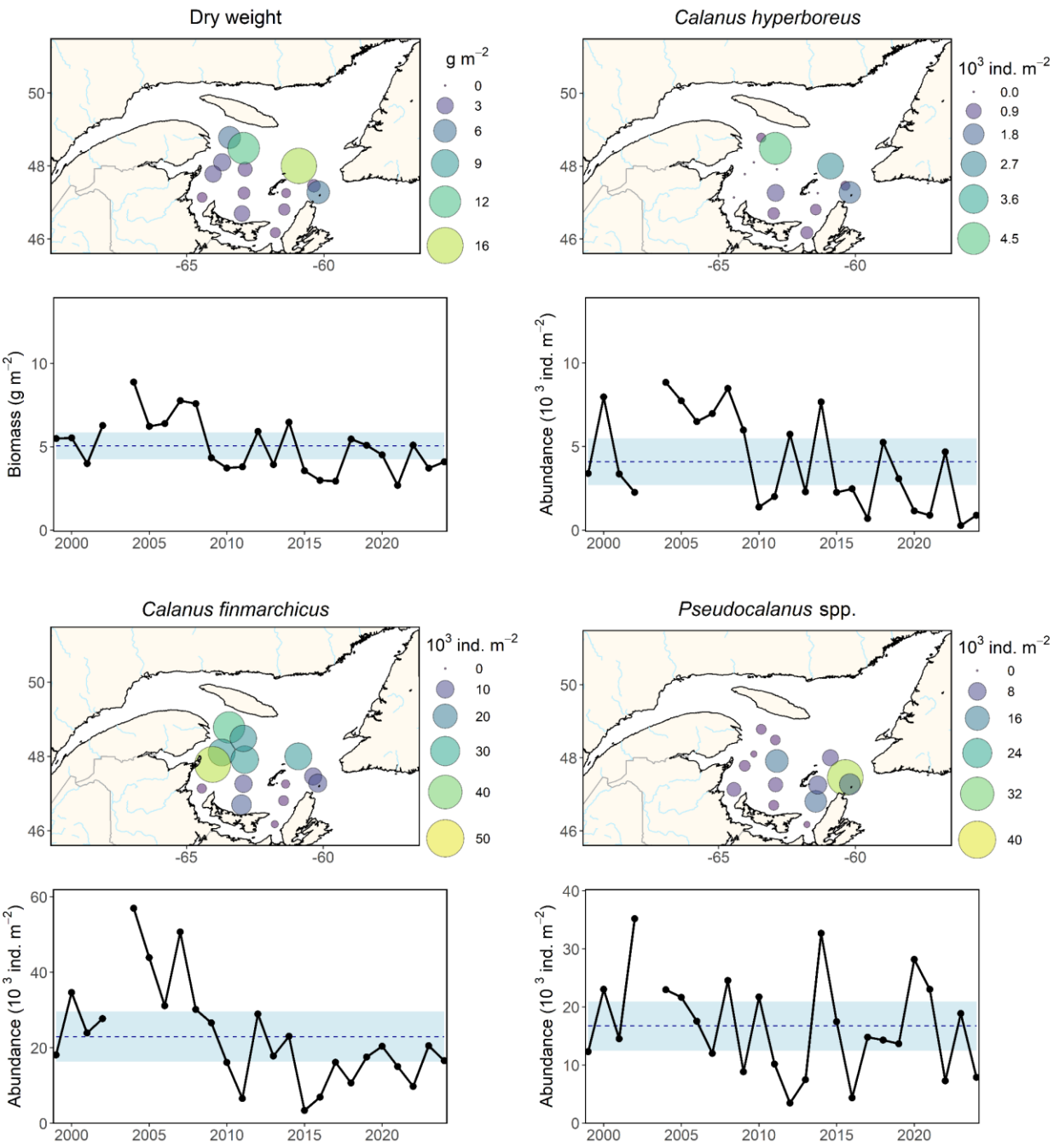

Figure 50. Biomass (g m^{-2}) and abundances (10^3 individuals m^{-2}) of main zooplankton taxa at each sampling station during late summer multidisciplinary survey on the Magdalen Shallows in September 2024. The seasonal time series of mean biomass (g m^{-2}) and total abundances for these taxa are also shown (10^3 individuals m^{-2}; bottom panels). Dashed lines represent the climatology (2000–2020) averages (blue shading represents ± 0.5 SD).

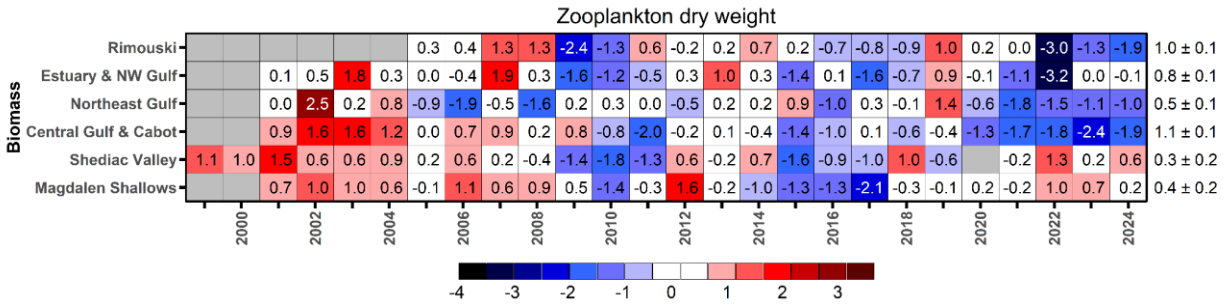

Figure 51. Time series of normalized annual anomalies of zooplankton biomass (dry weight) for the high-frequency monitoring stations and the regions of the Gulf of St. Lawrence. The numbers on the right are the 2001–2020 (2005–2020 for Rimouski; 1999–2019 for Shediac Valley) climatological means and standard deviations in units of $\log_{10}(g\ m^{-2})$. Blue colours indicate below-normal levels (negative anomalies), reds are above-normal levels (positive anomalies), and white represents normal levels. Gray cells indicate unavailable data. Biomass at the Shediac Valley station in 1999 may be overestimated, as it includes macrozooplankton dry weight, which typically accounts for less than 10% of the total dry weight.

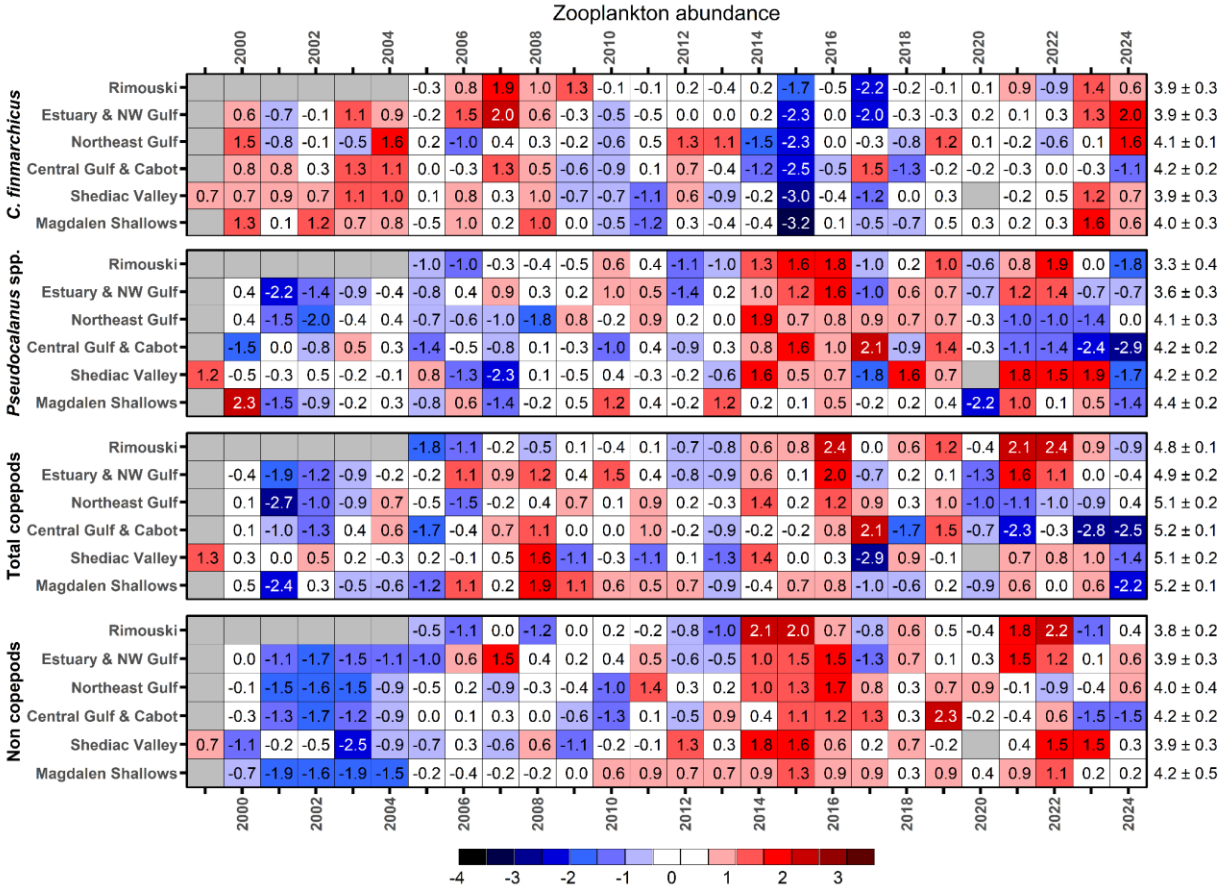

Figure 52. Time series of normalized annual anomalies for the abundance of four zooplankton categories for the high-frequency monitoring stations and regions of the Gulf of St. Lawrence. The numbers on the right are the 2000–2020 (2005–2020 for Rimouski; 1999–2019 for Shediac Valley) climatological means and standard deviations in units of $\log_{10}(\text{individuals}\ m^{-2})$. Blue colours indicate below-normal levels (negative anomalies), reds are above-normal levels (positive anomalies), and white represents normal levels. Gray cells indicate unavailable data.

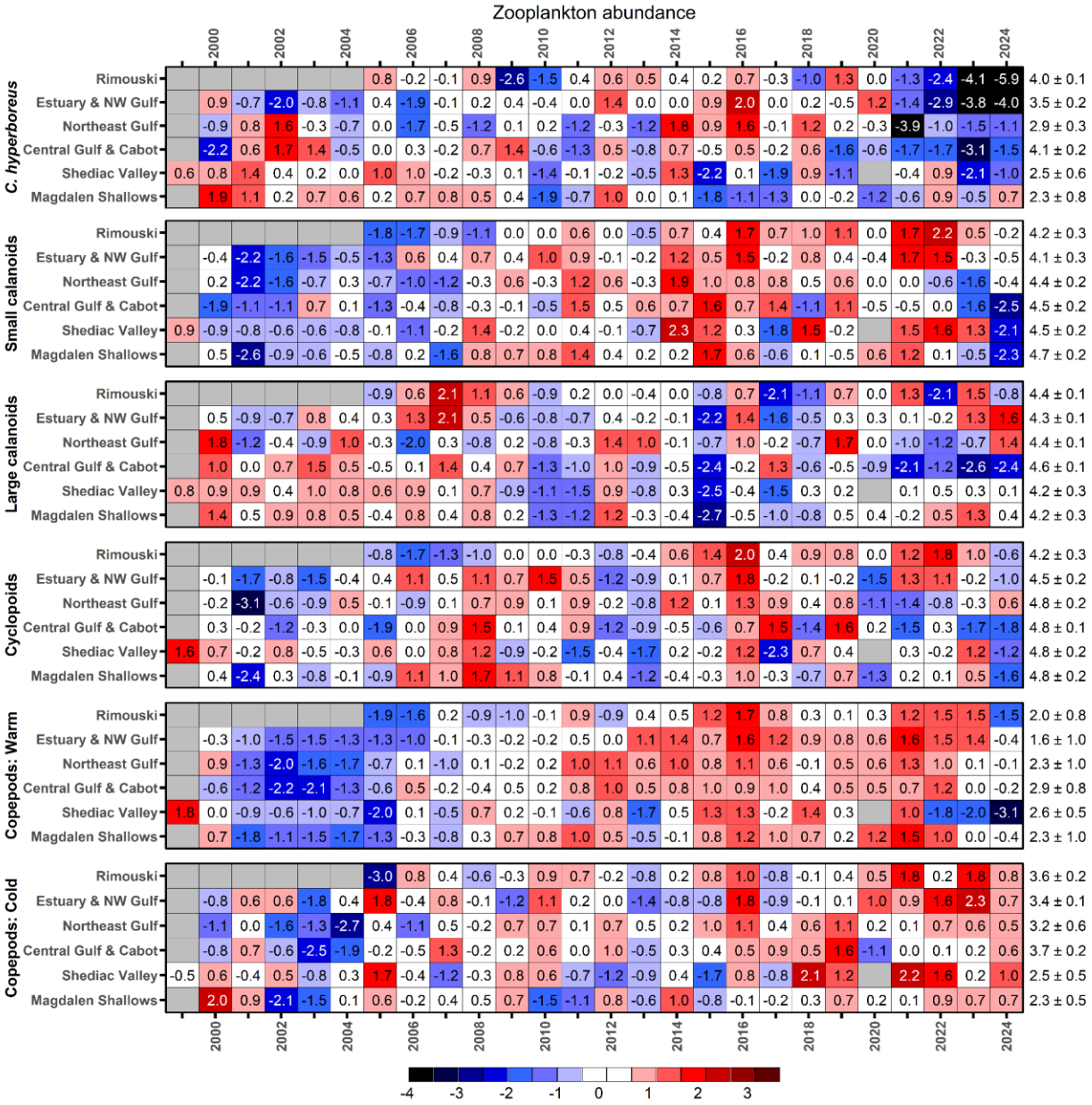

Figure 53. Time series of normalized annual anomalies for the abundance of six categories of zooplankton assemblages for the high-frequency monitoring stations and the regions of the Gulf of St. Lawrence. The numbers on the right are the 2000–2020 (2005–2020 for Rimouski; 1999–2020 for Shediac Valley) climatological means and standard deviations in units of $\log_{10}$(individuals m^{-2}). Blue colours indicate below-normal levels (negative anomalies), reds are above-normal levels (positive anomalies), and white represents normal levels. Gray cells indicate unavailable data. A detailed list of species included in each copepod index is presented in Appendix 1.

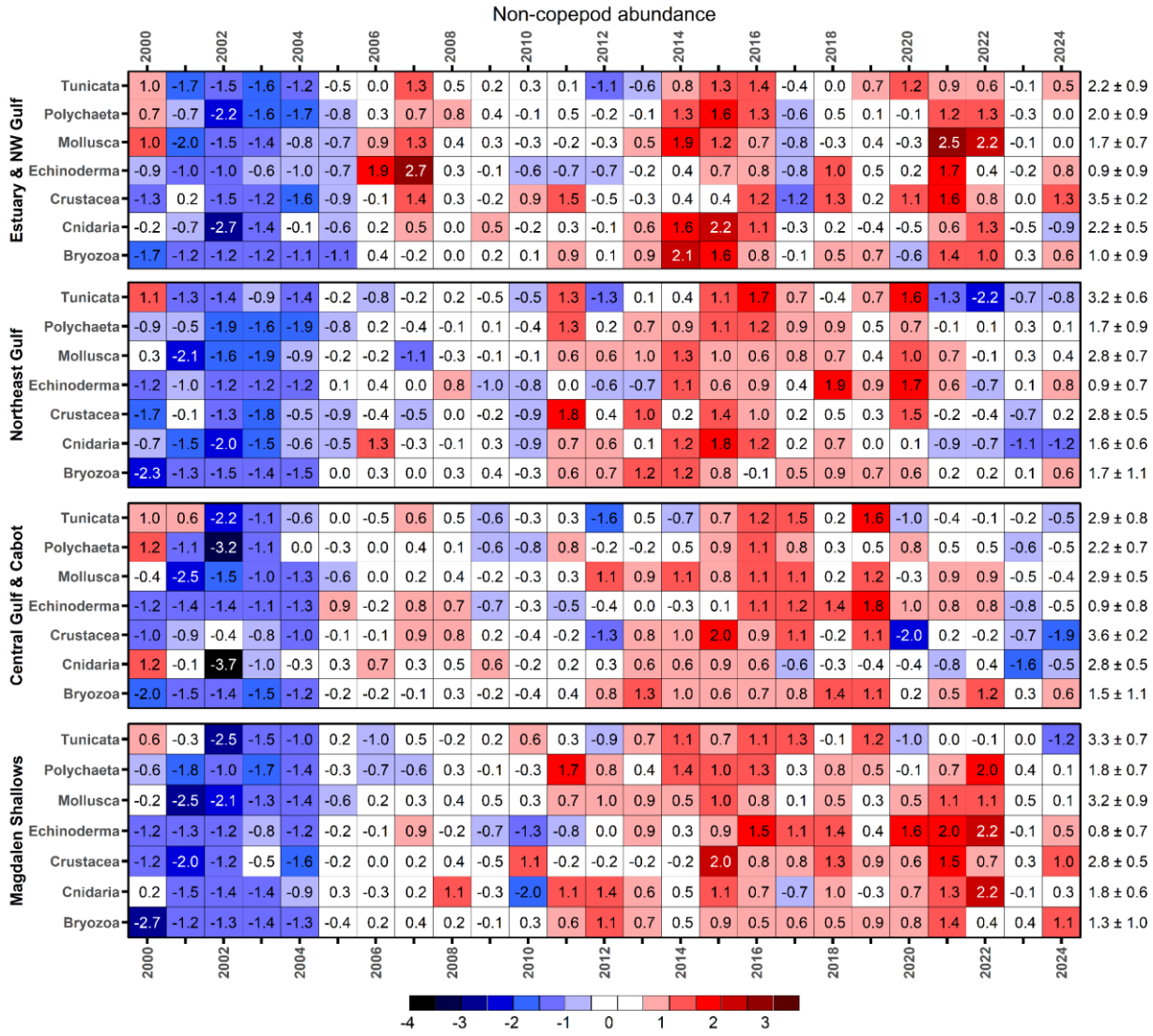

Figure 54. Time series of normalized annual anomalies for the abundance of main non-copepod zooplankton taxa for the regions of the Gulf of St. Lawrence. The numbers on the right are the 2000–2020 climatological means and standard deviations in units of $\log_{10}$(individuals m^{-2}). Blue colours indicate below-normal levels (negative anomalies), reds are above-normal levels (positive anomalies), and white represents normal levels.

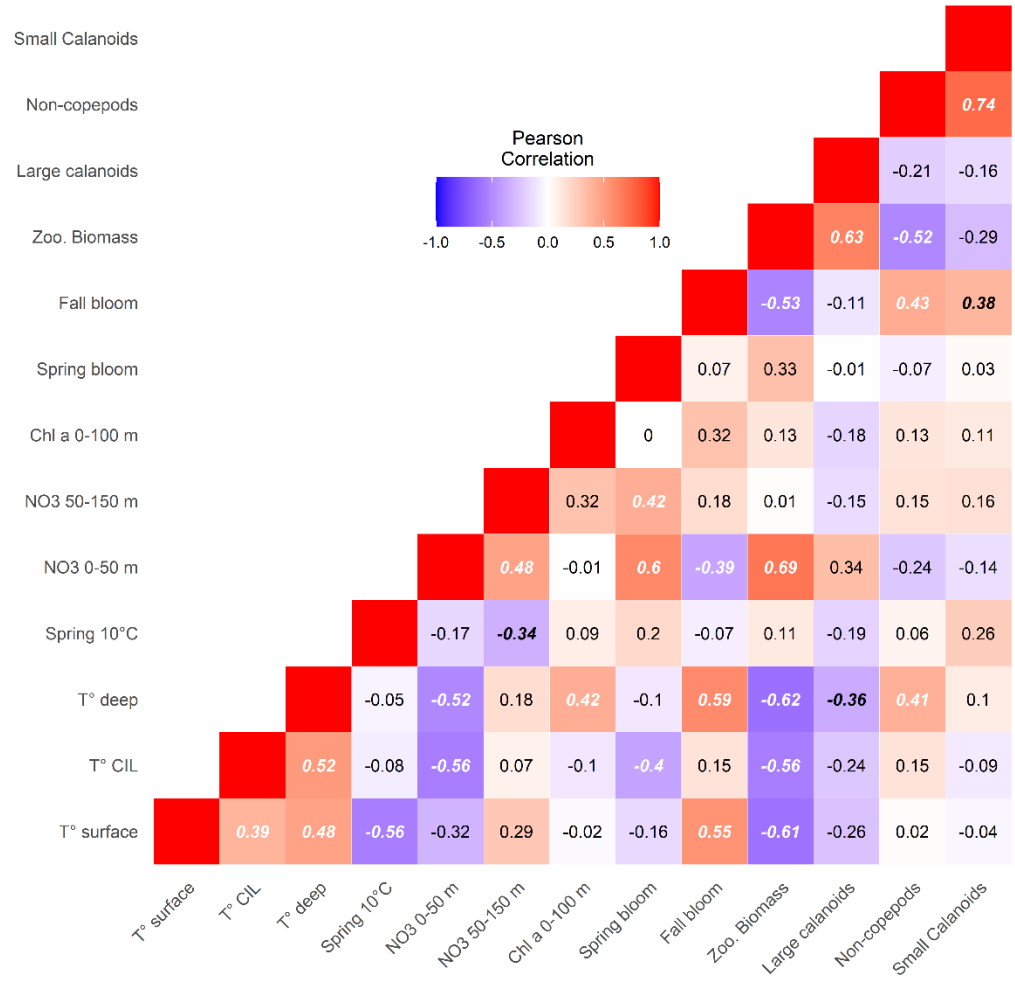

Figure 55. Correlation matrix of weighted averaged anomalies for key Gulf indices. Blue colours indicate negative correlations, and reds are positive correlations. Significant correlations are indicated in black bold italic ($p < 0.1$) or in white bold-italic ($p < 0.05$). CIL: cold intermediate layer. Spring 10 °C is an index of spring timing based on the date at which average Gulf temperature at the surface warms to 10 °C. Spring and fall blooms refer to their timing.

APPENDICES

Appendix 1 : List of taxa associated with each copepod index.

Small calanoids	*Acartia* spp.
	Aetideidae
	Centropages spp.
	Clausocalanus spp.
	Eurytemora spp.
	Microcalanus spp.
	Nannocalanus minor
	Paracalanus parvus
	Pseudocalanus spp.
	Scolecithricella spp.
	Spinocalanus spp.
	Temora spp.
	Tortanus spp.
Large calanoids	*Anomalocera* spp.
	Calanus finmarchicus
	Calanus glacialis
	Calanus hyperboreus
	Euchaeta spp.
	Metridia spp.
	Paraeuchaeta
	Pleuromamma borealis
	Pleuromamma robusta
Warm copepods	*Centropages* spp.
	Clausocalanus spp.
	Metridia lucens
	Nannocalanus minor
	Paracalanus spp.
	Pleuromamma borealis
	Pleuromamma robusta
Cyclopoids	*Oithona* spp.
	Oncaea spp.
	Triconia borealis
	Triconia conifer
	Triconia similis
Cold copepods	*Metridia longa*
	Calanus glacialis

Appendix 2 : Spring and fall bloom fits for 2024 in all Gulf ocean colour polygons using the Phytofit application v1.0.0 (Clay et al. 2021) with the parameters listed below. These bloom fits are used to define spring (peak; plots 1–4) and fall (start; plots 5–8) timing of the bloom, as well as to define season boundaries. Different "flagged fit" warning may arise if the offset between observed and modelled parameters is too large or if parameters are on the boundary of the allowed range. These flags exist in the PhytoFit app to aid the user in detecting bad fits.

1.

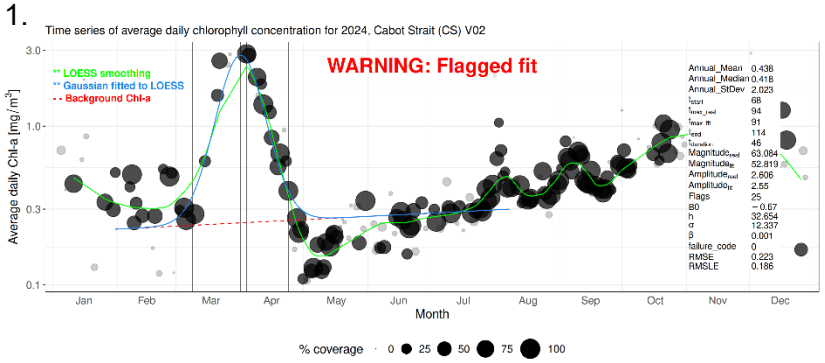

2.

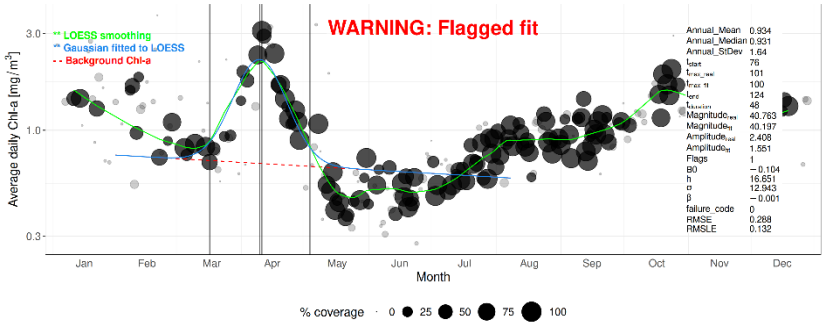

3.

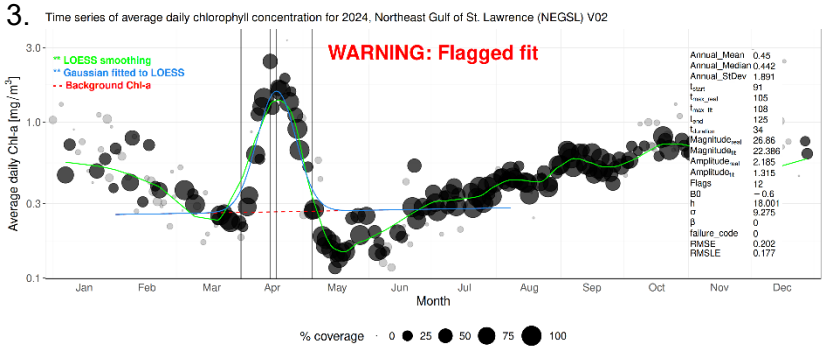

4.

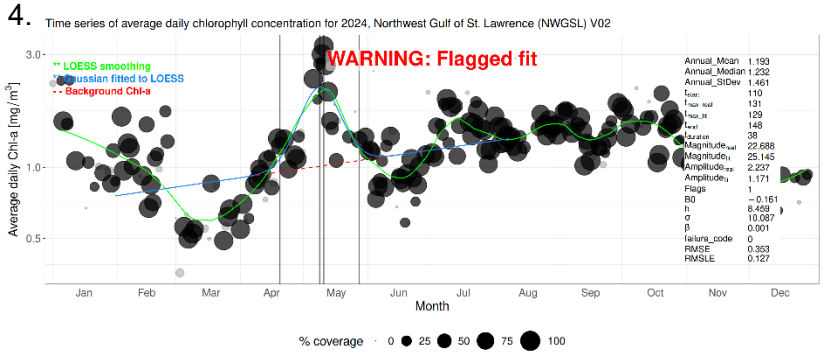

5. Time series of average daily chlorophyll concentration for 2024, Cabot Strait (CS) V02

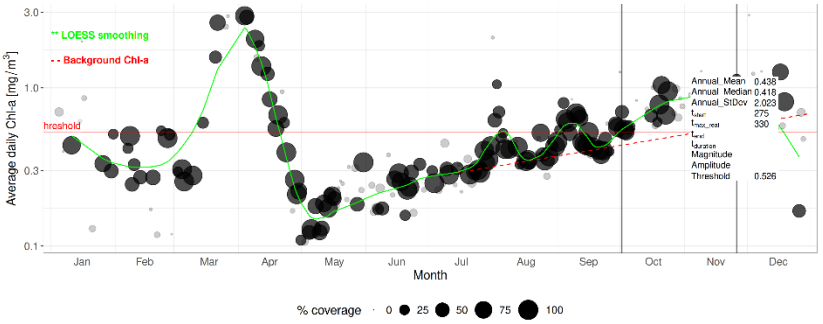

6. Time series of average daily chlorophyll concentration for 2024, Magdalen Shallows (MS) V02

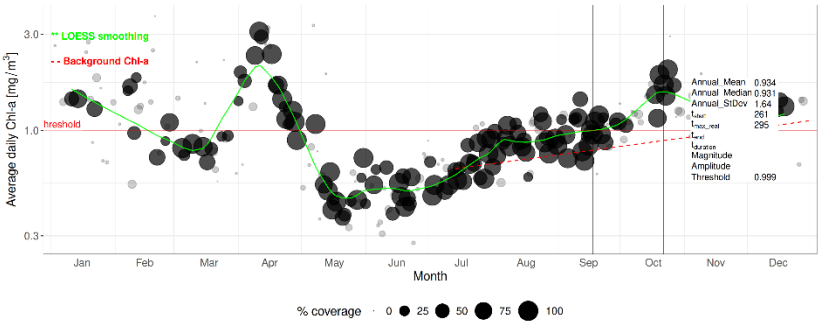

7. Time series of average daily chlorophyll concentration for 2024, Northeast Gulf of St. Lawrence (NEGSL) V02

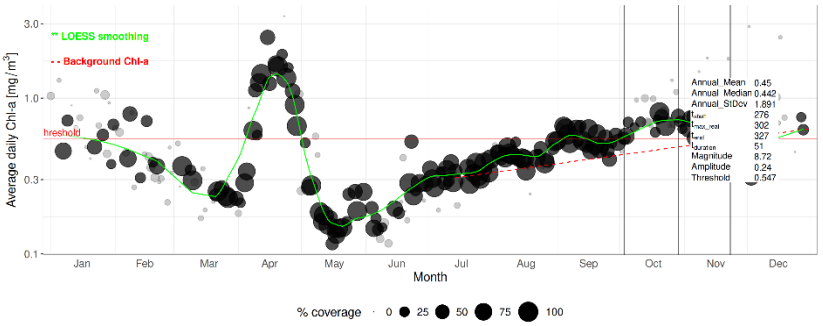

8.

Time series of average daily chlorophyll concentration for 2024, Northwest Gulf of St. Lawrence (NWGSL) V02

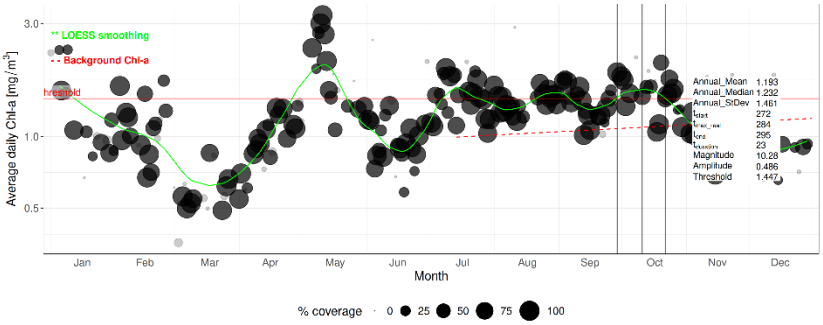

Parameters	Spring	Fall
Settings_region	Gulf of Saint Lawrence 4km	Gulf of Saint Lawrence 4km
Settings_sat_alg	occciv6.0_chlpoly4	occciv6.0_chlpoly4
Settings_concentration_type	full	full
Settings_interval	daily	daily
Settings_log_chla	TRUE	TRUE
Settings_percent	20	20
Settings_outlier	sd3	sd3
Settings_dailystat	average	average
Settings_pixrange1	-	-
Settings_pixrange2	-	-
Settings_fitmethod	gauss	thresh
Settings_bloomShape	symmetric	asymmetric
Settings_smoothMethod	loess	loess
Settings_loessSpan	0.2	0.2
Settings_t_range	31, 220	195, 365
Settings_ti_limits	58, 150	196, 354
Settings_tm_limits	91,181	197, 364
Settings_ti_threshold_type	percent_thresh	-
Settings_ti_threshold_percent	20	-
Settings_threshcoef	-	1.05
Settings_tm	TRUE	-
Settings_beta	TRUE	-
Settings_use_weights	TRUE	FALSE
Settings_rm_bkrnd	TRUE	TRUE
Settings_flag1_lim1	0.75	0.75
Settings_flag1_lim2	1.25	1.25
Settings_flag2_lim1	0.85	0.85
Settings_flag2_lim2	1.15	1.15

Appendix 3 : General linear model results for Rimouski and Shediac Valley stations. Significance of the year and month effects as well as the adjusted coefficients (R^2) of the regression for nutrients and chlorophyll *a* are presented.

Station	Index	Year (*p*)	Month (*p*)	R^2
Rimouski	Chlorophyll *a* (0–100 m)	<0.0001	<0.0001	0.43
	Nitrate (0–50 m)	<0.0001	<0.0001	0.38
	Nitrate (50–150 m)	<0.0001	<0.0001	0.28
	Nitrate (150–320 m)	<0.0001	<0.0001	0.49
Shediac Valley	Chlorophyll *a* (0–100 m)	0.003	<0.0001	0.29
	Nitrate (0–50 m)	<0.0001	<0.0001	0.48
	Nitrate (50–84 m)	<0.0001	<0.0001	0.45

Appendix 4 : General linear model results for Rimouski and Shediac Valley stations. Significance of the year and month effects as well as the adjusted coefficients (R^2) of the regression for phytoplankton groups are presented.

Station	Index	Year (*p*)	Month (*p*)	R^2
Rimouski	Diatoms	<0.0001	<0.0001	0.35
	Dinoflagellates	<0.0001	<0.0001	0.5
	Flagellates	<0.0001	<0.0001	0.36
	Total	<0.0001	<0.0001	0.26
Shediac Valley	Diatoms	<0.0001	<0.0001	0.34
	Dinoflagellates	<0.0001	0.002	0.31
	Flagellates	<0.0001	<0.0001	0.39
	Total	0.002	0.1	0.17

Appendix 5: General linear model results for Gulf regions. Significance of the year, season, and station effects as well as the adjusted coefficients (R^2) squared of the regression for nutrients or chlorophyll *a* are presented. Btm: Bottom.

Region	Index	Year (*p*)	Season (*p*)	Station(*p*)	R^2
Estuary/ Northwest Gulf	Chlorophyll *a* (0–100 m)	<0.0001	<0.0001	<0.0001	0.36
	Nitrate (0–50 m)	<0.0001	<0.0001	<0.0001	0.59
	N:P (0–50 m)	<0.0001	<0.0001	<0.0001	0.65
	Si:N (0–50 m)	<0.0001	<0.0001	<0.0001	0.16
	Nitrate (50–150 m)	<0.0001	<0.0001	<0.0001	0.71
	N:P (50–150 m)	<0.0001	<0.0001	<0.0001	0.39
	Si:N (50–150 m)	<0.0001	<0.0001	<0.0001	0.32
	Nitrate (150-btm)	<0.0001	<0.0001	<0.0001	0.95
	N:P (150-btm)	<0.0001	0.04	<0.0001	0.69
	Si:N (150-btm)	<0.0001	<0.0001	<0.0001	0.77
Northeast Gulf	Chlorophyll *a* (0–100m)	<0.0001	<0.0001	0.2	0.25
	Nitrate (0–50m)	<0.0001	<0.0001	0.04	0.73
	N:P (0–50m)	<0.0001	<0.0001	<0.0001	0.85
	Si:N (0–50m)	0.01	0.03	1	0.02
	Nitrate (50–150m)	<0.0001	<0.0001	<0.0001	0.85
	N:P (50–150m)	<0.0001	<0.0001	<0.0001	0.69
	Si:N (50–150m)	<0.0001	0.4	<0.0001	0.24
	Nitrate (150-btm)	<0.0001	<0.0001	<0.0001	0.92
	N:P (150-btm)	<0.0001	<0.0001	<0.0001	0.63
	Si:N (150-btm)	<0.0001	<0.0001	<0.0001	0.68
Central Gulf/Cabot Strait	Chlorophyll *a* (0–100m)	<0.0001	<0.0001	0.06	0.15
	Nitrate (0–50m)	<0.0001	<0.0001	<0.0001	0.7
	N:P (0–50m)	<0.0001	<0.0001	<0.0001	0.78
	Si:N (0–50m)	<0.0001	0.02	<0.0001	0.25
	Nitrate (50–150m)	<0.0001	<0.0001	<0.0001	0.54
	N:P (50–150m)	<0.0001	<0.0001	<0.0001	0.35
	Si:N (50–150m)	<0.0001	<0.0001	<0.0001	0.53
	Nitrate (150-btm)	<0.0001	<0.0001	<0.0001	0.95
	N:P (150-btm)	<0.0001	0.07	<0.0001	0.47
	Si:N (150-btm)	<0.0001	<0.0001	<0.0001	0.61
Magdalen Shallows	Chlorophyll *a* (0–100m)	<0.0001	<0.0001	<0.0001	0.34
	Nitrate (0–50m)	<0.0001	<0.0001	<0.0001	0.63
	N:P (0–50m)	<0.0001	<0.0001	<0.0001	0.67
	Si:N (0–50m)	<0.001	<0.0001	<0.0001	0.18
	Nitrate (50–150m)	<0.0001	<0.0001	<0.0001	0.75
	N:P (50–150m)	<0.0001	<0.0001	<0.0001	0.54
	Si:N (50–150m)	<0.0001	0.09	<0.0001	0.33

Appendix 6: General linear model results for Rimouski and Shediac Valley stations. Significance of the year and month effects as well as the adjusted coefficients (R^2) of the regression for each zooplankton index are presented.

Station	Index	Year (*p*)	Month (*p*)	R^2
Rimouski	*Calanus finmarchicus*	<0.0001	<0.0001	0.52
	Pseudocalanus spp.	<0.0001	<0.0001	0.57
	Total copepods	<0.0001	<0.0001	0.59
	Non-copepods	<0.0001	<0.0001	0.44
	Calanus hyperboreus	<0.0001	<0.0001	0.62
	Small calanoids	<0.0001	<0.0001	0.69
	Large calanoids	<0.0001	<0.0001	0.35
	Cyclopoids	<0.0001	<0.0001	0.59
	Copepods: Warm	<0.0001	0.6	0.53
	Copepods: Cold	<0.0001	<0.0001	0.45
	Dry weight	<0.0001	<0.0001	0.7
	Bryozoa	<0.0001	<0.0001	0.23
	Cnidaria	<0.0001	<0.0001	0.62
	Crustacea	<0.0001	<0.0001	0.50
	Echinoderma	<0.0001	0.001	0.22
	Mollusca	<0.0001	<0.0001	0.36
	Polychaeta	<0.0001	<0.0001	0.42
	Tunicata	<0.0001	<0.0001	0.47
	Ostracoda	<0.0001	0.2	0.29
Shediac Valley	*Calanus finmarchicus*	<0.0001	<0.0001	0.32
	Pseudocalanus spp.	0.03	0.2	0.09
	Total copepods	0.1	<0.0001	0.17
	Non-copepods	<0.001	0.002	0.2
	Calanus hyperboreus	<0.0001	<0.0001	0.68
	Small calanoids	0.001	<0.001	0.21
	Large calanoids	<0.0001	<0.0001	0.35
	Cyclopoids	0.2	<0.0001	0.22
	Copepods: Warm	0.01	0.2	0.1
	Copepods: Cold	0.02	<0.0001	0.31
	Dry weight	<0.0001	<0.0001	0.36
	Bryozoa	<0.001	<0.0001	0.43
	Cnidaria	<0.0001	<0.001	0.4
	Crustacea	0.005	<0.0001	0.33
	Echinoderma	0.05	<0.0001	0.17
	Mollusca	<0.001	<0.0001	0.33
	Polychaeta	<0.0001	<0.0001	0.49
	Tunicata	0.01	<0.0001	0.25
	Ostracoda	0.9	0.6	-0.06

Appendix 7: General linear model results for Gulf regions. Significance of the year, season, and station effects as well as the adjusted coefficients (R^2) of the regression for each zooplankton index are presented.

Region	Index	Year (*p*)	Season (*p*)	Station(*p*)	R^2
Estuary/ Northwest Gulf	*Calanus finmarchicus*	<0.0001	<0.001	<0.0001	0.64
	Pseudocalanus spp.	<0.0001	<0.0001	<0.0001	0.52
	Total copepods	<0.0001	<0.0001	<0.0001	0.72
	Non-copepods	<0.0001	<0.0001	<0.0001	0.56
	Calanus hyperboreus	<0.0001	<0.0001	<0.0001	0.62
	Small calanoids	<0.0001	<0.0001	<0.0001	0.64
	Large calanoids	<0.0001	<0.001	<0.0001	0.75
	Cyclopoids	<0.0001	<0.0001	<0.0001	0.68
	Copepods: Warm	<0.0001	0.003	<0.0001	0.55
	Copepods: Cold	<0.0001	0.01	<0.0001	0.66
	Dry weight	<0.0001	0.005	<0.0001	0.78
	Bryozoa	<0.0001	<0.0001	<0.0001	0.44
	Cnidaria	<0.0001	0.006	<0.0001	0.71
	Crustacea	<0.0001	<0.0001	<0.0001	0.55
	Echinoderma	<0.0001	<0.001	<0.0001	0.37
	Mollusca	<0.0001	<0.001	<0.0001	0.49
	Polychaeta	<0.0001	<0.0001	<0.0001	0.58
	Tunicata	<0.0001	<0.0001	<0.0001	0.44
	Ostracoda	<0.0001	0.9	<0.0001	0.71
Northeast Gulf	*Calanus finmarchicus*	<0.0001	<0.0001	0.008	0.23
	Pseudocalanus spp.	<0.0001	<0.0001	<0.0001	0.33
	Total copepods	<0.0001	<0.0001	<0.001	0.36
	Non copepods	<0.0001	<0.001	<0.0001	0.44
	Calanus hyperboreus	<0.001	<0.0001	<0.0001	0.59
	Small calanoids	<0.0001	0.6	<0.0001	0.41
	Large calanoids	0.005	<0.0001	<0.0001	0.45
	Cyclopoids	<0.0001	<0.0001	0.02	0.46
	Copepods: Warm	<0.0001	<0.0001	0.009	0.45
	Copepods: Cold	<0.0001	<0.0001	<0.0001	0.42
	Dry weight	<0.0001	<0.0001	<0.0001	0.65
	Bryozoa	<0.0001	<0.0001	0.9	0.62
	Cnidaria	<0.0001	0.9	<0.001	0.34
	Crustacea	<0.0001	<0.0001	0.002	0.52
	Echinoderma	<0.0001	0.06	0.07	0.20
	Mollusca	<0.0001	0.9	<0.001	0.31
	Polychaeta	<0.0001	<0.0001	0.9	0.53
	Tunicata	<0.0001	<0.0001	<0.0001	0.39
	Ostracoda	0.1	0.001	<0.0001	0.29

Appendix 7 (continued): General linear model results for Gulf regions. Significance of the year, season, and station effects as well as the adjusted coefficients (R^2) of the regression for each zooplankton index are presented.

Region	Index	Year (*p*)	Season (*p*)	Station(*p*)	R^2
Central Gulf/ Cabot Strait	*Calanus finmarchicus*	<0.0001	<0.0001	<0.001	0.26
	Pseudocalanus spp.	<0.0001	<0.0001	<0.0001	0.35
	Total copepods	<0.0001	<0.0001	<0.001	0.24
	Non-copepods	<0.0001	<0.0001	<0.0001	0.47
	Calanus hyperboreus	<0.0001	<0.0001	<0.0001	0.54
	Small calanoids	<0.0001	0.6	<0.0001	0.36
	Large calanoids	<0.0001	0.6	<0.0001	0.38
	Cyclopoids	<0.0001	<0.0001	0.007	0.21
	Copepods: Warm	<0.0001	<0.0001	<0.0001	0.48
	Copepods: Cold	<0.0001	0.6	0.09	0.11
	Dry weight	<0.0001	0.3	<0.0001	0.64
	Bryozoa	<0.0001	<0.0001	0.4	0.48
	Cnidaria	<0.0001	<0.0001	<0.0001	0.47
	Crustacea	<0.0001	<0.0001	0.07	0.46
	Echinoderma	<0.0001	0.005	<0.001	0.26
	Mollusca	<0.0001	0.03	0.003	0.17
	Polychaeta	<0.0001	<0.0001	<0.0001	0.58
	Tunicata	<0.0001	<0.0001	0.001	0.42
	Ostracoda	<0.001	0.2	<0.0001	0.37
Magdalen Shallows	*Calanus finmarchicus*	<0.0001	<0.001	<0.0001	0.33
	Pseudocalanus spp.	<0.0001	<0.0001	0.7	0.13
	Total copepods	<0.0001	<0.0001	<0.0001	0.21
	Non copepods	<0.0001	<0.0001	<0.0001	0.49
	Calanus hyperboreus	<0.0001	<0.0001	<0.0001	0.49
	Small calanoids	<0.0001	0.1	<0.001	0.19
	Large calanoids	<0.0001	<0.0001	<0.0001	0.49
	Cyclopoids	<0.0001	<0.0001	<0.0001	0.30
	Copepods: Warm	<0.0001	<0.0001	0.005	0.49
	Copepods: Cold	<0.0001	<0.0001	<0.0001	0.39
	Dry weight	<0.0001	<0.0001	<0.0001	0.43
	Bryozoa	<0.0001	<0.0001	0.4	0.64
	Cnidaria	<0.0001	0.09	<0.0001	0.30
	Crustacea	<0.0001	<0.0001	<0.0001	0.44
	Echinoderma	<0.0001	0.02	0.006	0.22
	Mollusca	<0.0001	0.09	<0.0001	0.58
	Polychaeta	<0.0001	<0.0001	0.01	0.65
	Tunicata	<0.0001	<0.0001	<0.0001	0.34
	Ostracoda	0.01	0.4	<0.0001	0.26